

Mass Transfer Effects on Reactive Separation Processes –
Discovery of Reactive Arrheotropes

Einfluss des Stoffübergangs auf reaktive Trennprozesse –
Die Entdeckung von reaktiven Arrheotropen

Dissertation
zur Erlangung des akademischen Grades

Doktoringenieur
(Dr.-Ing.)

von Master of Science Yuan-Sheng Huang
geb. am 18.06.1973 in Hualien

genehmigt durch die Fakultät für Verfahrens- und Systemtechnik
der Otto-von-Guericke-Universität Magdeburg

Gutachter: Prof. Dr.-Ing. Kai Sundmacher
Prof. Dr.-Ing. Achim Kienle

Promotionskolloquium am 13.12.2005

Acknowledgement

This dissertation presents the major results of my research work performed during November 2000 to October 2005 at the Max-Planck Institute for Dynamics of Complex Technical Systems in Magdeburg, Germany.

First of all, I want to thank God Almighty for seeing me through these days, no matter in the good times or bad times. His words of wisdom always encourage me when I suffered from the experimental difficulties and almost gave up.

“Ask and it will be given to you; seek and you will find; knock and the door will be opened to you. For everyone who asks receives; he who seeks finds; and to him who knocks, the door will be opened.”

~*Matthew 7, 7-8*

I would like to thank Prof. Kai Sundmacher for offering me this opportunity to carry out my PhD research at the Max-Planck Institute, and for his inspiring guidance and helpful advices to my study.

I would also like to show my sincere gratitude to Prof. Ernst-Ulrich Schlünder for his illuminating discussion and encouragement. It is always my honor and pleasure to work with such a famous but kind mentor.

Thanks also go to all colleagues at the Max-Planck Institute, in particular to the Physical and Chemical Process Engineering group. Special acknowledgements are given to the following people who have directly helped this work: Dr. Eileen Yu, Dr. Michael Mangold, Dr. Zhiwen Qi, Frank Steyer, Jignesh Gangadwala, Bianka Stein, Samuel Tulashie, Valentin Chernev, and Ravinder Seggyam.

The selfless supports from Pi-Ju Wu and my sister, Hui-Ling, are personally acknowledged.

Finally, I want to express my deepest thank to my family members, especially my parents, for approving of my decision to continue my education abroad. Their constant love is the strongest support for me during these years.

Magdeburg, October 2005

Table of Contents

Nomenclature	vii
Abstract.....	xi
Zusammenfassung.....	xii
1. Introduction	1
1.1 Literature review	2
1.2 Research objective and outline.....	4
2. Theoretical approach	6
2.1 Model formulation of retentate phase diagrams.....	7
2.1.1 Reaction kinetics and mass balance.....	7
2.1.2 Heating policies	9
2.1.3 Vapor-liquid equilibrium	10
2.1.4 Degeneration to reactive distillation	11
2.1.5 Equivalent continuous process	11
2.2 Kinetics of mass transfer through membranes	14
2.2.1 Explicit expression for pressure-driven membrane permeation	14
2.2.2 Diffusion through porous membranes – Dusty gas model	15
2.3 Singular point analysis and transformed composition variables	17
2.3.1 Singular points	17
2.3.2 Transformed composition variables	19
2.4 Chapter conclusions	20
3. Examples of ternary systems.....	22
3.1 Ideal ternary system	22
3.1.1 Residue curve maps and retentate phase diagrams.....	23
3.1.2 Singular point analysis.....	27
3.1.3 Generalization.....	29
3.1.4 Influence of membranes on singular points	30
3.2 Non-ideal system: THF synthesis reaction	34

3.2.1 Residue curve maps and retentate phase diagrams.....	35
3.2.2 Singular point analysis.....	38
3.3 Chapter conclusions.....	41
4. Examples of quaternary systems	42
4.1 Ideal quaternary system	42
4.1.1 Residue curve maps and retentate phase diagrams.....	43
4.1.2 Singular point analysis.....	47
4.2 Non-ideal system: esterification of acetic acid with <i>n</i> -propanol.....	51
4.2.1 Residue curve maps and retentate phase diagrams.....	52
4.2.2 Singular point analysis.....	56
4.3 Chapter conclusions.....	59
5. Kinetics of propyl acetate synthesis reaction	60
5.1 Experiments.....	60
5.1.1 Materials	60
5.1.2 Experimental setup	61
5.1.3 Analysis of liquid phase composition	62
5.1.4 Procedure	63
5.2 Results	63
5.2.1 Exclusion of external mass transfer influence.....	63
5.2.2 Chemical equilibrium constant.....	63
5.2.3 Reaction enthalpy, entropy and free energy	64
5.2.4 Effect of catalyst amount.....	65
5.2.5 Effect of temperature	66
5.2.6 Effect of initial mole fraction.....	66
5.2.7 Mathematical formulation of kinetic models	67
5.2.8 Parameter identification	68
5.3 LHHW model parameter identification issue.....	70
5.4 Chapter conclusions.....	71

6. Experimental validation of proposed theory	72
6.1 Experimental setup for reactive distillation process	73
6.2 Validation of reactive azeotrope	74
6.3 Experimental setup for membrane reactor process	75
6.3.1 Mass transfer resistance through the boundary layer	76
6.3.2 Capillary condensation in the membrane pores.....	77
6.3.3 Selection of polymer membrane material.....	78
6.3.4 Control of permeation flux.....	79
6.4 Validation of reactive azeotrope.....	80
6.5 Chapter conclusions	81
7. Conclusions and outlook	82
Appendix.....	85
A.1 Derivation of transformed composition variables.....	85
A.2 Matrix formulation of dusty gas model.....	87
A.3 Thermodynamic data of THF reaction system.....	88
A.4 Thermodynamic data of propyl acetate reaction system	89
A.5 Derivation of heterogeneous kinetic models for propyl acetate reaction system	91
A.6 Influence of temperature on the quaternary unstable node in propyl acetate reaction system.....	96
References.....	97

Nomenclature

Latin symbols

a	m^2/m	interfacial area per unit column length, Eq.(2.17)
a_i	-	liquid phase activity of component i
$a_1 - a_6$	-	coefficients in the quadratic equation, Eq.(3.9)
A	m^2	permeation area
A_c	m^2	sectional area
A, B, C, D	-	chemical species
B_0	m^2	permeability constant of porous membranes, Eq.(2.28)
$[B^e]$	$(\text{m}^2/\text{s})^{-1}$	the inverse matrix of $[k]$ in dusty gas model, Eq.(2.32)
B^e_{ii}, B^e_{ij}	$(\text{m}^2/\text{s})^{-1}$	elements of $[B^e]$
c	mol/m^3	molar density of vapour, Eq.(6.2)
Da	-	Damköhler number
D_{ij}	m^2/s	binary diffusivity
D^e_{ij}	m^2/s	effective binary diffusivity in porous media effective
$D^e_{K,i}$	m^2/s	Knudsen diffusivity of i
E_f	J/mol	activation energy
$\Delta_f G$	J/mol	free energy of formation
$\Delta_r G$	J/mol	reaction free energy change
H	mol	molar liquid holdup
H_0	mol	initial molar liquid holdup
H_r	mol	holdup in which the reaction proceeds
$H_{r,0}$	mol	initial holdup in which the reaction proceeds
$\Delta_f H$	J/mol	enthalpy of formation
$\Delta_r H$	J/mol	reaction enthalpy
k_A	$1/\text{Pa}$	dimerization equilibrium constant
k_f	$\text{mol}/(\text{mol}\cdot\text{s})$ or $\text{mol}/(M_{cat}\cdot\text{s})$	forward reaction rate constant
k_{f0}	$\text{mol}/(\text{mol}\cdot\text{s})$ or $\text{mol}/(M_{cat}\cdot\text{s})$	frequency factor of k_f
$k_{f,ref}$	$\text{mol}/(\text{mol}\cdot\text{s})$ or $\text{mol}/(M_{cat}\cdot\text{s})$	forward reaction rate constant at reference point

$[k]$	m/s	matrix of effective mass transfer coefficients
k_{ij}	m/s	effective binary mass transfer coefficients of pair i - j
K	-	chemical equilibrium constant
K_{BD}	-	adsorption constant of 1,4-butanediol
K_{H_2O}	-	adsorption constant of water
$K_{S,i}$	-	absorption constant of component i
L	mol/s	total molar flow rate
L_i	mol/s	component molar flow rate
M_{cat}	g	mass of catalyst
M_i	-	molecular weight of component i
n_i	mol/(m ² ·s)	molar flux of component i through membrane
n_T	mol/(m ² ·s)	total molar flux through membrane
$n_{T,ref}$	mol/(m ² ·s)	total molar flux at a reference state
NC	-	number of reacting species
N_{ij}	-	interaction parameter for NRTL model
N_{tot}	mol	total number of moles in kinetics study, Chapter 5
p_i^{sat}	Pa	saturated vapor pressure of component i
p^{cond}	Pa	capillary condensation pressure, Eq.(6.2)
p	Pa	system pressure
QS	-	quadratic sum of deviation, Eq.(5.9)
r	mol/(mol·s) or mol/(M_{cat} ·s)	reaction rate per unit catalyst amount
r_i	mol/(mol·s) or mol/(M_{cat} ·s)	reaction rate per unit catalyst amount
r_c	m	radius of curvature, Eq.(6.2)
R	J/(mol·K)	universal gas constant, 8.314 J/(mol·K)
R_i	mol/s	apparent reaction rate, Eqs.(5.5)-(5.7)
\mathcal{R}	-	dimensionless reaction rate
$\Delta_r S$	J/(mol·K)	reaction entropy
t	s	time
T	K	temperature
V	mol/s	total molar flow rate for open evaporation
V_{ref}	mol/s	total molar flow rate at a reference state

(x)	-	vector of liquid phase mole fractions
x_i	-	liquid phase mole fraction of component i
$x_{i,0}$	-	initial mole fraction at $t = 0$
X_i	-	transformed liquid phase mole fraction of component i
y_i	-	mole fraction of component i in vapor phase
Y_i	-	transformed vapor phase mole fraction of component i
z	m	axial coordinate of reactor column
z^*	-	dimensionless axial coordinate
z_A, z_N	-	dimerization correction factor
z_i	-	dimerization correction factor

Greek symbols

α_{ij}	-	relative volatility of i with respect to j
γ_i	-	liquid phase activity coefficient of component i
δ	m	membrane thickness
ε	-	membrane porosity
ε_{cat}	(mol·cat)/m ³	catalyst loading density
η	-	water inhibition factor, Eq.(3.16)
θ	-	contact angle, Eq.(6.2)
κ_{ij}	-	dimensionless binary mass transfer coefficient
$\lambda_{1,2}$	-	eigenvalues of matrix $[A]$
μ	Pa·s	viscosity of vapor mixture
ν_i	-	stoichiometric coefficient of component i
ν_T	-	total mole change of reaction
ξ	-	dimensionless time, $d\xi = (n_T/H) \cdot dt$
σ	N/m	interfacial tension, Eq.(6.2)
σ_{ij}	-	interaction parameter for NRTL model
τ	-	tortuosity of membrane pores

Subscripts

<i>A, B, C, D</i>	components A, B, C and D respectively
<i>AcAc</i>	acetic acid
<i>BD</i>	1,4-butanediol
<i>H₂O</i>	water
<i>i, j</i>	components <i>i, j</i>
<i>PrAc</i>	propyl acetate
<i>PrOH</i>	propanol
<i>p</i>	permeation side
<i>THF</i>	tetrahydrofurane
<i>1, 2, 3, 4</i>	acetic acid, propanol, propyl acetate, water

Abbreviations

<i>DGM</i>	dusty gas model
<i>LHHW</i>	Langmuir-Hinshelwood-Hougen-Watson model
<i>MR</i>	membrane reactor
<i>PC</i>	polycarbonate
<i>PET</i>	polyester
<i>PH</i>	pseudo-homogeneous model
<i>PSPC</i>	potential singular point curve
<i>RCM</i>	residue curve map
<i>RD</i>	reactive distillation
<i>RE</i>	Rideal-Eley model
<i>RED</i>	relative energy difference number, Table (6.1)
<i>RMS</i>	reactive membrane separation

Abstract

A new feasibility analysis methodology generalized from reactive distillation is applied to membrane reactors. A model is formulated to depict the dynamic behavior of the reactive liquid phase composition on the retentate side of membrane reactors. The effects of both chemical reaction kinetics and membrane mass transfer kinetics on the feasible products are elucidated by means of retentate phase diagrams and singular point analysis. The proposed method is applicable to various kinds of membrane processes due to the fact that the flux through membranes can be formulated independently within the frame of the method.

Singular points represent stationary compositions of the system and thus are important for conceptual process design. To get deeper insights into the singular point analysis, a new set of composition variables is proposed to transform the original model equations into an analogous form to simple distillation. This results in the singular point conditions of membrane reactors, which define the curve where all singular points of different Damköhler numbers (Da) are located. The new terminology “*arrheotrope*” is introduced to convey the concept of stationary compositions of membrane separation, and correspondingly “*reactive arrheotropes*” stand for those of membrane reactors.

Two ternary reaction systems and two quaternary systems are studied to exemplify the methodology. It is shown in all examples that the selective mass transfer through membranes can change the topology and the singular points of the retentate phase diagrams. This implies certain desired products which are not attainable in an open distillation process can be feasible by means of suitable membranes. Furthermore, it is also demonstrated that the singular point analysis can be carried out with respect to the Damköhler number (Da) as well as to the properties of membranes (e.g. the membrane pore size), which can be very helpful for the selection of membrane materials.

In the last example, the esterification of acetic acid with *n*-propanol, the commercial porous polyester membrane is employed to exert mass transfer effects. The permeation through the considered membrane is quantified by the dusty gas model. The system exhibits a quaternary reactive azeotrope as an unstable node, and its location is shifted to the reactive arrheotrope by the applied membrane. Experiments are then carried out to validate the existence of the reactive azeotrope and reactive arrheotrope.

Zusammenfassung

Eine neue Methode der Machbarkeitsbewertung, die aus der Analyse von Reaktivdestillationskolonnen hergeleitet und verallgemeinert wurde, wurde auf Membranreaktoren angewendet. Es wurde ein Modell hergeleitet, das das dynamische Verhalten der Zusammensetzung der Flüssigphase auf der reaktiven Retentatseite von Membranreaktoren beschreibt. Der Einfluss von chemischer Reaktion und Stofftransportkinetik auf die erzielbaren Produkte wurden mit Hilfe von Retentat-Phasendiagrammen und der Analyse der singulären Punkte gezeigt. Die vorgeschlagene Methode ist auf verschiedene Arten von Membranprozessen anwendbar.

Singuläre Punkte stellen stationäre Zusammensetzungen des Systems dar und sind daher wichtig für den konzeptionellen Prozessentwurf. Ein neuer Satz an Zusammensetzungsvariablen wurde vorgeschlagen, um die ursprünglichen Modellgleichungen in eine der einfachen Destillation analoge Form zu bringen. Das Resultat hieraus ist ein Satz an Bedingungen für singuläre Punkte von Membranreaktoren, die die Kurve beschreiben, auf der alle singulären Punkte bei verschiedenen Damköhlerzahlen (Da) liegen. Der neue Begriff „Arheotrop“ wurde eingeführt, um das neue Konzept der stationären Punkte in der Membrantrennung zu beschreiben. Dementsprechend stellt ein „reaktives Arheotrop“ einen stationären Punkt in einem Membranreaktor dar.

Zwei ternäre und zwei quaternäre Reaktionssysteme wurden untersucht, um die Methode beispielhaft darzustellen. Es wurde in allen Beispielen gezeigt, dass der selektive Transport durch die Membran in der Lage ist, die Topologie und die Position der singulären Punkte im Phasendiagramm der Retentatphase zu verändern. Daraus ergibt sich, dass gewisse gewünschte Produkte bei Vorhandensein einer geeigneten Membran erreichbar sind, die durch einen offenen Destillationsprozess nicht erreichbar wären. Außerdem wurde gezeigt, dass die Analyse der singulären Punkte in Abhängigkeit der Damköhlerzahl und der Membraneigenschaften (z.B. der Porengröße der Membran) möglich ist, was sehr hilfreich bei der Membranauswahl ist. Im letzten Beispiel, der Veresterung von Essigsäure mit n-Propanol, wurde eine kommerziell verfügbare, poröse Polyestermembran verwendet, um einen Einfluss auf den Stofftransport auszuüben. Das System zeigt ein quaternäres, reaktives Azeotrop als instabilen Knoten, der durch Anwendung der Membran zum reaktiven Arheotrop verschoben wird. Dies wurde experimentell validiert.

1. Introduction

Separation of liquid mixtures has been a fundamental task of scientists and engineers over a hundred years. In former times, separation by boiling species of different volatilities was first applied as the ordinary manner. To overcome the separation barriers laid by the well-known “azeotropes”, manifold designs were then proposed to enhance the process efficiency¹. Among these elaborate possibilities, the focus is oriented towards two major principles in this work.

The first approach, conventionally termed as reactive distillation (RD), is to integrate the distillation process into a chemical reactor. The simultaneous occurrence of a chemical reaction can support the distillation process by “reacting away” the azeotropes [1]. Moreover, the benefit of such integration is not unilateral; the distillation process can also facilitate the reaction conversion by continuous removal of the byproduct. Besides, other potential advantages such as more efficient heat utilization, lower capital and operational cost etc., all made RD receive a lot of attention during the last decades. In consequence, RD has been amply studied and many theories around this topic have been developed and are now ready for use (e.g. [1-3]).

The other principle to raise the separation efficiency is to exert the selectivity brought forth by mass transfer effects. One representative of this approach is the membrane separation process wherein the separation effect is enhanced by the different permeation rates through the membrane, instead of urging repeated evaporation-condensation cycles. Thus, the operating temperature and the energy consumption can be expected to be much lower, and this is particularly advantageous for mixtures that are not compatible with high temperatures of distillation process.

The coupling of a membrane separation process and simultaneous chemical reaction provides an even more promising process alternative, which could have the joint advantages

¹ Such as extraction, adsorption, crystallization, membrane separation, and integrated reaction-separation processes.

of the two types of approaches mentioned above. Such a process can be termed as reactive membrane separation (RMS) according to an analogous terminology with RD, or more often called membrane reactor (MR). In this work, the abbreviation “MR” is used, to avoid any confusing alteration between MR and RMS. Despite its numerous potential advantages, there still exist a lot of unsolved issues in applying and analyzing MR. The first crucial hurdle is the property of the membranes. Generally speaking, the selectivity and permeability of real membrane materials are limited and usually contradictory to each other. Additionally, the stability and membrane fouling issues also make the membrane reactors less reliable than conventional reactors. To overcome these problems, in principle, new membrane materials have to be developed and synthesized.

The second problem that retards the development of MR is concerned with engineering aspects. The complexity of the process behavior of membrane reactors increases drastically due to the interaction of the chemical reaction with the membrane transport phenomena. Thus the majority of works on membrane reactors heretofore mainly performed experimental investigations (see e.g. [4-12]); some attempts have also been made to model membrane reactors [13-16]. However to the best of our knowledge, so far there is no systematic approach for the feasibility analysis of membrane reactors, i.e. to assess the influence of membrane mass transfer and the operating parameters on the attainable products for a given target reaction. In the literature, methodologies for the analysis, synthesis and control of membrane reactors have been rarely addressed. Therefore, this work aims to set up a new methodology of feasible product analysis for membrane reactors.

1.1 Literature review

Due to the reason that the theory proposed in this work is generalized from reactive distillation, this section will review the literature on RD that are related to this dissertation, mainly on residue curve maps and feasible product analysis. For the purpose of a broad review on other subjects of RD, two representative review articles are recommended [1-2]. Furthermore, some previous works investigating interfacial mass transfer effects in distillation process, which also stimulate the ideas of this work, will be mentioned subsequently.

For the conceptual design of RD processes, the residue curve maps (RCM) were introduced as a very important and powerful tool and were used by many researchers (e.g.

[17-21]). RCM represent the dynamic behavior of the liquid phase composition in a batch reactive distillation process as depicted in Fig.1.1. The analysis of the location and stability of the singular points in the RCM, i.e. the stationary compositions of this simple process, yields valuable information on the attainable products of a RD process. The existence of these stationary points was also proven experimentally [22-24].

For the stationary points in a distillation system undergoing equilibrium-controlled chemical reactions the term *reactive azeotrope* was introduced by Doherty and coworkers [25-27]. In RD systems with kinetically controlled chemical reactions, the singular points were called *kinetic azeotropes* by Rev [28] who investigated the general situation of the simultaneous occurrence of a chemical reaction and a separation process. Several groups studied the bifurcations of kinetic azeotropes in homogeneous systems [19, 29-30] and also in mixtures undergoing liquid phase splitting [31]. Most of these singularity analyses were carried out using the Damköhler number of first kind, Da , as most important bifurcation parameter. As important limiting cases, at $Da = 0$ the classical azeotropes of non-reactive distillation are recovered, and at $Da \rightarrow \infty$ the (chemical equilibrium controlled) reactive azeotropes are found.

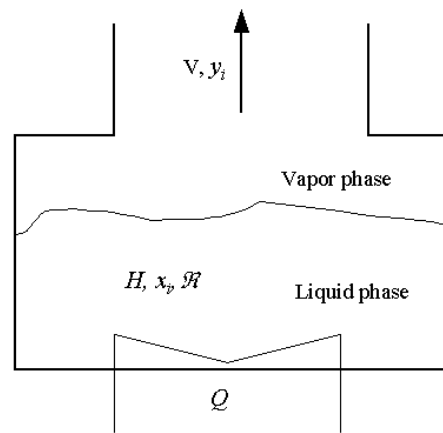


Figure 1.1 Batch reactive distillation.

In most research works mentioned above it was assumed that the liquid and vapor bulks were in phase equilibrium. In practical situations, however, the phase equilibrium can hardly be established unless sufficient contact time is allowed. Therefore numerous attempts have been made to consider the vapor-liquid interface mass transfer effect on the separation process (e.g. [2, 32-34]). For example, in non-reactive azeotropic distillation processes, Castillo and Towler [33] and Springer et al. [34] investigated the importance of vapor-liquid

interface mass transfer with respect to the feasible products. The latter authors announced that it is possible to cross distillation boundaries by interfacial mass transfer effects. Additionally, Schlünder et al. [35-37] demonstrated that separational limitations imposed by azeotropes can be overcome by application of an entraining medium. Due to different diffusion rates of the components in the entrainer, the azeotropic points are shifted. Since these points are formed under mass transfer control, the term “pseudo-azeotrope” was proposed. Analogously, Nguyen and Clement [38] observed and analyzed pseudo-azeotropic points which appear in the separation of water-ethanol mixtures at pervaporation membranes.

From the analysis of non-reactive systems it can be imagined that vapor-liquid interfacial mass transfer will also have some effect on the attainable products of reactive distillation processes [2, 39]. In particular, the stationary points of reactive distillation processes might be influenced more significantly by selective membranes, as has been shown by Aiouache and Goto [40] who integrated a pervaporation membrane into a reactive distillation process.

1.2 Research objective and outline

One can expect that the selective mass transfer induced by an intermediate phase (i.e. the membrane) can influence the feasible products of reactive separation process in a desired manner. The objective of this work is therefore to develop a methodology to predict this mass transfer effect on the products. The proposed method will be elucidated with some examples of ternary and quaternary systems, by means of *retentate phase diagrams* and *singular point analysis* (also called *bifurcation analysis*). Relevant experiments will then be performed to validate the proposed theory.

In Chapter 2, the theoretical part of this work will be addressed. The model equations will first be derived, accompanied with the discussion on the influence of heating policy, recapture of RD analysis from the proposed model, and the equivalence between the batch and continuous processes. Afterwards the membrane mass transport kinetics applied in this work will be introduced. The last part of this chapter covers the singular points analysis with the help of a set of transformed composition variables proposed in this work.

Chapter 3 provides two examples of ternary systems to illustrate the proposed theory. The first one is an ideal ternary mixture. Such a simple system has been often used in the literature of (reactive) distillation process, since its phase diagram can be easily visualized in

the 2-dimensional space, and the singular point condition can be further manipulated to give a simple criterion of whether a reaction system exhibits stationary compositions of ternary mixtures. The other example of technical relevance is the synthesis reaction of tetrahydrofuran (THF) from 1,4-butanediol (1,4-BD), in which it can be seen how a Knudsen membrane can influence the feasible products.

In addition to ternary systems, Chapter 4 delivers two more examples of quaternary systems wherein the composition space is a tetrahedron. In particular it is shown in this chapter that the singular point analysis can be carried out not only with respect to the Damköhler number Da , but also to parameters of membrane properties; this can be very helpful for the selection of suitable membrane materials. In the first ideal system, it is revealed that the derived singular point condition still gives a curve as the intersection of two surfaces in the 3-dimensional space. The second example is the esterification of acetic acid with *n*-propanol, coupled with mass transfer through porous membranes. The significance of this example is to demonstrate that the proposed theory can be applied to real mass transfer mechanisms which may contain variable mass transfer coefficients. It also predicts the occurrence of a *reactive arrheotrope*² in this system.

Chapter 5 and 6 convey the experimental aspects of this work. Chapter 5 is dedicated to the determination of reaction kinetics of the above mentioned esterification system, which is needed for the kinetically controlled reactive separation process. In Chapter 6 the residue curve map and retentate phase diagram are measured both for reactive distillation and for a membrane reactor at the chemical equilibrium condition. The experimental detection of the predicted reactive arrheotrope confirms the proposed theory. In the end the concluding remark and an outlook based on this work are given in Chapter 7.

² *Arrheotrope* comes from the Greek origin and represents in translation “a point at which the liquid composition is not changing with flux”.

2. Theoretical approach

In this chapter, a model is developed to describe the concentration profiles in the retentate liquid phase in which the chemical reaction takes place. The batch membrane reactor wherein vacuum is applied on the permeation side is schematically shown in Figure 2.1. Residue curve maps, or being more precise, "*retentate phase diagrams*" for a membrane process, and *singular point analysis* are applied to elucidate the influence of chemical reaction and mass transfer kinetics.

In section 2.1, the model equation for retentate phase diagram is derived. The necessary information such as reaction kinetics, vapor-liquid equilibrium will be also addressed. Since the autonomous heating policy [17] conventionally assumed in reactive distillation is convenient for theoretical analysis, but not practically achievable for a membrane process, some other heating policies are considered. The influence of different heat input strategies will be further discussed, aiming at releasing the autonomous heating policy assumption for the subsequent experimental validation. Additionally, the analogy between the model equations of a batch process and a continuous process at steady state conditions is clarified so that the information acquired from the batch process can be used for the design of a continuous process.

The validity of the model equations derived in section 2.1 holds regardless of the flux equation to be applied for a specific membrane which is under consideration. However, for feasibility analysis, adequate flux equations have to be formulated to close the set of governing equation. Thus in section 2.2, two types of flux expressions, which are applied in the following examples will be introduced.

Section 2.3 discusses about the classification of singular points in different processes. A new set of transformed composition variables is then proposed, which significantly transforms the model equation into a form being analogous to simple distillation, and thus leads to the condition of singular points for membrane reactors. Similar as in reactive distillation, the singular points of a membrane reactor at different Damköhler numbers are located on the curve defined by the singular point condition.

2.1 Model formulation of retentate phase diagrams

The process model is based on the following assumptions:

- The liquid phase and the retentate vapor bulk phase are assumed to be in phase equilibrium based on the fact that the membrane exerts the major mass transfer resistance.
- Vacuum is applied on the permeate side of the membrane ($p_p \rightarrow 0$).
- The chemical reaction takes place in the reactive holdup H_r of the liquid phase, i.e. either as a homogeneous reaction in the liquid bulk ($H_r = H$), or at a heterogeneous catalyst which is fully immersed in the liquid bulk ($H_r = H_{cat}$).
- In Figure 2.1, the model equations are formulated for a vapor permeation process, i.e. there is a buffer vapor phase between the membrane and the reactive liquid phase. Nevertheless, the derived can be also applied to a pervaporation process, i.e. the liquid phase is in direct contact with the membrane.
- Accumulation of components within the retentate vapor phase and within the membrane are neglected, i.e. process dynamics are considered to be dominated by the liquid phase.

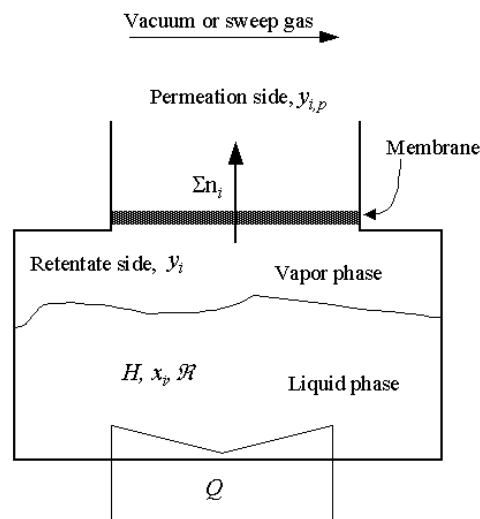


Figure 2.1 Batch membrane reactor.

2.1.1 Reaction kinetics and mass balance

The chemical reaction taking place in the liquid phase is represented by



where ν_i is the stoichiometric coefficient of component i . By convention, $\nu_i < 0$ if component i is a reactant, $\nu_i > 0$ if component i is a product. A_r and A_p are the reacting species, C_r is the number of reactants and C_p is the number of products. Thus, the total number of components is $NC = C_r + C_p$. The rate expression of this reaction is given by

$$r = k_f(T) \cdot \mathfrak{R}(a) \quad (2.2)$$

where k_f is the temperature-dependent rate constant of the forward reaction, and \mathfrak{R} is the dimensionless reaction rate depending on the liquid phase composition, expressed in terms of activities $a_i = x_i \cdot \gamma_i$.

The component and the total material balances in the liquid phase (*cf.* Figure 2.1) are formulated in molar units as following:

$$\frac{d(H \cdot x_i)}{dt} = -n_i \cdot A + \nu_i \cdot H_r \cdot k_f \cdot \mathfrak{R} \quad i = 1 \dots NC - 1 \quad (2.3)$$

$$\frac{dH}{dt} = -n_T \cdot A + \nu_T \cdot H_r \cdot k_f \cdot \mathfrak{R} \quad (2.4)$$

where H represents the total molar liquid holdup, H_r the reactive holdup in which the reaction proceeds, n_i the component molar flux, $n_T = \sum_{i=1}^{NC} n_i$ the total molar flux, A the effective permeation area, and $\nu_T = \sum_{i=1}^{NC} \nu_i$ the total mole change of the chemical reaction. Expanding

the time derivative in Eq.(2.3) and combining the result with Eq.(2.4) yields

$$\frac{dx_i}{d\xi} = \left(x_i - \frac{n_i}{n_T} \right) + \frac{H_r}{n_T \cdot A} \cdot (\nu_i - \nu_T x_i) \cdot k_f \cdot \mathfrak{R} \quad i = 1 \dots NC - 1 \quad (2.5)$$

where ξ stands for the dimensionless time with $d\xi = (n_T \cdot A / H) \cdot dt$. Now, the Damköhler number Da is introduced which is defined as the ratio of the characteristic reaction rate ($H_{r,0} \cdot k_{f,ref}$) and the characteristic vapor flow rate $n_{T,ref} \cdot A$:

$$Da \equiv \frac{H_{r,0} \cdot k_{f,ref}}{n_{T,ref} \cdot A} \quad (2.6)$$

where $H_{r,0}$ is the initial reactive holdup; $n_{T,ref}$ and $k_{f,ref}$ are the total molar flow rate and the forward reaction rate constant at a reference point within the composition space, usually chosen as the lightest component of the considered reaction system. Incorporating Eq.(2.6), the mass balances, Eq.(2.5), are rewritten as

$$\frac{dx_i}{d\xi} = \left(x_i - \frac{n_i}{n_T} \right) + Da \cdot (v_i - v_T x_i) \cdot \frac{H_r}{H_{r,0}} \cdot \frac{n_{T,ref}}{n_T} \cdot \frac{k_f}{k_{f,ref}} \cdot \mathfrak{R} \quad i = 1 \cdots NC - 1 \quad (2.7)$$

2.1.2 Heating policies

Eq.(2.7) cannot be solved without specifying the policy of heat input, which affects the relative importance of the separation term and the chemical reaction term. The most convenient strategy for theoretical analysis is the autonomous heating policy whereby Eq.(2.7) can be reduced to

$$\frac{dx_i}{d\xi} = \left(x_i - \frac{n_i}{n_T} \right) + Da \cdot (v_i - v_T x_i) \cdot \frac{k_f}{k_{f,ref}} \cdot \mathfrak{R} \quad i = 1 \cdots NC - 1 \quad (2.8)$$

This autonomous heating policy was first proposed by Venimadhavan and coworkers [17], and it has been widely used for the simulation of reactive distillation. This operating condition can be achieved if

- (i) $n_T / n_{T,ref} = H_r / H_{r,0}$, when the chemical reaction takes place as a homogeneous reaction in the whole liquid bulk phase, or
- (ii) $n_T = n_{T,0} = \text{const.}$, when the chemical reaction takes place in a solid catalyst phase whose molar holdup is constant during the process ($H_r = H_{r,0} = \text{const.}$).

At both strategies the reaction kinetic effect is characterized by a single parameter, i.e. the Damköhler number Da .

The autonomous heating policy applied above is rather useful for theoretical analysis since it results in a concise governing equation. However, it is hardly achievable in practice, especially when a membrane is incorporated in the process. Thus, to adapt the proposed formulation to practical membrane reactors, it is essential to replace the autonomous heating policy by a heating policy which can be realized in the laboratory. For instance, Eq.(2.9) represents the governing equation under isothermal conditions:

$$\frac{dx_i}{d\xi} = \left(x_i - \frac{n_i}{n_T} \right) + Da \cdot (v_i - v_T x_i) \cdot \frac{H_r}{H_{r,0}} \cdot \frac{n_{T,ref}}{n_T} \cdot \mathfrak{R} \quad i = 1 \cdots NC - 1 \quad (2.9)$$

(Isothermal operation)

Furthermore, for a non-volatile catalyst (i.e. solid catalyst) the reactive holdup term vanishes as in Eq.(2.10).

$$\frac{dx_i}{d\xi} = \left(x_i - \frac{n_i}{n_T} \right) + Da \cdot (v_i - v_T x_i) \cdot \frac{n_{T,ref}}{n_T} \cdot \frac{k_f}{k_{f,ref}} \cdot \mathfrak{R} \quad i = 1 \dots NC - 1 \quad (2.10)$$

(Heterogeneous catalyst)

For the experimental validation to be addressed later in Chapter 6, the experiment is carried out under the isothermal conditions, and the reaction is catalyzed heterogeneously so that the governing equations can be re-formulated as

$$\frac{dx_i}{d\xi} = \left(x_i - \frac{n_i}{n_T} \right) + Da \cdot (v_i - v_T x_i) \cdot \frac{n_{T,ref}}{n_T} \cdot \mathfrak{R} \quad i = 1 \dots NC - 1 \quad (2.11)$$

(Isothermal operation & heterogeneous catalyst)

For the examples in Chapters 3 and 4, the autonomous heating policy, Eq.(2.8), is used for the first three purely theoretical examples, while Eq.(2.11) is adopted for the last esterification example which was validated experimentally. (See Chapter 6)

2.1.3 Vapor-liquid equilibrium

Based on the assumption that the membrane holds the major mass transfer resistance, possible mass transfer resistances at the vapor-liquid interface are neglected. The composition of the retentate vapor phase below the membrane is quantified by the mole fractions y_i (See Figure 2.1).

For the autonomous operation, the liquid bulk is assumed to be in the boiling state such that it is in phase equilibrium with the retentate vapor phase at any time. Assuming ideal gas phase behavior at moderate pressures, y_i can be calculated from

$$y_i = \frac{x_i \cdot \gamma_i(x_j, T) \cdot p_i^{sat}(T)}{p} \quad i = 1 \dots NC \quad (2.12)$$

where p is the total system pressure, p_i^{sat} the saturated vapor pressure of component i , T the boiling temperature at the given pressure and liquid phase composition, γ_i the liquid phase activity coefficient. The boiling temperature T is determined from the vapor phase summation equation

$$\sum_{i=1}^{NC} y_i = 1 \quad (2.13)$$

For isothermal conditions, it is straightforward to calculate the vapor phase mole fractions. The partial pressure of each component at the operating temperature is given by

$$p_i = x_i \cdot \gamma_i(x_j, T) \cdot p_i^{sat}(T) \quad i = 1 \dots NC \quad (2.14)$$

and the mole fraction in the vapor phase is quantified by

$$y_i = \frac{p_i}{p} = \frac{p_i}{\sum p_i} \quad i = 1 \dots NC \quad (2.15)$$

2.1.4 Degeneration to reactive distillation

The advantage of adopting the expression n_i / n_T in the model equation is that the mass transfer kinetics of the separation process can be formulated subordinately. It can be reduced also to the specific case of open distillation when there is no selectivity induced by mass transfer. In such a case, the flux ratio (n_i / n_T) equals the vapor phase mole fraction y_i , which is often assumed to be in phase equilibrium with x_i , and the total molar flow rate is usually denoted as V , which is proportional to the total vapor pressure of the system. Thus, the model equations of RD in accordance with Eqs.(2.8) and (2.11) can be written as:

$$\frac{dx_i}{d\xi} = (x_i - y_i) + Da \cdot (v_i - v_T x_i) \cdot \mathfrak{R} \quad i = 1 \dots NC - 1 \quad (2.16a)$$

(Autonomous heating policy)

$$\frac{dx_i}{d\xi} = (x_i - y_i) + Da \cdot (v_i - v_T x_i) \cdot \frac{V_{ref}}{V} \cdot \mathfrak{R} \quad i = 1 \dots NC - 1 \quad (2.16b)$$

(Isothermal operation & heterogeneous catalyst)

2.1.5 Equivalent continuous process

For practical use, a continuous type membrane reactor is sometimes of higher interest. It is shown here that the governing equation of a continuous membrane reactor at steady state is analogous to the batch process considered above, except that the time coordinate is replaced by the axial coordinate. Therefore, the information obtained from a batch vessel can be very informative for continuous process design.

As in Figure 2.2, the reaction is assumed to take place in the liquid retentate phase only. The membrane is assumed to be gas-filled with the vapor-liquid interface being placed at the retentate side of the membrane surface. At steady state, the component and total material balance equations for any segment dz can be written as

$$L_i = L_i + dL_i + n_i a dz - A_c dz \varepsilon_{cat} \nu_i r \quad i = 1 \cdots NC - 1 \quad (2.17)$$

$$L = L + dL + n_T a dz - A_c dz \varepsilon_{cat} \nu_T r \quad (2.18)$$

where L_i stands for the component molar flow rate, L the total molar flow rate, n_i the molar flux through the membrane, $n_T = \sum_{i=1}^{NC} n_i$ the total molar flux, a the interfacial area per unit column length, A_c the cross sectional area, and ε_{cat} the catalyst loading density. ν_i is the stoichiometric coefficient, $\nu_T = \sum_{i=1}^{NC} \nu_i$ the total mole change of the chemical reaction. With the help of the dimensionless reaction rate defined in Eq.(2.2), Eq.(2.17) and (2.18) can be rewritten as

$$\frac{d(L \cdot x_i)}{dz} = -n_i a + A_c \varepsilon_{cat} \nu_i k_f \mathfrak{R} \quad i = 1 \cdots NC - 1 \quad (2.19)$$

$$\frac{dL}{dz} = -n_T a + A_c \varepsilon_{cat} \nu_T k_f \mathfrak{R} \quad (2.20)$$

rearranging the above equations and introducing the dimensionless Damköhler number Da yield:

$$\frac{dx_i}{dz^*} = \left(x_i - \frac{n_i}{n_T} \right) + Da (\nu_i - \nu_T x_i) \frac{n_{T,ref}}{n_T} \frac{k_f}{k_{f,ref}} \mathfrak{R} \quad i = 1 \cdots NC - 1 \quad (2.21)$$

(Heterogeneous catalyst)

where

$$dz^* = \frac{n_T a}{L} dz \quad (2.22)$$

stands for the dimensionless axial coordinate, $n_{T,ref}$ and $k_{f,ref}$ again represent the total mass flux and the forward reaction rate constant at a reference point within the composition space, respectively. The Damköhler number Da is defined as the ratio of the characteristic reaction rate and the characteristic permeation rate:

$$Da = \frac{A_c \varepsilon_{cat} k_{f,ref}}{n_{T,ref} a} \quad (2.23)$$

Eq.(2.21) describes the retentate concentration profile along the axial reactor coordinate at steady state. With the sufficiently long reactor length, the liquid phase will reach stationary compositions. This is equivalent to the temporal concentration profile of a corresponding batch process, except that the former process is expressed in terms of its axial coordinate, while the latter is expressed in terms of time. Depending on the Damköhler number, Eq.(2.21) describes non-reactive operation ($Da = 0$), chemical kinetics controlled operation ($0 < Da < \infty$), or chemical equilibrium controlled operation ($Da \rightarrow \infty$).

To transfer mass from the retentate phase through the membrane to the permeate side, energy has to be supplied to the process. As discussed in section 2.1.2, different heating policies will result in different variants of the model equations; here it is not intended to address the similar discussion for the continuous MR again.

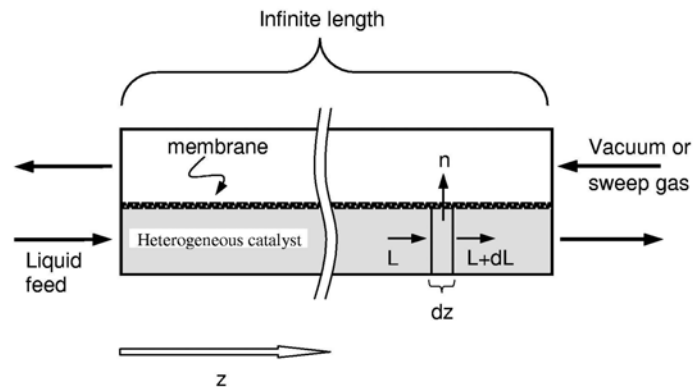


Figure 2.2 Equivalent continuous membrane reactor (MR).

2.2 Kinetics of mass transfer through membranes

In this work, two types of flux formulations will be applied. First, for the hypothetical systems, the permeation fluxes are expressed in terms of the partial pressure difference across the membrane. In the practical example of the esterification reaction, the fluxes through the porous membrane are described by the dusty gas model.

2.2.1 Explicit expression for pressure-driven membrane permeation

In a partial pressure-driven membrane diffusion process, the NC -dimensional vector of molar fluxes through the membrane (n_i) can be expressed as

$$(n_i) = \frac{1}{RT} \cdot [k] \cdot (y_i \cdot p - y_{i,p} \cdot p_p) \quad (2.24)$$

where $[k]$ is the $NC \times NC$ -dimensional matrix of effective binary mass transfer coefficients k_{ij} , (y_i) and p are the vector of mole fractions and the total system pressure on the retentate side of the membrane. ($y_{i,p}$) and p_p denote the vector of mole fractions and the total pressure on the membrane permeate side, respectively. It is convenient to formulate Eq.(2.24) in terms of dimensionless mass transfer coefficients κ_{ij} which are defined as the ratios of the effective mass transfer coefficients k_{ij} related to a reference coefficient. Here, the first main diagonal element k_{11} is taken as reference coefficient. This yields:

$$(n_i) = \frac{1}{RT} \cdot k_{11} [\kappa] \cdot (y_i \cdot p - y_{i,p} \cdot p_p) \quad \text{with} \quad \kappa_{ij} \equiv \frac{k_{ij}}{k_{11}} \quad (2.25a,b)$$

When vacuum is applied on the permeate side, the partial pressures of the diffusing components on the permeate side are negligible ($p_p \rightarrow 0$). Then, Eq.(25a) becomes

$$(n_i) = \frac{p}{RT} \cdot k_{11} [\kappa] \cdot (y_i) \quad (2.26)$$

In Eq.(2.26), the membrane properties are reflected by the $[\kappa]$ -matrix. Different membrane material structures (e.g. pore size), lead to different elements in the $[\kappa]$ -matrices. In general, all elements of the mass transfer matrix can depend on the process variables, in particular on the adjacent vapor phase composition (y_i). The mass transfer mechanisms through membranes can be rather complicated and diverse, and usually predicated by applicable models or acquired by membrane characterization. However, for the conceptual analysis of the considered membrane process, it is not helpful to go into the mechanistic

details of membrane mass transport immediately. Therefore, in the following the membrane diffusion mechanisms can be categorized by the mathematical structure of the $[k]$ -matrix wherein the effective binary mass transfer coefficients k_{ij} are assumed to be constants:

- (i) scalar $[k]$ -matrix if the membrane is non-selective, i.e. it has no separation effect on the components. In this case the membrane process coincides with the distillation process (Figure 1.1) and the $[\kappa]$ -matrix in Eq.(2.26) is equal to the identity matrix.
- (ii) diagonal $[k]$ -matrix if the permeating components are only driven by their own partial pressure differences. This case is valid e.g. for a Knudsen membrane.
- (iii) non-diagonal $[k]$ -matrix if the permeating components interact with each other within the membrane. This will be the case if e.g. bulk diffusion and/or competitive adsorption effects are involved.

Despite the fact that the matrix elements can be positive or negative, the $[k]$ -matrix has to be positive definite because of the constraints imposed by the second law of thermodynamics [41]. Furthermore, for the case of a non-diagonal $[k]$ -matrix, the off-diagonal elements in the i^{th} row should vanish when the concentration of component i is zero, to ensure the flux and mole fraction remaining in the physically meaningful domain.

2.2.2 Diffusion through porous membranes – Dusty gas model

The dusty gas model (DGM) is a well-established tool to quantify the flux of components through porous membranes [42-43]. This model is based on the Maxwell-Stefan equations, in which the porous medium is considered as the $(NC+1)^{th}$ component with infinite molar mass and zero flux. The flux equation for species i in a NC -component mixture can be derived as

$$-\frac{1}{RT} \nabla p_i - \frac{1}{RT} \frac{B_0 p_i}{\mu D_{K,i}^e} \nabla p = \sum_{j=1}^{NC} \frac{y_j n_i - y_i n_j}{D_{ij}^e} + \frac{n_i}{D_{K,i}^e} \quad \text{with} \quad i = 1 \cdots NC \quad (2.27)$$

Eq.(2.27) accounts for three transport mechanisms, namely bulk diffusion, Knudsen diffusion and viscous flow. B_0 is the permeability constant of the porous membrane

$$B_0 = (\varepsilon/\tau) \frac{d_p^2}{32} \quad (2.28)$$

and $D_{K,i}^e$ stands for the effective Knudsen diffusivity

$$D_{K,i}^e = \left(\frac{\varepsilon}{\tau}\right) \frac{d_p}{3} \sqrt{\frac{8RT}{\pi M_i}} \quad (2.29)$$

where d_p is the pore diameter, M_i the molar mass, ε and τ are the porosity and the tortuosity of the membrane, respectively. D_{ij}^e , the effective binary diffusivity in the porous medium, is related to the corresponding free space value by

$$D_{ij}^e = (\varepsilon/\tau) D_{ij} \quad (2.30)$$

where D_{ij} is calculated by Fuller's method (see e.g. [44]); μ is the viscosity of the mixture, which is calculated by the methods of Reichenberg (viscosity of pure substances) and Wilke [44].

The membrane pores are assumed to be fully filled with vapor, i.e. the pressure on the retentate side of the membrane is calculated as the saturated vapor pressure of the liquid mixture, while the permeate side pressure is negligible if vacuum is applied. The pressure within the membrane is taken as the average value of the pressures on both sides.

Eq.(2.27) can be cast into an explicit NC-dimensional matrix form (see Appendix A.2) as:

$$(n_i) = -\frac{1}{RT} [k] (\Delta p_i + \frac{y_i \cdot p \cdot B_0}{\mu \cdot D_{K,i}^e} \Delta p) \quad (2.31)$$

where

$$[k] = [B^e]^{-1} / \delta \quad (2.32a)$$

with δ as the membrane thickness. The elements of the $[B^e]$ -matrix are given by

$$B_{ii}^e = \frac{1}{D_{K,i}^e} + \sum_{\substack{j=1 \\ j \neq i}}^{NC} \frac{y_j}{D_{ij}^e} \quad (2.32b)$$

$$B_{ij}^e = -\frac{y_i}{D_{ij}^e} \quad (2.32c)$$

Based on Eqs.(2.31) and (2.32a-c) it can be seen that the dusty gas model is equivalent to a non-diagonal $[\kappa]$ -matrix (in Eq.2.26) whose elements are functions of the state variables, i.e. the vapor phase composition y_i . Furthermore, it should be noticed that the right hand side of Eq.(2.31) contains two driving force terms, since diffusion described by the DGM is driven by the partial pressure difference (Knudsen and molecular diffusion), as well as the

total pressure difference (viscous flow), while in section 2.2.1 it was assumed that the permeation is driven by the partial pressure difference only.

2.3 Singular point analysis and transformed composition variables

2.3.1 Singular points

The singular points of model equations derived in Section 2.1 are of special interest for the conceptual design, because those points represent the stationary compositions of the process and structure the topology of the retentate phase diagrams. Singular points can be classified as stable nodes, unstable nodes and saddle points according to their stability. Stable nodes in particular stand for the feasible products of the considered reactive separation process.

The locations of the singular points in the composition space depend on the type of the separation process applied (distillation/membrane separation) and on the presence of chemical reactions (non-reactive/reactive operation). Four cases can be distinguished (*cf.* Table 2.1):

(i) Non-reactive distillation

For non-reactive membrane separation, i.e. $Da = 0$, and for the special case that $[k]$ is a scalar matrix, i.e. no separation effect by the membrane, the stationary points correspond to those obtained for phase equilibrium controlled distillation. The condition is:

$$x_i = y_i \quad \text{with} \quad i = 1 \cdots NC - 1 \quad (2.33)$$

Eqs.(2.33) are fulfilled by pure components and by non-reactive azeotropic mixtures.

(ii) Non-reactive membrane separation

If the mass transfer effects brought forth by the membranes are involved, $[k]$ is a non-scalar matrix and the following singularity condition results from Eq.(2.8) or (2.21):

$$x_i = \frac{n_i}{n_T} \quad \text{with} \quad i = 1 \cdots NC - 1 \quad (2.34)$$

Eqs.(2.34) are valid for mass transfer controlled non-reactive separation and corresponds to the azeotropic condition for equilibrium controlled non-reactive distillation,

Eqs.(2.33). In the literature, these singular points were termed as *pseudo-azeotropes* [35, 38] because they behave as if they were azeotropes. Since the meaning of the prefix “pseudo-” is quite non-specific, a new terminology is proposed here to precisely convey the concept of stationary compositions of membrane separation [45].

Considering the Greek origin of the word “*azeotrope*”, it is composed of three fragments [46-47]: “*a*” means “not”, “*zeo*” means “boiling” and “*trope*” means “changing”. The complete meaning of “*azeotrope*” is therefore “the liquid composition is not changing with boiling”. Following the same nomenclature logic, we propose the term “*arrheotrope*” representing the stationary points in mass transfer controlled processes³, where “*rheo*” means “flux”. The full meaning of “*arrheotrope*” can be stated as “the liquid composition is not changing with flux”.

(iii) Reactive distillation

Formally, a conventional reactive distillation process can be interpreted as a special case of a membrane reactor with a scalar $[k]$ -matrix, i.e. no separation effect is exerted by the membrane, Eqs.(2.8) yields the following singularity condition:

$$0 = (x_i - y_i) + Da \cdot (v_i - v_T x_i) \cdot \frac{k_f}{k_{f,ref}} \cdot \mathfrak{R} \quad \text{with} \quad i = 1 \cdots NC - 1 \quad (2.35)$$

The stationary points defined by Eqs.(2.35) are termed as “*kinetic azeotropes*” for kinetically-controlled reactive distillation [28, 48] and as “*reactive azeotropes*” for chemical equilibrium-controlled reactive distillation [25-26]. It is important to note that the term *kinetic* refers to the chemical reaction kinetics rather than to the mass transfer kinetics.

(iv) Membrane reactor / reactive membrane separation

The most general case is a membrane reactor whose $[k]$ -matrix is a non-scalar matrix, i.e. a diagonal or a non-diagonal matrix. From Eq.(2.8) the following conditions for stationary points are obtained:

$$0 = \left(x_i - \frac{n_i}{n_T} \right) + Da \cdot (v_i - v_T x_i) \cdot \frac{k_f}{k_{f,ref}} \cdot \mathfrak{R} \quad \text{with} \quad i = 1 \cdots NC - 1 \quad (2.36)$$

³ Here, “arrheotrope” (double “r”) is adopted instead of “arheotrope” (single “r”) because of Greek grammar. The author would like to thank Prof. Dr.-Ing. E. Tsotsas for his linguistic advice.

According to the terminology proposed above, the stationary points can be denoted as *kinetic arrheotropes* ($0 < Da < \infty$) or as *reactive arrheotropes* ($Da \rightarrow \infty$). In the latter case, the reaction approaches the chemical equilibrium. The mixture composition of kinetic arrheotropes is determined by both the chemical reaction kinetics and the mass transfer kinetics through the membrane.

Table 2.1 Classification of singular points in (non-)reactive distillation and membrane separation processes

Separation \ Reaction	Phase equilibrium controlled separation: Distillation $[\kappa] = \begin{bmatrix} 1 & 0 & 0 \\ 0 & 1 & 0 \\ 0 & 0 & 1 \end{bmatrix}$	Mass transfer controlled separation: Membrane Permeation $[\kappa] = \begin{bmatrix} 1 & \kappa_{AB} & \kappa_{AC} \\ \kappa_{BA} & \kappa_{BB} & \kappa_{BC} \\ \kappa_{CA} & \kappa_{CB} & \kappa_{CC} \end{bmatrix}$
No reaction: $Da = 0$	<i>Azeotrope</i> , $x_i = y_i$ First introduced by Wade and Merriman [46]	<i>Arrheotrope</i> , $x_i = n_i/n_T$ First introduced as “Pseudo-azeotrope” by Schlünder [35]
Kinetically controlled reaction: $Da \in (0, \infty)$	<i>Kinetic Azeotrope</i> , $X_i^{BD} = Y_i^{BD} *$ First studied by [17, 28]	<i>Kinetic Arrheotrope</i> , $X_i = Y_i$ This work, Eq.(2.37)
Chemical equilibrium controlled reaction: $Da \rightarrow \infty$	<i>Reactive Azeotrope</i> , $X_i^{BD} = Y_i^{BD} *$ First introduced by Barbosa and Doherty [25-26]	<i>Reactive Arrheotrope</i> , $X_i = Y_i$ This work, Eq.(2.37)

* The superscript “BD” denotes the abbreviation of initiators’ names.

2.3.2 Transformed composition variables

As has been demonstrated for the singular point analysis of reactive distillation systems [25-26, 48], it is useful to separate the influences of the chemical reaction kinetics and of the vapor-liquid equilibrium. The same is true for the analysis of membrane reactors. By elimination of the reaction term from the (NC-1) singularity conditions, Eq.(2.36), it is possible to fix the potential singular point curve (PSPC) on which all possible singular points

will be located. The PSPC is defined by a set of equations which can be formulated analogously to the azeotropic conditions for non-reactive distillation, Eq.(2.33), by introducing transformed composition variables [45] for the liquid phase, X_i , and for the vapor phase, Y_i (see derivation in Appendix A.1). By means of these transformed variables, the singularity conditions of the here discussed separation processes can be expressed in a compact manner:

$$X_i = Y_i \quad \text{with} \quad i = 1 \cdots NC - 2 \quad (2.37a)$$

where

$$X_i = \frac{(v_k x_i - v_i x_k)}{(v_k - v_T x_k)}, \quad Y_i = \frac{(v_k n_i - v_i n_k)}{(v_k n_T - v_T n_k)} \quad (2.37b,c)$$

With the flux equation given as Eq.(2.26), the transformed vapor composition variable, Y_i , can be successively expanded for the different possible structures of the mass transfer matrix:

$$\begin{aligned} Y_i &= \frac{\left(v_k \sum_{j=1}^{NC} \kappa_{ij} y_j - v_i \sum_{j=1}^{NC} \kappa_{kj} y_j \right)}{\left(v_k \sum_{i=1}^{NC} \sum_{j=1}^{NC} \kappa_{ij} y_j - v_T \sum_{j=1}^{NC} \kappa_{kj} y_j \right)} && \text{for a non - diagonal } [\kappa] \text{- matrix} \\ &= \frac{(v_k \kappa_{ii} y_i - v_i \kappa_{kk} y_k)}{\left(v_k \sum_{i=1}^{NC} (\kappa_{ii} y_i) - v_T \kappa_{kk} y_k \right)} && \text{for a diagonal } [\kappa] \text{- matrix} \\ &= \frac{(v_k y_i - v_i y_k)}{(v_k - v_T y_k)} && \text{for a scalar } [\kappa] \text{- matrix} \end{aligned} \quad (2.38a,b,c)$$

The definition in Eq.(38c) is identical to the Y_i -definition which was proposed first by Barbosa and Doherty [25-26] for reactive distillation processes.

2.4 Chapter conclusions

In this chapter, the theoretical part of this work has been addressed. First the model equations of the retentate phase diagram are derived. Different heat input policies are then considered, aiming at releasing the autonomous heating policy assumption. In particular, the isothermal operating condition is employed in order to realize the experimental validation which will be presented in Chapter 6.

The flux-based formulation in this work can degenerate into the specific case of reactive distillation wherein there is no extra separation selectivity in addition to the thermodynamic phase equilibrium. It is also shown that the model equations of a batch process and a continuous process at steady state are structurally analogous except that the former is of the time coordinate while the latter is of the axial coordinate. Therefore, the information acquired from the simple batch process can be used for the design of continuous processes.

In section 2.2 two types of flux formulations used in the subsequent examples are introduced. In the first partial pressure driven permeation process, the properties of membranes are embedded in the mass transfer coefficients $[k]$ -matrix whose elements are assumed constant for comprehensive discussion. The second flux formulation is the conventional dusty gas model (DGM). It can be cast into an explicit matrix form, and the corresponding $[k]$ -matrix is a non-diagonal matrix with elements as a function of the state variable y_i . It should be noted that the driving force for mass transfer in DGM consists of both the partial pressure difference (Knudsen and molecular diffusion) and total pressure difference (viscous flow) across the membrane. The ratio of the non-selective viscous flow increases with the total system pressure.

The occurrence of singular points in membrane separation is a kinetic phenomenon, instead of a pure thermodynamic phenomenon. Therefore, the singular points of a membrane reactor are denoted as “reactive arrheotrope”. The condition of arrheotropy can be formulated in terms of a set of transformed composition variables proposed in this work. This condition yields the potential singular point curve (PSPC) whose shape depends on the reaction stoichiometry, the vapor-liquid equilibrium, and on the mass transfer properties of the membrane applied.

3. Examples of ternary systems

In this chapter, two examples of ternary systems are investigated by means of retentate phase diagrams and singular point analysis to illustrate the theory proposed in Chapter 2 [45]. The first example is an ideal ternary system with constant relative volatilities. It is particularly illustrative since it allows the successive manipulation of reactive arrheotrope conditions to give a simple criterion for the shape of the singular point curve. In the second example, the synthesis reaction of tetrahydrofurane (THF) by dehydration of 1,4-butanediol (1,4-BD), the influence of a Knudsen membrane is studied. The emphasis is laid on the agreement between the shapes of the PSPC in this strongly non-ideal system and the criterion inferred from the preceding ideal one.

3.1 Ideal ternary system

As the first example, the effect of a selective membrane on the ternary mixture A/B/C undergoing a single reversible chemical reaction in an ideal liquid phase is considered:



The dimensionless rate of the chemical reaction is assumed to obey the kinetic law

$$\mathfrak{R} = x_A - \frac{x_B x_C}{K} \quad (3.2)$$

with K as chemical equilibrium constant. For the sake of a simplified analysis, the following assumptions are made:

- The chemical equilibrium constant is independent of temperature: $K = 0.2$.
- The rate constant k_f is independent of temperature: $k_f / k_{f,ref} = 1$.
- The relative volatilities of the product B and the byproduct C with respect to the reactant A, α_{BA} and α_{CA} , are assumed to be constants. Then, the vapor phase equilibrium composition can be calculated as

$$y_i = \frac{\alpha_{iA} x_i}{\sum_{m=A}^C \alpha_{mA} x_m} \quad (3.3)$$

- Three $[\kappa]$ -matrix structures are considered here: identity matrix, diagonal matrix and non-diagonal matrix.

3.1.1 Residue curve maps and retentate phase diagrams

The effect of a membrane is studied with the help of retentate phase diagrams, i.e. phase portraits of the liquid phase composition. They are determined both for a reactive distillation process and for the corresponding membrane reactor so that the effect of incorporating membranes can be explicitly exhibited by the direct comparison. The selected volatility values are $\alpha_{BA} = 5.0$ and $\alpha_{CA} = 3.0$, viz. the reactant A is the high boiler, the main product B is the low boiler and the byproduct C is the intermediate boiler.

Figure 3.1 shows residue curve maps for the classical reactive distillation process at three different Damköhler numbers. In the non-reactive case, i.e. $Da = 0$ (Figure 3.1a), the map topology is structured by one unstable node (pure B), one saddle point (pure C) and one stable node (pure A). The arrows along the residue curves indicate increasing time. Since pure A is the only stable node of non-reactive distillation, this is the feasible bottom product to be expected in a continuous distillation process.

At kinetically controlled chemical reaction ($Da = 1$, Figure 3.1b), the stable node moves from the pure A vertex into the composition triangle, i.e. the feasible product is a ternary mixture instead of pure A. According to the classification in Table 2.1, this stable node is a kinetic azeotrope. At equilibrium controlled chemical reaction ($Da \rightarrow \infty$, Figure 3.1c), the reaction approaches its chemical equilibrium, and therefore the stable node is exactly located on the equilibrium curve. In this case, the residue curves are first dominated by the reaction stoichiometry and then move along the equilibrium curve towards the stable node which is a reactive azeotrope.

In the analogous manner, retentate phase diagrams of membrane reactors are determined with the proposed theory. First, a diagonal $[\kappa]$ -matrix is considered with $\kappa_{CC} > 1$ and $\kappa_{BB} = 1$, i.e. the undesired by-product C permeates preferentially through the membrane ($\kappa_{CC} > 1$), while A and B are assumed to have the same mass transfer coefficients. The retentate phase diagrams are depicted for two different κ_{CC} -values (Figure 3.2a-c: $\kappa_{CC} = 5$;

Figure 3.2d-f: $\kappa_{CC} = 10$) at three different Damköhler numbers. Figures 3.2a and 3.2d reveal the effects of membranes at the non-reactive condition. The trajectories move from pure C to pure A, while in non-reactive distillation (Figure 3.1a) they move from pure B to pure A. Thus, by application of a C-selective membrane, the C vertex becomes an unstable node, while the B vertex becomes a saddle point. This can be understood as that the membrane changes the effective volatilities (i.e. the products $\kappa_{ii} \cdot \alpha_{iA}$) of the reaction system such that $\kappa_{CC} \cdot \alpha_{CA} > \kappa_{BB} \cdot \alpha_{BA}$.

At kinetically controlled reactive conditions ($Da = 1$), Figures 3.2b and 3.2e show that the stable node (kinetic arrheotrope) moves into the composition triangle as in reactive distillation (Figure 3.1b). But, this node moves towards the B vertex with increasing C-selectivity of the membrane. At infinite Damköhler number the system is chemical equilibrium controlled (Figures 3.2c,f), and therefore the stable node (reactive arrheotrope) is located exactly on the chemical equilibrium curve. The different stable node locations in Figure 3.2c ($\kappa_{CC} = 5$) and in Figure 3.2f ($\kappa_{CC} = 10$) reveal that pure B is a feasible product if the membrane selectivity with respect to C exceeds a certain critical value.

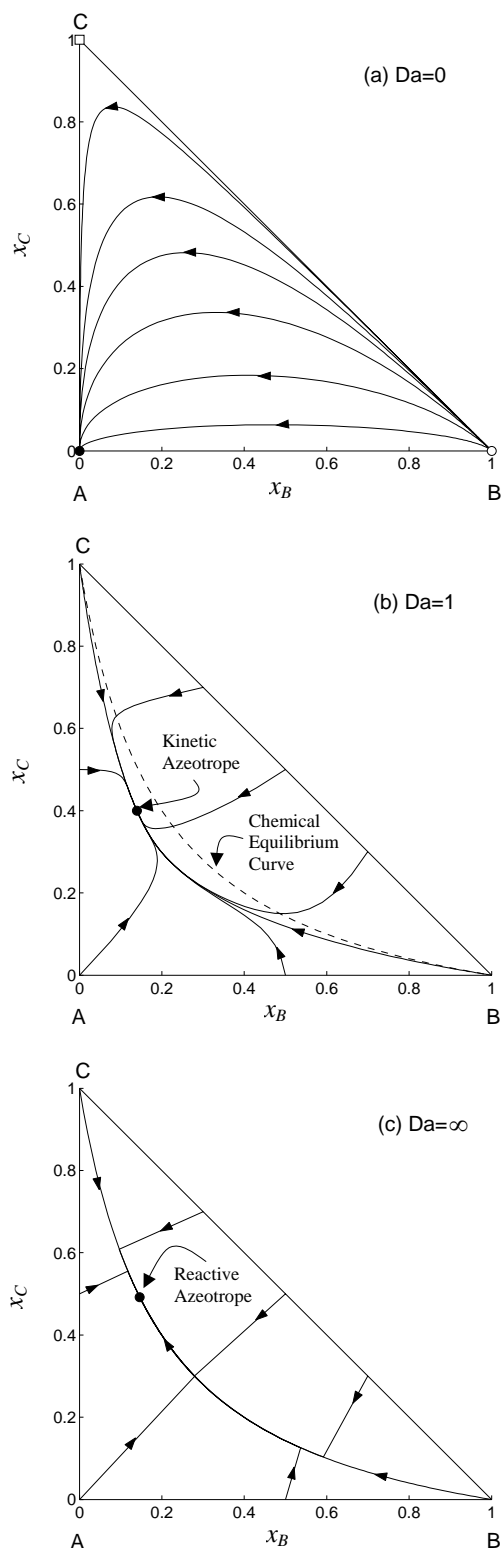


Figure 3.1 Residue curve maps for reactive distillation; $A \rightleftharpoons B + C$; $K = 0.2$; constant relative volatilities: $\alpha_{BA} = 5.0$; $\alpha_{CA} = 3.0$. (a) no chemical reaction (i.e. non-reactive distillation), (b) kinetically controlled chemical reaction, (c) equilibrium controlled chemical reaction. Legend: \square Unstable Node, \square Saddle Point, \bullet Stable Node

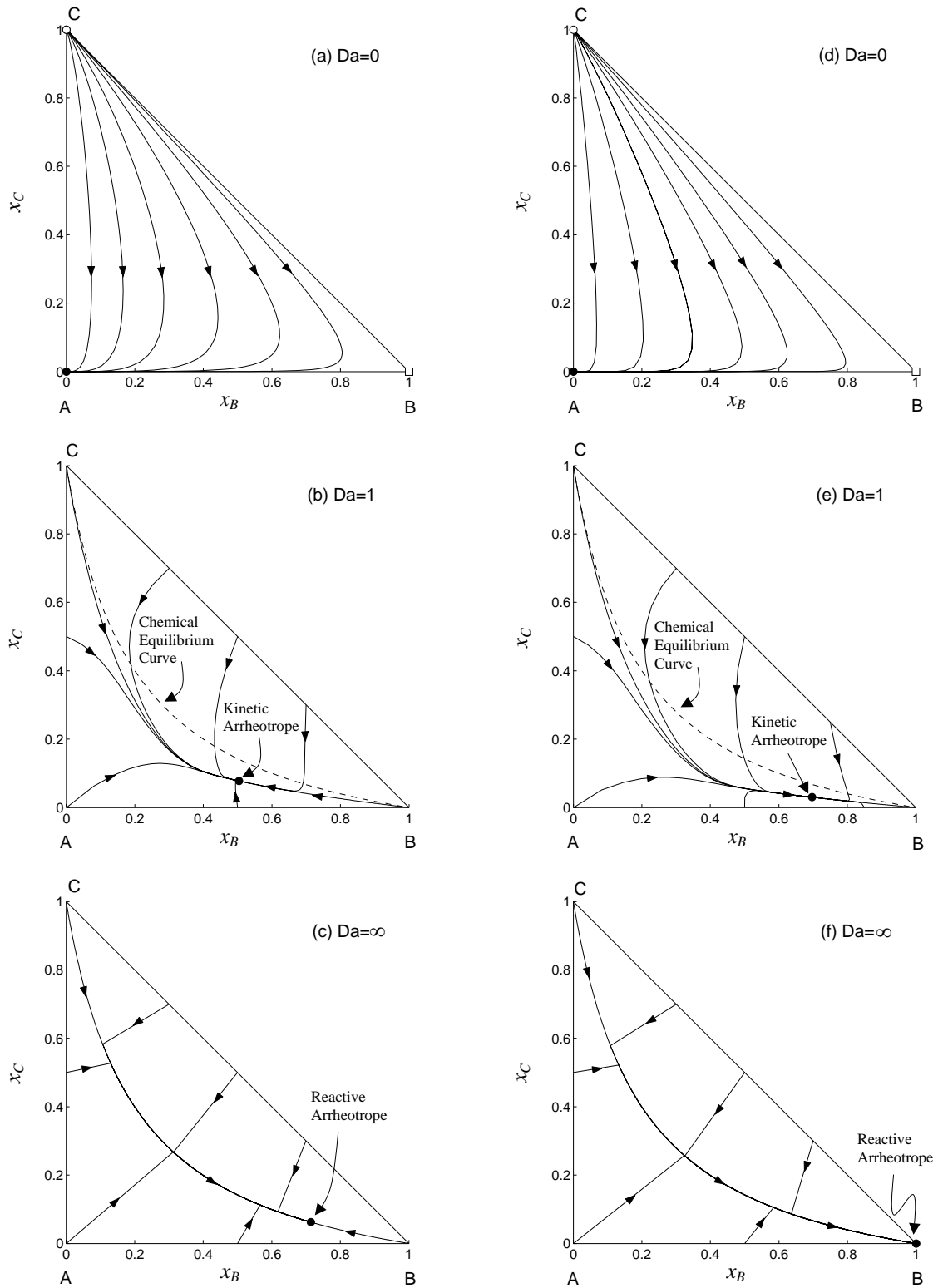


Figure 3.2 Retentate phase diagrams for membrane reactors; $A \rightleftharpoons B + C$, $K = 0.2$; constant relative volatilities: $\alpha_{BA} = 5.0$, $\alpha_{CA} = 3.0$; membrane: diagonal $[\kappa]$ -matrix. Legend: o Unstable Node, □ Saddle Point, • Stable Node.

$$(3.2 \text{ a,b,c}): [\kappa] = \begin{bmatrix} 1 & 0 & 0 \\ 0 & 1 & 0 \\ 0 & 0 & 5 \end{bmatrix}$$

$$(3.2 \text{ d,e,f}): [\kappa] = \begin{bmatrix} 1 & 0 & 0 \\ 0 & 1 & 0 \\ 0 & 0 & 10 \end{bmatrix}$$

3.1.2 Singular point analysis

For practical applications, the mixture compositions at the singular points are of major interest. As discussed in Section 2.3.2, all potential singular points of a certain system are located on a unique curve (PSPC) whose location is defined by Eq.(2.37). In the considered case, the PSPC is given by

$$X_B = Y_B \quad (3.4)$$

where the reactant A is chosen as the reference component because $\nu_T > 0$ (see Appendix A.1). For conventional reactive distillation, Eq.(2.38c) defines the transformed vapor phase composition Y_B and this yields in combination with Eq.(3.4):

$$\frac{(-x_B - x_A)}{(-1 - x_A)} = \frac{(-y_B - y_A)}{(-1 - y_A)} \quad (\text{Reactive distillation}) \quad (3.5)$$

At the given set of relative volatilities ($\alpha_{BA} = 5.0$, $\alpha_{CA} = 3.0$), the PSPC defined by Eq.(3.5) is a hyperbola (see Figure 3.3). For the sake of completeness, the PSPC is also shown outside the physically relevant composition space. The left part of the hyperbola intersects the chemical equilibrium curve at the reactive azeotrope. Between this point ($Da \rightarrow \infty$) and the origin of the triangle ($Da = 0$), the branch of stable nodes is located (solid line). Each point along this branch corresponds to a certain value of the Damköhler number.

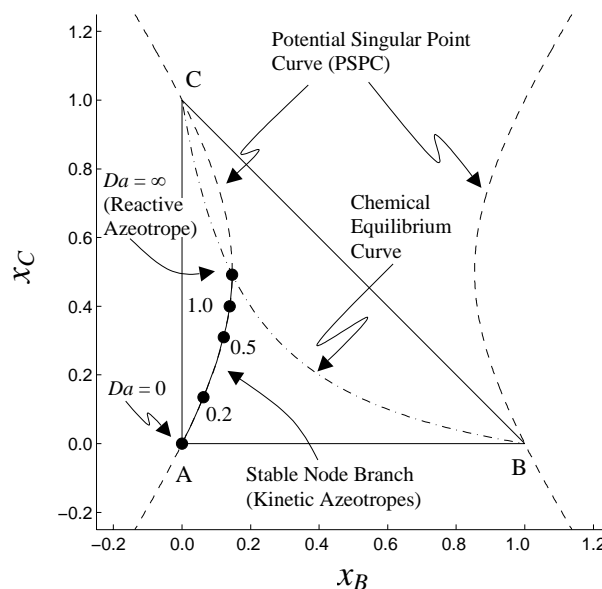


Figure 3.3 Potential singular point curve and stable node bifurcation behavior for reactive distillation; $A \rightleftharpoons B + C$; $K = 0.2$; constant relative volatilities: $\alpha_{BA} = 5.0$, $\alpha_{CA} = 3.0$. Legend:
 • Branch of Stable Nodes.

As mentioned, the reactive distillation process can be regarded as a special case of membrane reactors wherein the membrane itself does not induce any selectivity, namely a membrane process with a scalar $[k]$ -matrix. However, now the question arises how the PSPC and the branch of stable singular points are influenced by a membrane having a diagonal mass transfer matrix. In Figure 3.4 the PSPC of the reactive distillation process is depicted along with those of membrane reactors for three different κ_{CC} -values. Only the physically relevant composition space is considered in this diagram. The solid lines represent the different branches of stable nodes. Obviously, there exists a critical value, $\kappa_{CC,crit} = 5/3$, above which the PSPC is turned from the C vertex towards the B vertex. At the intersections of the PCPCs with the chemical equilibrium curve ($Da \rightarrow \infty$), reactive arrheotropes are located. They are moved towards the B vertex with increasing C-selectivity of the membrane, i.e. increasing κ_{CC} -value. Above a certain value the reactive arrheotrope coincides with the pure B vertex and at this point the PSPC is tangential to the chemical equilibrium curve.

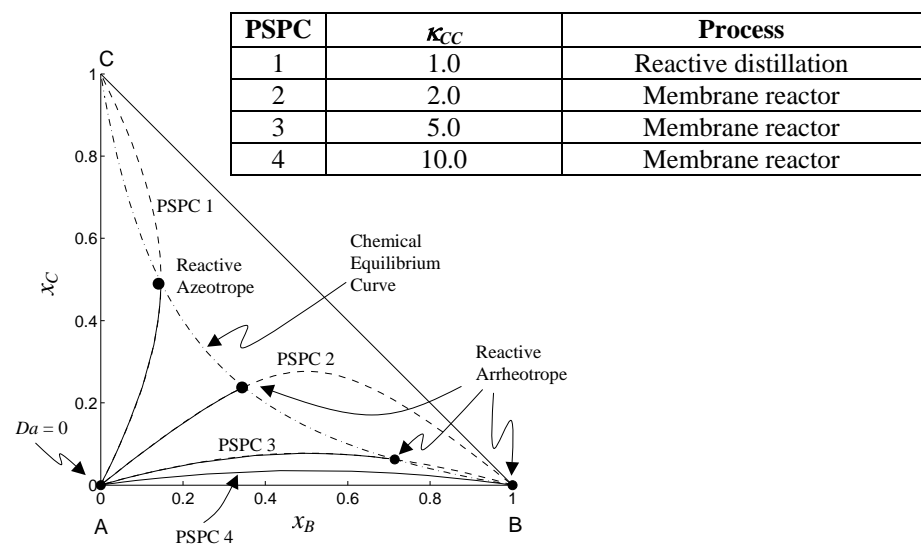


Figure 3.4 Potential singular point curves (PSPCs) and stable node bifurcation behavior of membrane reactors at different mass transfer conditions; $A \Leftrightarrow B + C$, $K = 0.2$; constant relative volatilities: $\alpha_{BA} = 5.0$, $\alpha_{CA} = 3.0$; membrane with diagonal $[k]$ -matrix \Rightarrow

$$[k] = \begin{bmatrix} 1 & 0 & 0 \\ 0 & 1 & 0 \\ 0 & 0 & \kappa_{CC} \end{bmatrix}$$

Legend: ●—● Branch of Stable Nodes (Damköhler numbers: $Da \in (0, \infty)$)

3.1.3 Generalization

For a more generalized analysis of the qualitative influence of membranes on the singular points, now the membrane mass transfer is considered with a non-diagonal $[\kappa]$ -matrix. Then, Eqs.(2.37) in combination with Eqs.(2.38a) yield the condition for *kinetic arheotropy*:

$$X_B = Y_B \Rightarrow \frac{(-x_B - x_A)}{(-1 - x_A)} = \frac{(-n_B - n_A)}{(-n_T - n_A)} \quad (\text{Membrane reactor}) \quad (3.6)$$

By expanding Eq.(3.6) and collecting terms, it can be shown that the above equation can be cast into the following quadratic form:

$$(x)^T \cdot [A] \cdot (x) + (b)^T \cdot (x) + c = 0 \quad (3.7)$$

with $(x)^T = (x_B, x_C)$ and the following matrix-vector definitions (note that $\alpha_{AA} = 1$):

$$[A] = \begin{bmatrix} a_1 & a_2/2 \\ a_2/2 & a_3 \end{bmatrix} \quad (b)^T = (a_4, a_5) \quad c = a_6 \quad (3.8a,b,c)$$

$$a_1 = -1 - \kappa_{BA} + \kappa_{AB}\alpha_{BA} + \kappa_{BB}\alpha_{BA} \quad (3.9a)$$

$$a_2 = -\kappa_{BA} + \kappa_{CA} - \kappa_{AB}\alpha_{BA} - \kappa_{CB}\alpha_{BA} + \kappa_{AC}\alpha_{CA} + \kappa_{BC}\alpha_{CA} \quad (3.9b)$$

$$a_3 = 1 + \kappa_{CA} - \kappa_{AC}\alpha_{CA} - \kappa_{CC}\alpha_{CA} \quad (3.9c)$$

$$a_4 = 1 + 2 \cdot \kappa_{BA} - \kappa_{CA} - \kappa_{BB}\alpha_{BA} + \kappa_{CB}\alpha_{BA} \quad (3.9d)$$

$$a_5 = -1 + \kappa_{BA} - 2 \cdot \kappa_{CA} - \kappa_{BC}\alpha_{CA} + \kappa_{CC}\alpha_{CA} \quad (3.9e)$$

$$a_6 = -\kappa_{BA} + \kappa_{CA} \quad (3.9f)$$

In the composition triangle, Eq.(3.7) describes a second-order curve whose shape is fixed by the signs of the eigenvalues λ_1 and λ_2 of the symmetric matrix $[A]$. The following cases can be distinguished:

$$\begin{aligned} \lambda_1 \cdot \lambda_2 < 0 & \Rightarrow \text{hyperbolic system} \\ \lambda_1 \cdot \lambda_2 > 0 & \Rightarrow \text{elliptic system} \\ \lambda_1 = 0 \text{ or } \lambda_2 = 0 & \Rightarrow \text{parabolic system} \end{aligned} \quad (3.10)$$

For the special case of a membrane being characterized by a diagonal $[\kappa]$ -matrix, Eqs. (3.9a-f) reduce to

$$a_1 = -1 + \kappa_{BB}\alpha_{BA} \quad , \quad a_2 = 0 \quad (3.11a,b)$$

$$a_3 = 1 - \kappa_{CC}\alpha_{CA} \quad , \quad a_4 = -a_1 \quad (3.11c,d)$$

$$a_5 = -a_3 \quad , \quad a_6 = 0 \quad (3.11e,f)$$

In this case, the shape of the PSPC can be classified as follows:

$$\begin{aligned} (-1 + \kappa_{BB}\alpha_{BA}) \cdot (1 - \kappa_{CC}\alpha_{CA}) < 0 & \Rightarrow \text{hyperbolic system} \\ (-1 + \kappa_{BB}\alpha_{BA}) \cdot (1 - \kappa_{CC}\alpha_{CA}) > 0 & \Rightarrow \text{elliptic system} \\ (-1 + \kappa_{BB}\alpha_{BA}) = 0 \quad \text{or} \quad (1 - \kappa_{CC}\alpha_{CA}) = 0 & \Rightarrow \text{parabolic system} \end{aligned} \quad (3.12)$$

For the simple case of a scalar mass transfer matrix, the criterion for the shape of the PSPC is

$$\begin{aligned} (-1 + \alpha_{BA}) \cdot (1 - \alpha_{CA}) < 0 & \Rightarrow \text{intrinsically hyperbolic system} \\ (-1 + \alpha_{BA}) \cdot (1 - \alpha_{CA}) > 0 & \Rightarrow \text{intrinsically elliptic system} \\ (-1 + \alpha_{BA}) = 0 \quad \text{or} \quad (1 - \alpha_{CA}) = 0 & \Rightarrow \text{intrinsically parabolic system} \end{aligned} \quad (3.13)$$

In Eq.(3.13), the term “intrinsically” reflects the fact that, if no membrane is applied, the shape of the PSPC only depends on the relative volatilities of the reaction components. Eq.(3.13) is in full agreement with the conclusion stated in the literature [25-26] that the ranking of the volatilities of the reaction components determines whether a reactive distillation system exhibits reactive azeotropy or not. If the reactant A is highest boiler or lowest boiler of the reaction system (as assumed in Figure 3.3: $\alpha_{BA} = 5.0$, $\alpha_{CA} = 3.0$), one has an intrinsically hyperbolic system in which the PSPC intersects with the chemical equilibrium line within the physically relevant composition range, i.e. a reactive azeotrope will appear.

Due to the fact that, in Eqs.(3.8) and (3.9) the eigenvalues λ_1 and λ_2 of [A] are dependent on the binary mass transfer coefficients, κ_{ij} , the shape and the orientation of the PSPC of a reactive separation process (i.e. the attainable products) can thus be changed by application of membranes. This is illustrated in the next subsection.

3.1.4 Influence of membranes on singular points

An intrinsically hyperbolic system is studied under the influence of membrane permeation (Figures 3.5). The applied parameters (volatilities α_{iA} , mass transfer coefficients κ_{ij}) and the corresponding eigenvalues of the [A]-matrix are summarized in Table 3.1.

Table 3.1 Parameters used for the potential singular point curves presented in Figure 3.5

Fig.	Parameters		Eigenvalues of [A]		PSPC shape	Physical meaning
	Volatilities	[κ]-matrix	λ_1	λ_2		
(3.5a)	$\alpha_{BA}=3.0$ $\alpha_{CA}=2.0$	scalar $\begin{bmatrix} 1 & 0 & 0 \\ 0 & 1 & 0 \\ 0 & 0 & 1 \end{bmatrix}$	2	-1	Vertical hyperbola	intrinsic hyperbolic system, (membrane without any separation effect, corresponds to reactive distillation)
(3.5b)	$\alpha_{BA}=3.0$ $\alpha_{CA}=2.0$	diagonal $\begin{bmatrix} 1 & 0 & 0 \\ 0 & 1 & 0 \\ 0 & 0 & 5 \end{bmatrix}$	2	-9	Horizontal hyperbola	selective membrane which preferentially transfers C
(3.5c)	$\alpha_{BA}=3.0$ $\alpha_{CA}=2.0$	diagonal $\begin{bmatrix} 1 & 0 & 0 \\ 0 & 1 & 0 \\ 0 & 0 & 0.2 \end{bmatrix}$	2	0.6	Ellipse	(improper) membrane creates a stable node at the undesired by-product C, membrane causes change to elliptic system
(3.5d)	$\alpha_{BA}=3.0$ $\alpha_{CA}=2.0$	non-diagonal $\begin{bmatrix} 1 & 0 & 0.5 \\ 0 & 1 & 0 \\ 0.5 & 0 & 5 \end{bmatrix}$	2.05	-9.55	Rotated and deformed hyperbola	interaction of A and C in selective membrane creates non-reactive binary azeotrope at A-B edge

For comparison, again the PSPC for the reactive distillation process is given in Figure 3.5a. This situation is equivalent to a membrane reactor with a scalar mass transfer matrix, i.e. $[\kappa] = [I]$. The branch of stable nodes is indicated by a solid line for all positive Damköhler numbers $Da \in [0, \infty)$. In Figure 3.5b, the effect of a selective membrane having a diagonal $[\kappa]$ -matrix is illustrated. It is assumed that the membrane preferentially removes the undesired byproduct C from the liquid phase ($\kappa_{CC} = 5$, see Table 3.1). The membrane changes the vertically oriented hyperbola to a horizontally oriented hyperbola. Based on Eqs.(3.8) and (3.11a,c), one can show that the coefficients a_1 and a_3 fix the orientation of the hyperbola:

$$|a_1| > |a_3|, \text{ i.e. } |-1 + \kappa_{BB}\alpha_{BA}| > |1 - \kappa_{CC}\alpha_{CA}| \Rightarrow \text{vertical hyperbola} \quad (3.14a)$$

$$|a_1| < |a_3|, \text{ i.e. } |-1 + \kappa_{BB}\alpha_{BA}| < |1 - \kappa_{CC}\alpha_{CA}| \Rightarrow \text{horizontal hyperbola} \quad (3.14b)$$

The PSPC has an elliptic shape if an (improper) membrane, which preferentially retains the byproduct C, is applied (Figure 3.5c). In this case, the pure C vertex is the only stable

node of the system. That means the only feasible product is the pure byproduct C at reactive and also at non-reactive conditions.

It is possible that the permeating species exert some influence on each other, apart from the effect induced by the membrane; for instance, when the bulk diffusion takes place within porous media, or when the competitive adsorption plays a role in the diffusion mechanism. In such cases, the $[\kappa]$ -matrix may contain off-diagonal elements. In principle, the off-diagonal elements of $[\kappa]$ in the i^{th} row should vanish when the concentration of component i is zero, to ensure the flux and mole fraction remaining in the physically meaningful domain.

Nevertheless, in order to avoid the higher order equations than the operable quadratic form Eq.(3.7), the effect of off-diagonal elements of $[\kappa]$ -matrix are interpreted here with constant values. As illustrated in Figure 3.5d, the interaction of A and C is embodied in the $[\kappa]$ -matrix by assuming $\kappa_{AC}=0.5$ and $\kappa_{CA}=0.5$. All other parameters are equal to the case in Figure 3.5b. As can be seen the horizontal hyperbola is slightly rotated and shifted. As a result, a binary mixture on the A-B edge appears to be a stable node when Da exceeds a critical value 0.27. Moreover, pure B is achievable at $Da \rightarrow \infty$ which cannot be attained in the absence of A-C interactions at the given parameter settings (compare to diagonal case in Figure 3.5b).

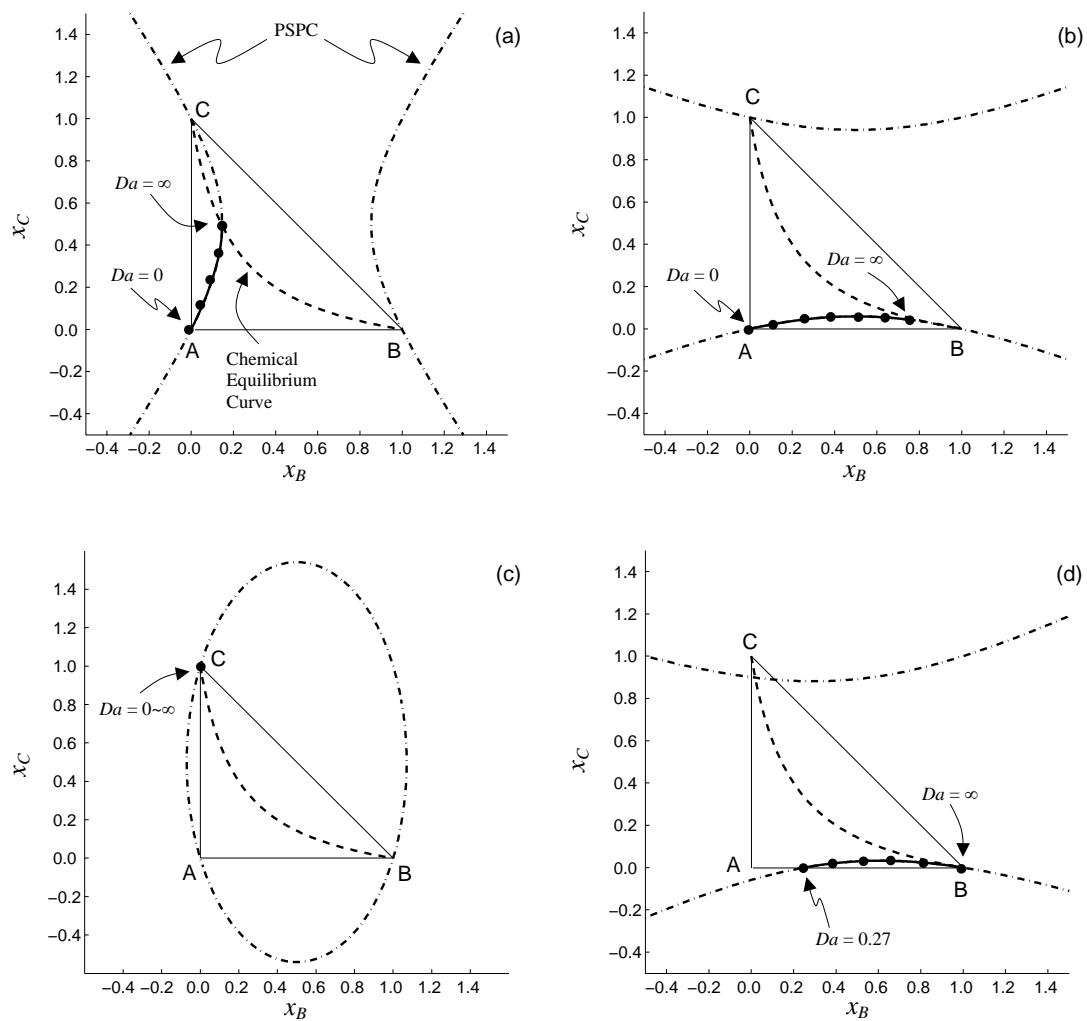
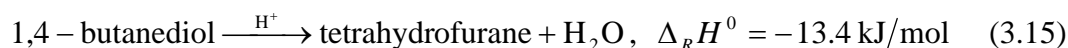


Figure 3.5 Potential singular point curves (PSPC) and stable node bifurcation behavior for an intrinsically hyperbolic system; $A \Leftrightarrow B + C$; $K = 0.2$ (For parameters see Table 3.1). Legend:
 • Branch of Stable Nodes

3.2 Non-ideal system: THF synthesis reaction

Now, after the analysis of an ideal ternary reaction system, a non-ideal example of technical relevance is considered. This is the heterogeneously catalyzed cyclisation of 1,4-butanediol (1,4-BD) to tetrahydrofuran (THF) and water:



Limbeck and coworkers [49] have studied the kinetics of this irreversible reaction at macroporous acidic ion exchange resins as catalysts. In this reaction, the byproduct water has a significant affinity with the catalyst and this inhibits the catalytic reaction severely. Therefore, the authors proposed the rate expression in Eq.(3.16):

$$r = \eta(a_{\text{H}_2\text{O}}) \cdot \frac{k_f \cdot K_{BD} a_{BD}}{1 + K_{BD} a_{BD}} = \frac{1}{1 + K_{\text{H}_2\text{O}} \sqrt{a_{\text{H}_2\text{O}}}} \cdot \frac{k_f \cdot K_{BD} a_{BD}}{1 + K_{BD} a_{BD}} \quad (3.16)$$

where k_f represents the rate constant, K_{BD} and $K_{\text{H}_2\text{O}}$ the adsorption constants of 1,4-BD and water, and η the water inhibition factor. The expressions of k_f , K_{BD} and $K_{\text{H}_2\text{O}}$ as functions of temperature are as follows:

$$\frac{k_f}{k_{f,ref}} = \exp\left(\frac{-18282.42}{T/[K]}\right) / \exp\left(\frac{-18282.42}{404.2}\right) \quad (3.17)$$

$$K_{BD} = 6.29 \times 10^{-2} \times \exp\left(\frac{1335.1}{T/[K]}\right) \quad K_{\text{H}_2\text{O}} = 2.43 \times \exp\left(\frac{764.97}{T/[K]}\right) \quad (3.18a,b)$$

The boiling point of THF at the operating pressure $p = 5$ atm is chosen as the reference temperature. The vapor phase mole fraction y_i can be calculated by Eq.(2.12), wherein the saturated vapor pressures are calculated from the Antoine equations, and the liquid phase activity coefficients (γ_i) are calculated by the Wilson equation [50]. For detailed information of the thermodynamic model, please refer to Appendix A.3.

Since water is the byproduct and it has an additional undesired inhibition effect upon the catalyst, it has to be separated efficiently from the reaction mixture. To achieve this, both conventional reactive distillation (Figure 1.1) and the membrane (Figure 2.1) are considered as process alternatives. In the second process, a Knudsen membrane is applied. Consequently, the mass transfer matrix $[\kappa]$ has a diagonal structure and the diagonal elements are the

Knudsen selectivities, i.e. the square roots of the ratios of the molecular weights M_i (1,4-BD as reference component):

$$[\kappa] = \begin{bmatrix} 1 & 0 & 0 \\ 0 & \sqrt{M_{BD} / M_{THF}} & 0 \\ 0 & 0 & \sqrt{M_{BD} / M_{H_2O}} \end{bmatrix} = \begin{bmatrix} 1 & 0 & 0 \\ 0 & 1.1 & 0 \\ 0 & 0 & 2.5 \end{bmatrix} \quad (3.19)$$

Thus, water will pass preferentially through the Knudsen membrane.

3.2.1 Residue curve maps and retentate phase diagrams

First, RCMs were determined for non-reactive distillation (Figure 3.6a), for reactive distillation at kinetically controlled reaction (Figure 3.6b) and for reactive distillation at equilibrium controlled reaction (Figure 3.6c). The topology of the maps at non-reactive conditions ($Da = 0$) is structured by a binary azeotrope (unstable node) between water and THF. Pure water and pure THF are saddle nodes while the 1,4-BD vertex is a stable node. It has the highest boiling point in this system.

At $Da = 0.4$ (Figure 3.6b), the two saddle points are moved from the pure vertices into the composition triangle. The same is true for the stable node which is moved from the 1,4-BD vertex to the kinetic azeotrope at $(x)^T = (0.0328, 0.6935)$. Pure water and pure THF are still singular points, but they become stable nodes under reactive conditions. The unstable node on the water-THF edge remains unmoved. It forms two separatrices with the two saddle points. Therefore, the whole composition space is divided into three subspaces which have each a stable node, namely pure water, pure THF and the kinetic azeotrope.

At $Da \rightarrow \infty$ (Figure 3.6c), only pure water and pure THF remain stable nodes. The residue curves first are dominated by the reaction stoichiometry and approach the water-THF edge, which is actually the chemical equilibrium line of this irreversible reaction, and then converge to the water vertex or to the THF vertex. When starting from pure 1,4-BD, the undesired by-product water will be the final product in the distillation still.

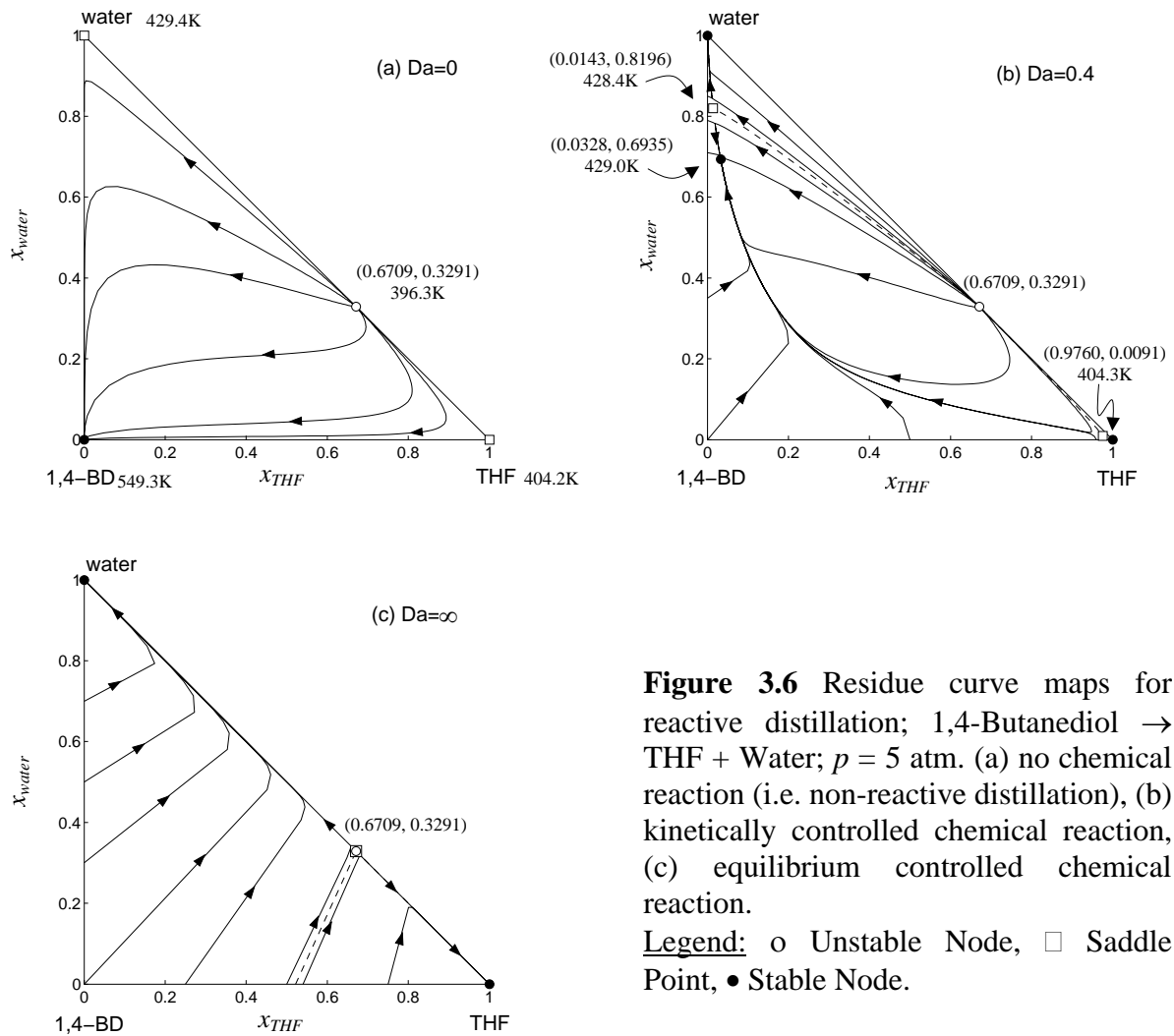


Figure 3.6 Residue curve maps for reactive distillation; 1,4-Butanediol \rightarrow THF + Water; $p = 5$ atm. (a) no chemical reaction (i.e. non-reactive distillation), (b) kinetically controlled chemical reaction, (c) equilibrium controlled chemical reaction.

Legend: o Unstable Node, □ Saddle Point, • Stable Node.

The effect of a Knudsen membrane on the process behavior is illustrated in Figure 3.7a which is valid at non-reactive conditions. Comparing Figure 3.6a and Figure 3.7a, the unstable node on the THF-water edge is moved closer to the water vertex by application of the Knudsen membrane, while the two saddle points and the stable node are not affected.

At $Da = 0.4$ (Figure 3.7b), the diagram is structured by one unstable node, two saddle points and three stable nodes (as in Figure 3.6b), whereas the locations of the two saddle points and the stable node are changed. In particular, the kinetic arrheotrope at $(x)^T = (0.2313, 0.2520)$ is located closer to the THF vertex than the kinetic azeotrope at $(x)^T = (0.0328, 0.6935)$.

Similar to the reactive distillation process, at $Da \rightarrow \infty$ the composition space is again divided into two subspaces which have either pure THF or pure water as attractors (Figure 3.7c). However, as a very important feature of this membrane reactor with Knudsen effect, when starting with pure 1,4-BD it is possible to attain pure THF as the desired product. This is not possible with conventional reactive distillation. The reason for this behavior is the fact that the saddle point on the THF-water edge is shifted towards the water vertex.

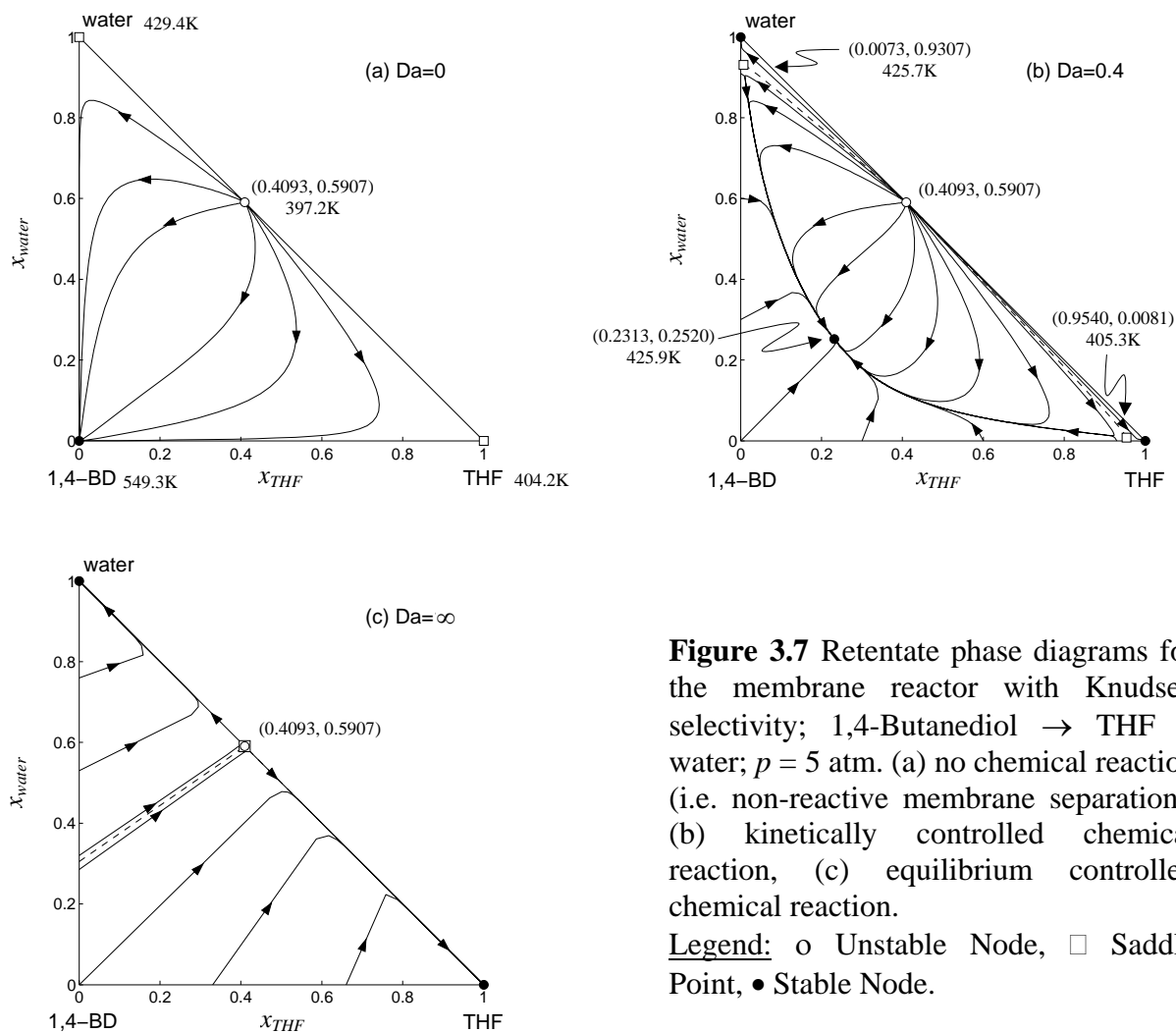


Figure 3.7 Retentate phase diagrams for the membrane reactor with Knudsen selectivity; 1,4-Butanediol \rightarrow THF + water; $p = 5$ atm. (a) no chemical reaction (i.e. non-reactive membrane separation), (b) kinetically controlled chemical reaction, (c) equilibrium controlled chemical reaction.

Legend: □ Unstable Node, □ Saddle Point, ● Stable Node.

3.2.2 Singular point analysis

Figure 3.8 shows the PSPC and the bifurcation behavior of a simple reactive distillation. Qualitatively, the curve of potential singular points is shaped like a hyperbola due to the boiling sequence of the involved components. Along the left hand part of the PSPC, the stable node branch and the saddle point branch 1 coming from the water vertex, meet each other at the kinetic tangent pinch point $(x)^T = (0.0246, 0.7462)$ where the critical Damköhler number is $Da = 0.414$. The right hand part of the PSPC is the saddle point branch 2 which runs from pure THF to the binary azeotrope between THF and water.

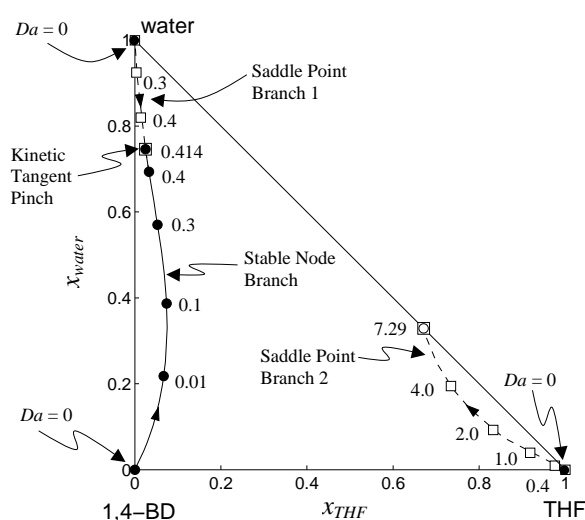


Figure 3.8 Potential singular point curve and bifurcation behavior for reactive distillation; 1,4-Butanediol \rightarrow THF + Water; $p = 5$ atm. Legend: o Unstable Node, □ Saddle Point, ● Stable Node.

In a similar manner, Figure 3.9 illustrates the PSPC for the membrane reactor case. In Figure 3.9a, the effect of a Knudsen membrane on the PSPC can be seen by comparison with the corresponding diagram for reactive distillation (i.e. $[\kappa]$ -matrix equals identity matrix) depicted in Figure 3.8. Generally speaking, the membrane turns the vertical hyperbola into a horizontal hyperbola. In particular, the membrane shifts the stable node branch towards the THF vertex such that THF-rich products can be achieved in the considered Knudsen membrane reactor.

Because the boiling temperature of 1,4-BD is much higher than of the two products and the cyclisation reaction is irreversible, the bifurcation behavior is only affected by the ratio of $\kappa_{water}/\kappa_{THF}$ if κ_{BD} is not extremely high or low. There exists a critical value of $\kappa_{water}/\kappa_{THF} = 2.1$, above which the stable node branch approaches the THF vertex.

Figure 3.9b shows the effect of a membrane which is assumed to have with a higher selectivity of water with respect to 1,4-BD than the Knudsen membrane, namely $\kappa_{water} = 11$ instead of 2.5 in the Knudsen case. With this higher selectivity the location of the stable node branch is closer to BD-THF edge, i.e. a higher THF content can be achieved in the final liquid residue.

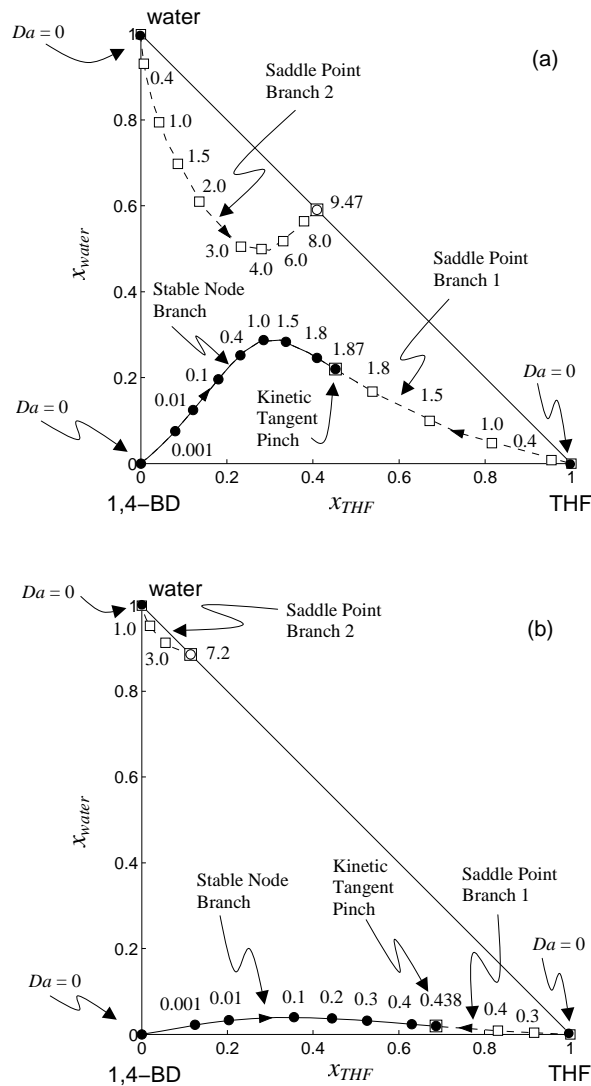


Figure 3.9 Potential singular point curves (PSPCs) and bifurcation behavior of membrane reactors at different mass transfer conditions; 1,4-Butanediol \rightarrow THF + Water; $p = 5$ atm.

(a) Knudsen membrane $[\kappa] = \begin{bmatrix} 1 & 0 & 0 \\ 0 & 1.1 & 0 \\ 0 & 0 & 2.5 \end{bmatrix}$, (b) membrane with $[\kappa] = \begin{bmatrix} 1 & 0 & 0 \\ 0 & 1.1 & 0 \\ 0 & 0 & 11 \end{bmatrix}$

Legend: o Unstable Node, \square Saddle Point, \bullet Stable Node.

In order to illustrate the difference between the two considered membranes on a quantitative basis, it is helpful to simultaneously integrate Eqs.(2.3) and (2.4) to get the two diagrams given in Figure 3.10. With the initial condition $x_{BD,0} = 1.0$ at $Da = 100$ (i.e. equilibrium controlled chemical reaction), Figure 3.10a shows the time needed for in-situ purification. A Knudsen membrane needs about four times longer than the more selective membrane process to achieve a reasonable product purity. In Figure 3.10b, the relative liquid holdup (H/H_0) is plotted versus the liquid mole fraction of the desired product THF. Although pure THF is a feasible product for a Knudsen membrane reactor, the final product amount is almost negligible, while the more selective membrane produces an acceptable amount of pure THF (ca. 70 % of max. value).

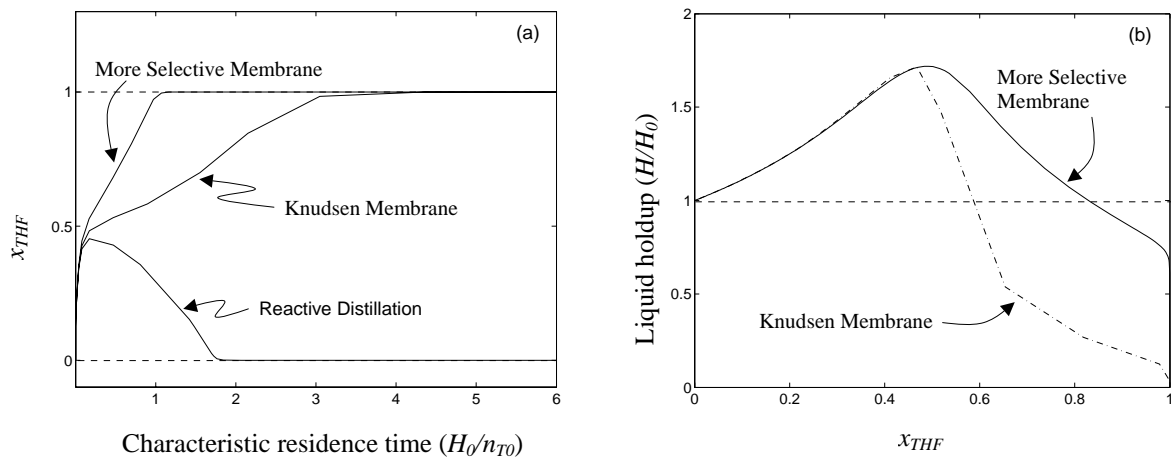


Figure 3.10 Transient behavior of membrane reactors of different selectivity (Knudsen membrane / more selective membrane); 1,4-Butanediol \rightarrow THF + Water; $p = 5$ atm; initial condition: $x_{BD,0} = 1.0$, $Da = 100$; (a) THF liquid mole fraction versus characteristic residence time, (b) Liquid holdup versus THF liquid mole fraction.

$$\text{Knudsen membrane } [\kappa] = \begin{bmatrix} 1 & 0 & 0 \\ 0 & 1.1 & 0 \\ 0 & 0 & 2.5 \end{bmatrix}; \text{ more selective membrane } [\kappa] = \begin{bmatrix} 1 & 0 & 0 \\ 0 & 1.1 & 0 \\ 0 & 0 & 11 \end{bmatrix}.$$

3.3 Chapter conclusions

From the retentate phase diagrams and singular point analysis, it is shown that selective mass transfer through a membrane can change the attainable products of a reactive separation process significantly.

This has been demonstrated for a simple ideal reaction system ($A \Leftrightarrow B + C$) and also for a selected non-ideal reaction example (cyclisation of 1,4-butanediol to THF). In both examples, the autonomous heating policy has been applied; and the influence of membranes is exhibited by comparing the phase diagrams with and without membranes.

In the first ideal example, the influences of different membrane selectivities and diffusion mechanisms are interpreted by the structure of effective mass transfer coefficients $[k]$ -matrix (scalar / diagonal / non-diagonal). The reactive arrheotrope conditions are further manipulated to give a simple criterion for the shape (hyperbola / ellipse) of potential singular point curves.

In the THF synthesis reaction example, the influence of a Knudsen membrane on the retentate phase composition is demonstrated. From the singular point analysis, it is found that a Knudsen membrane can shift the orientation of the PSPC from a vertical hyperbola to a horizontal one. This result is compatible with the predications of the ideal system in a qualitative way.

4. Examples of quaternary systems

Apart from the ternary examples, in this chapter two more quaternary examples are investigated [51]. The composition space for quaternary systems can be visualized in a 3-dimensional tetrahedron. In the first ideal system with constant relative volatilities, the emphasis in addition to the ternary example is laid on graphical interpretation of the reactive azeotrope condition and the PSPC, as well as on the bifurcation behavior with respect to the mass transfer coefficient. In the second example, the goal is set to demonstrate the existence of a reactive azeotrope. The propyl acetate synthesis reaction coupled with permeation through porous membranes is chosen wherein the permeation through the porous membrane is described by the dusty gas model. The isothermal heating policies (as discussed in Section 2.1.2) are applied so that the experimental validation can be realized in the laboratory (see Chapter 6).

4.1 Ideal quaternary system

The effect of a selective membrane on the quaternary mixture A/B/C/D undergoing a single reversible chemical reaction in the ideal liquid phase is considered:



The pseudo-homogeneous reaction kinetics of this quaternary system reads as

$$\mathfrak{R} = x_A x_B - \frac{x_C x_D}{K} \quad (4.2)$$

with K as chemical equilibrium constant. Again for the sake of a concise analysis, the following assumptions are made:

- The chemical equilibrium constant is independent of temperature: $K = 12$.
- The rate constant k_f is independent of temperature: $k_f / k_{f,ref} = 1$.
- The relative volatilities are assumed to be constant, and denoted as α_{BA} , α_{CA} , α_{DA} with respect to the reactant A. Therefore, the vapor phase equilibrium composition can be calculated as

$$y_i = \frac{\alpha_{iA} x_i}{\sum_{m=A}^D \alpha_{mA} x_m} \quad (4.3)$$

4.1.1 Residue curve maps and retentate phase diagrams

The effect of a membrane being integrated into a chemical reactor can be elucidated with the help of retentate phase diagrams. As mentioned in Section 2.1.4, distillation can be interpreted as a limiting case of a membrane process with the mass transfer matrix $[\kappa]$ being the identity matrix, i.e. no selective mass transfer effects. The values of the relative volatilities are chosen as $\alpha_{BA} = 1.7$, $\alpha_{CA} = 3.9$, and $\alpha_{DA} = 4.2$, so that the reactants A and B are higher boilers than the products C and D. The quaternary mixture with this set of volatilities was also studied by [25-26] for non-reactive distillation and for equilibrium controlled reactive distillation. Here, we consider this system for the purpose of comparison with a membrane reactor to see the effects of incorporating membranes.

Figure 4.1 shows residue curve maps for the classical reactive distillation process at three different Damköhler numbers. In the non-reactive case ($Da = 0$, Figure 4.1a), the map topology is structured by one unstable node (pure D), two saddle points (pure B and pure C) and one stable node (pure A). The arrows along the residue curves indicate the composition change along the axial direction in the continuous process, or with increasing time in the batch one. Since pure A is the only stable node of non-reactive distillation, this is the feasible bottom product to be expected in a continuous distillation column.

At kinetically controlled chemical reaction ($Da = 1$, Figure 4.1b), there appears another saddle point (called *kinetic azeotrope*), while pure C becomes an unstable node and B becomes a stable node. The quaternary saddle point forms two boundaries with the unstable nodes C and D such that the residue curves which originate from C and D move towards the saddle point and eventually converge to A and B, respectively.

When the reaction rate is much faster than the permeation rate ($Da \rightarrow \infty$, Figure 4.1c), the reaction approaches the chemical equilibrium, and therefore the quaternary saddle point (called *reactive azeotrope*) reaches the equilibrium surface (as shown later in Figure 4.4 or 4.5). In this case, the residue curves are first dominated by the reaction stoichiometry and then move along the equilibrium surface converging to the stable nodes A and B.

By the proposed method, the retentate phase diagrams of the membrane reactors can be determined analogously. First, a diagonal $[\kappa]$ -matrix is considered with $\kappa_{CC} = 0.8$, i.e. the membrane is slightly selective so that it retains the product C more than the other three components which are assumed to have the same mass transfer coefficients. Figure 4.2a shows the phase diagram of such a membrane process at non-reactive conditions ($Da = 0$). Due to the low selectivity of the membrane, it does not change the sequence of the relative volatilities. Thus, the topology of Figure 4.2a is similar to Figure 4.1a.

At kinetically controlled conditions ($Da = 1$, Figure 4.2b), it again shows an additional quaternary saddle point (called *kinetic arrheotrope*), and pure B becomes the stable node. Different from Figure 4.1b, the C vertex remains the saddle point. The unstable D forms two boundaries with the two saddle points, pure C and the just mentioned kinetic arrheotrope. The composition trajectory lines originate from the D vertex, move towards the C vertex and the quaternary saddle point, and finally end up at pure A or pure B.

At infinite Damköhler number ($Da \rightarrow \infty$, Figure 4.2c), the saddle point (called *reactive arrheotrope*) is located exactly on the chemical equilibrium surface. The C vertex becomes the unstable node when the Damköhler number exceeds a critical value. The composition trajectory lines again move along the equilibrium surface and converge to the stable nodes A or B, similar to Figure 4.1c, while the location of the reactive arrheotrope is closer to the C vertex than the reactive azeotrope in Figure 4.1c.

When the membrane is more selective, e.g. $\kappa_{CC} = 0.2$, the membrane changes the sequence of effective volatilities. Thus, C becomes the stable node, A and B are the saddle points and D remains the unstable node at any Damköhler numbers (as shown in Figures 4.2d-f). The reaction kinetics in this case can only influence the composition trajectory, but not the location and stability of singular points. For the non-reactive case (Figure 4.2d, $Da = 0$), the composition trajectory lines may spiral and travel through the whole composition tetrahedron; for $Da \rightarrow \infty$, the composition trajectory lines are constrained by the chemical equilibrium relationship so that they can only approach the equilibrium surface by the reaction stoichiometry first, and then move on the surface, i.e. the system loses a degree of freedom in the chemical equilibrium controlled case.

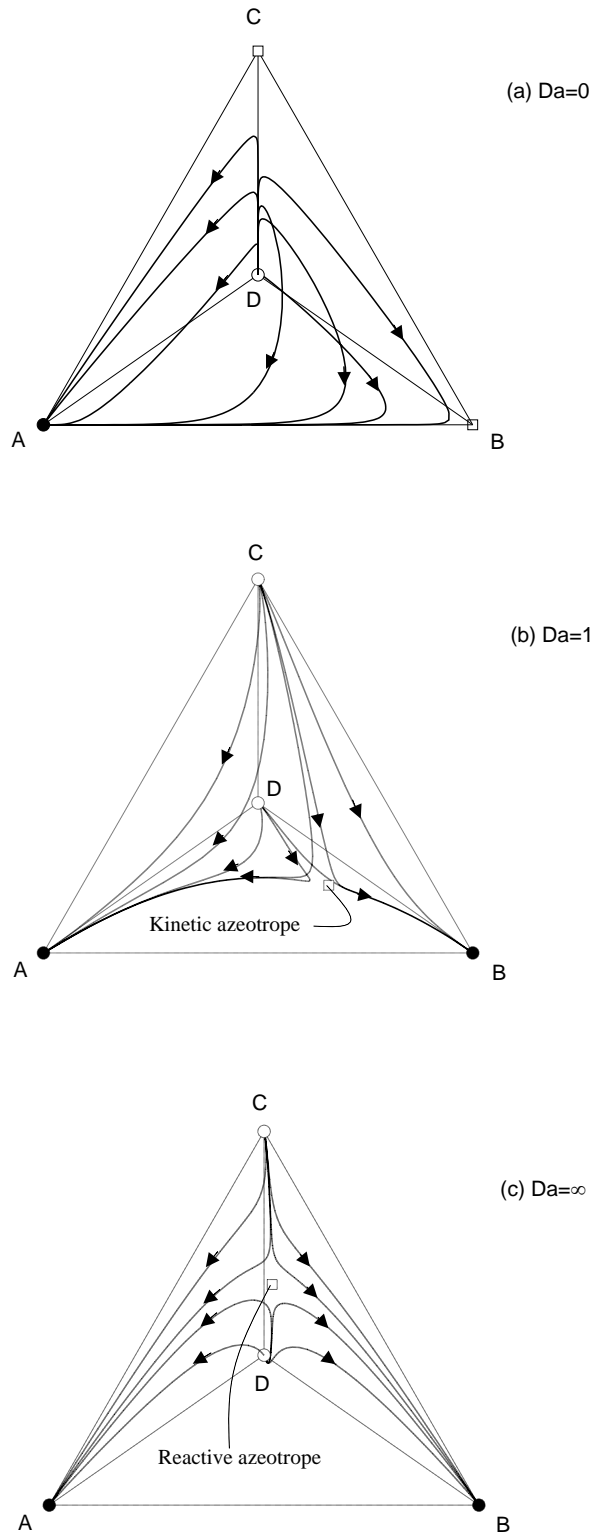


Figure 4.1 Residue curve maps for reactive distillation; $A + B \rightleftharpoons C + D$; $K = 12$; constant relative volatilities: $\alpha_{BA} = 1.7$; $\alpha_{CA} = 3.9$; $\alpha_{DA} = 4.2$. (a) no chemical reaction (i.e. non-reactive distillation), (b) kinetically controlled chemical reaction, (c) equilibrium controlled chemical reaction. Legend: \circ Unstable Node, \square Saddle Point, \bullet Stable Node.

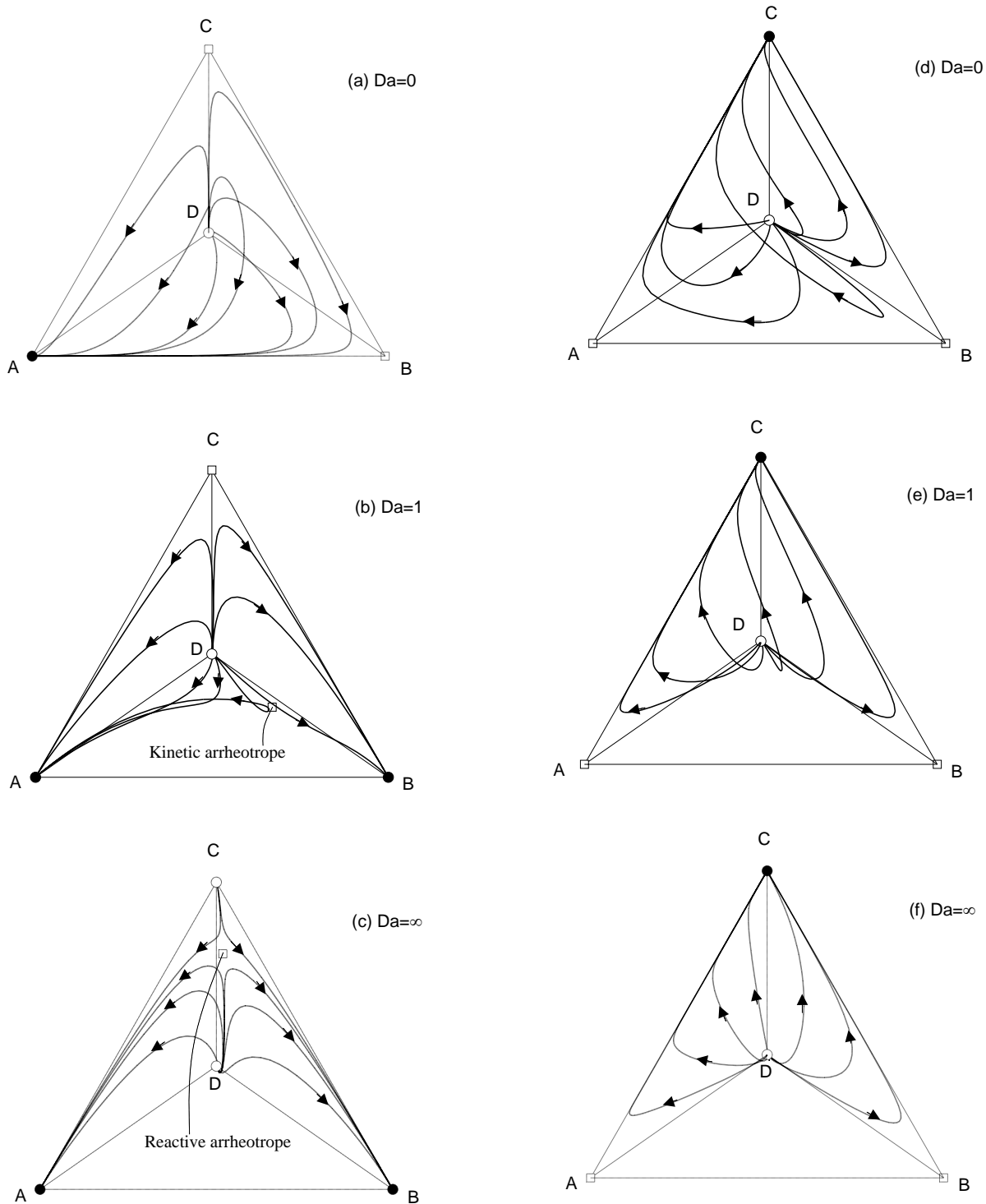


Figure 4.2 Retentate phase diagrams for membrane reactor; $A + B \rightleftharpoons C + D$; $K = 12$; constant relative volatilities: $\alpha_{BA} = 1.7$; $\alpha_{CA} = 3.9$; $\alpha_{DA} = 4.2$. **Legend:** o Unstable Node, □ Saddle Point, • Stable Node.

$$(4.2 \text{ a,b,c}): [K] = \begin{bmatrix} 1 & 0 & 0 & 0 \\ 0 & 1 & 0 & 0 \\ 0 & 0 & 0.8 & 0 \\ 0 & 0 & 0 & 1 \end{bmatrix}$$

$$(4.2 \text{ d,e,f}): [K] = \begin{bmatrix} 1 & 0 & 0 & 0 \\ 0 & 1 & 0 & 0 \\ 0 & 0 & 0.2 & 0 \\ 0 & 0 & 0 & 1 \end{bmatrix}$$

4.1.2 Singular point analysis

As revealed in the previous figures, the topology of retentate phase diagrams can be structured by the singular points. Thus, singular point analysis yields the key information on the feasibility of a membrane reactor. As mentioned in Section 2.3, all potential singular points of different Da -numbers are located on a unique curve (PSPC) whose location is fixed by Eq.(2.37). For the considered quaternary case, the PSPC is determined by solving the following set of equations simultaneously:

$$X_A = Y_A, X_B = Y_B \quad (4.4a,b)$$

where the main product C is chosen as the reference component. Eqs.(4.4a,b) are the reactive azeotropic conditions for the considered reaction example.

In Figure 4.3, the PSPC for $\kappa_{CC} = 0.8$ (*cf.* Figure 4.2a-c) is plotted (dashed line) as the intersection of the two surfaces described by Eqs.(4.4a,b). Only the PSPC branch within the physically relevant composition space is shown here. A certain subset of points along the PSPC are singular points of physical relevance, i.e. for $Da \in [0, \infty]$. Points which correspond to negative Da -numbers are physically not relevant.

At the given set of relative volatilities, the PSPC of the distillation process is depicted in Figure 4.4. For completeness, the PSPC is also shown outside the composition space. One branch of the PSPC passes through the composition tetrahedron and connects the B, C vertices. The quaternary saddle point emerges from the B vertex and moves along this PSPC branch with the increasing Damköhler number. It intersects the equilibrium surface and thus results in the reactive azeotrope at $Da \rightarrow \infty$. As for the pure component vertices, A and D remain the stable and unstable nodes, respectively, at any Damköhler number, while B changes from a saddle point to a stable node if $Da > 0.411$. The pure C vertex is a saddle point when $Da < 0.921$, and turns into an unstable node if the Damköhler number exceeds the critical value.

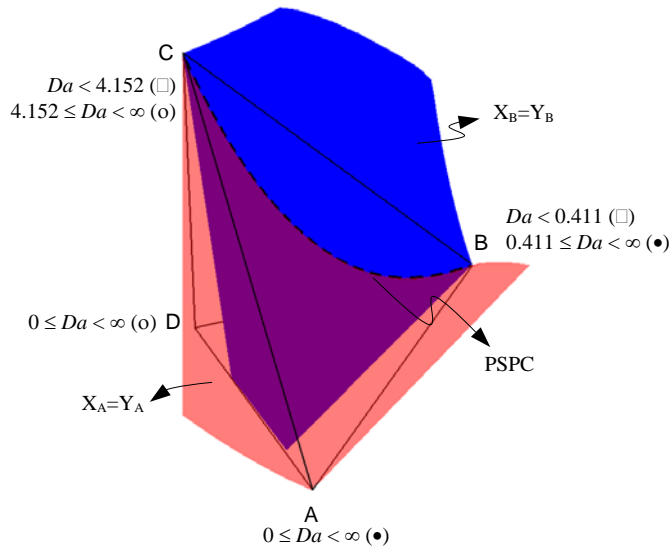


Figure 4.3 Reactive azeotropic conditions (red and blue surfaces) and potential singular point curve (PSPC); $A + B \rightleftharpoons C + D$; $K = 12$; constant relative volatilities: $\alpha_{BA} = 1.7$; $\alpha_{CA} = 3.9$; $\alpha_{DA} = 4.2$; $\kappa_{CC} = 0.8$. Legend: ○ Unstable Node, □ Saddle Point, ● Stable Node, --- PSPC.

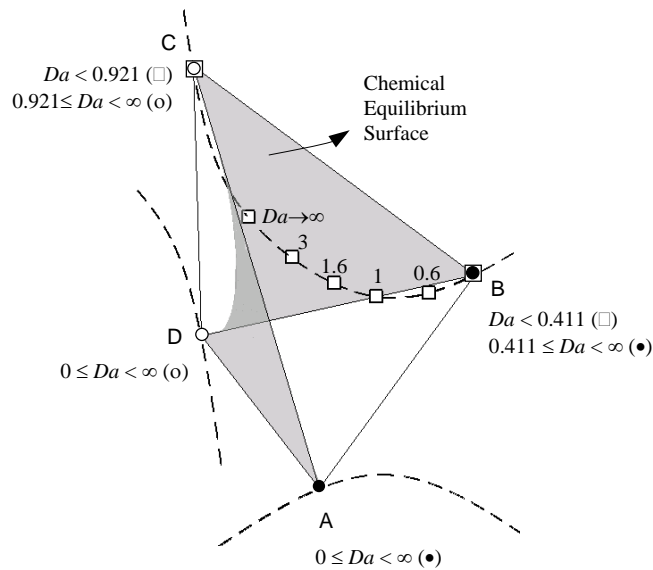


Figure 4.4 Potential singular point curve (PSPC) and bifurcation behavior for reactive distillation; $A + B \rightleftharpoons C + D$; $K = 12$; constant relative volatilities: $\alpha_{BA} = 1.7$; $\alpha_{CA} = 3.9$; $\alpha_{DA} = 4.2$. Legend: ○ Unstable Node, □ Saddle Point, ● Stable Node, --- PSPC.

Similarly, the PSPCs of membrane reactors for the conditions given in Figure 4.2a-c and Figure 4.2d-f are depicted in Figure 4.5a,b. For $\kappa_{CC} = 0.8$ (Figure 4.5a), the shape of the PSPC is similar to Figure 4.4, but the branch passing through the composition space is closer to the B-C edge. This leads to different locations for kinetic and reactive azeotropes compared to the azeotropes in the reactive distillation process. Furthermore, the pure C vertex

is an unstable node in Figure 4.1b, but a saddle point in Figure 4.2b, because the critical value for pure C turning from a saddle point into an unstable node is $Da = 4.152$ (as Figure 4.5a). For $\kappa_{CC} = 0.2$ (Figure 4.5b), the two branches of the PSPC do not move into the composition tetrahedron, but only intersect the four pure component vertices. For this case, A and B are saddle points, C is a stable node and D is an unstable node at all Damköhler numbers.

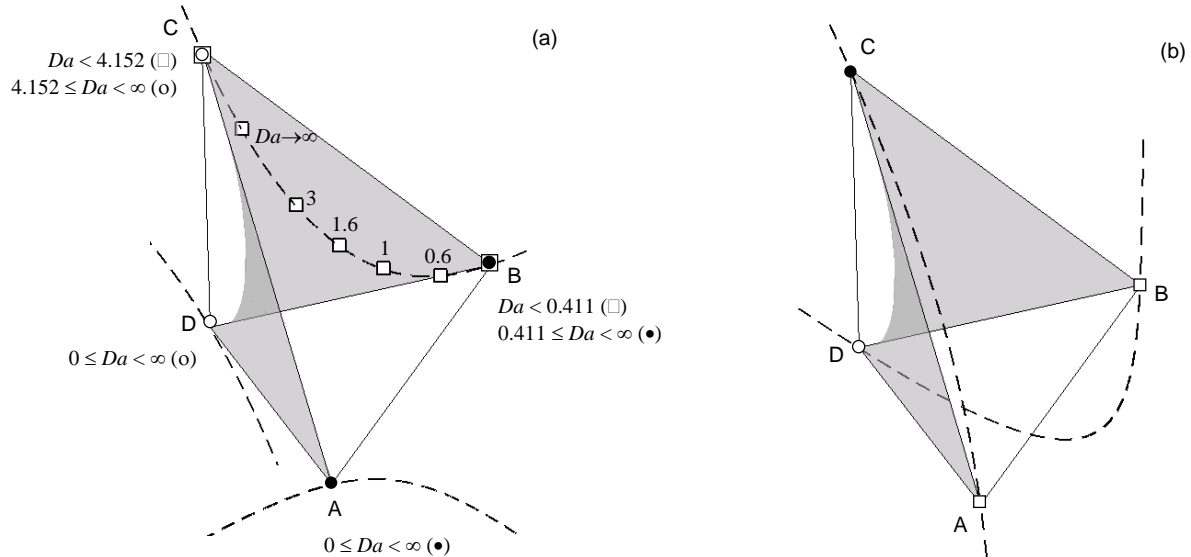


Figure 4.5 Potential singular point curve (PSPC) and bifurcation behavior for membrane reactors; $A + B \rightleftharpoons C + D$; $K = 12$; constant relative volatilities: $\alpha_{BA} = 1.7$; $\alpha_{CA} = 3.9$; $\alpha_{DA} = 4.2$; (a) $\kappa_{CC} = 0.8$, (b) $\kappa_{CC} = 0.2$. Legend: o Unstable Node, □ Saddle Point, ● Stable Node, --- PSPC.

For the selection of suitable membrane materials, it is helpful to track the location of the feasible product composition in dependence on the membrane mass transfer coefficients. For instance, Figure 4.6 shows the bifurcation behavior with respect to the relative mass transfer coefficient κ_{CC} . At equilibrium controlled conditions (i.e. $Da \rightarrow \infty$), the quaternary singular point moves from the reactive azeotrope ($\kappa_{CC} = 1$) towards the B-C edge with decreasing κ_{CC} as shown in Figure 4.6a. When κ_{CC} is smaller than the critical value 0.436 ($= \alpha_{BA} / \alpha_{CA}$), the quaternary branch vanishes within the composition space, and pure B changes from a stable node into a saddle point, while pure C from an unstable into a saddle point. When κ_{CC} becomes smaller than the value 0.256 ($= 1 / \alpha_{CA}$), C becomes the only stable node of the system, replacing the original stable node which was pure A (as in Figure 4.6b).

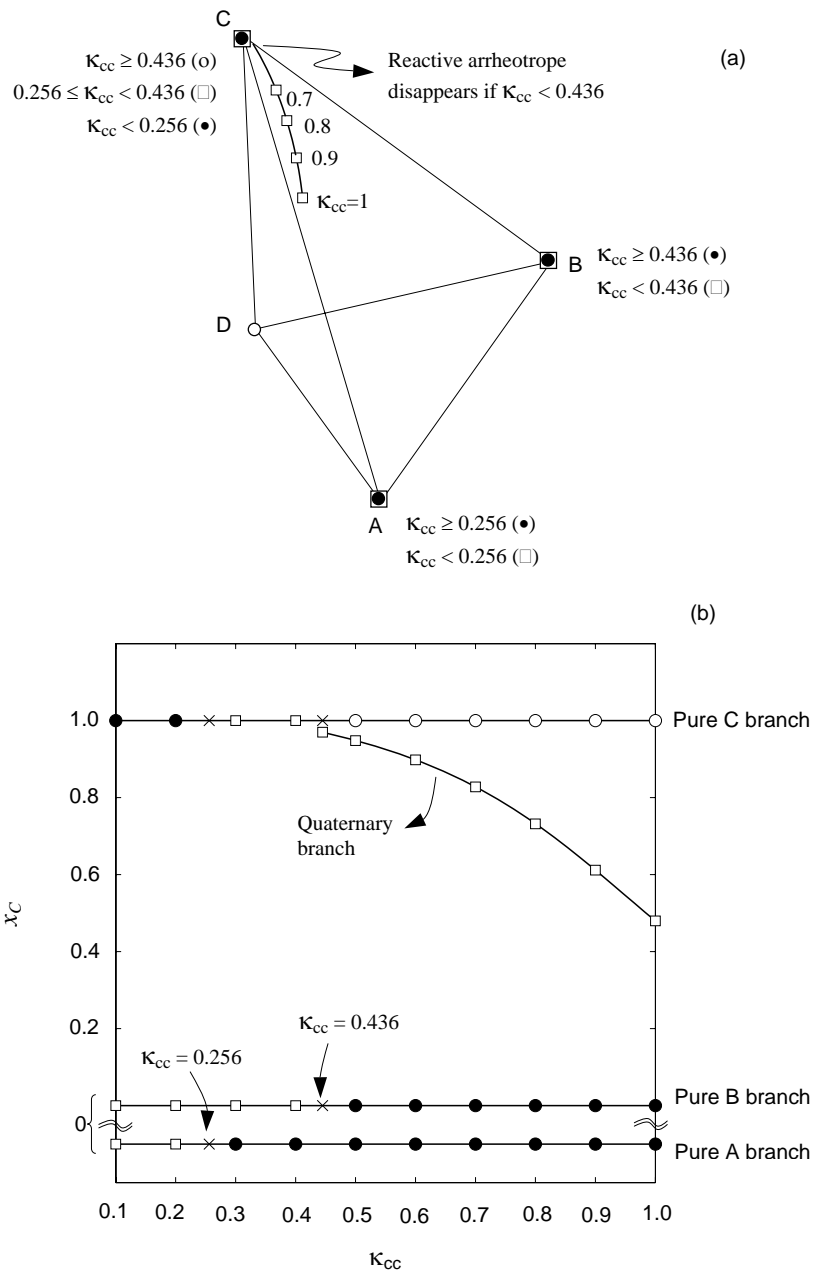


Figure 4.6 Bifurcation behavior with respect to κ_{CC} (at $Da \rightarrow \infty$); $A + B \rightleftharpoons C + D$; $K = 12$; constant relative volatilities: $\alpha_{BA} = 1.7$; $\alpha_{CA} = 3.9$; $\alpha_{DA} = 4.2$. Legend: o Unstable Node, \square Saddle Point, \bullet Stable Node. (a) within the composition tetrahedron. (b) x_C versus κ_{CC} .

4.2 Non-ideal system: esterification of acetic acid with *n*-propanol

Now a non-ideal reaction system of technical relevance is considered: the synthesis reaction of propyl acetate, coupled with the permeation through porous polyester membranes. This system was chosen mainly for two reasons: (i) to show how a realistic permeation model (dusty gas model) can be implemented in the frame of the proposed methodology, and (ii) to give a technically relevant example for the existence of a *reactive azeotrope*. As mentioned in section 2.2.2, the $[\kappa]$ -matrix of the dusty gas model can be regarded as a non-diagonal matrix and its elements are functions of the composition. The esterification reaction of acetic acid with propanol reads as:



The kinetics of this reaction catalyzed by commercial cation-exchange resin Amberlyst 15, is studied in Chapter 5 [52]. A pseudo-homogeneous kinetic model was chosen in the simulations. The reaction rate is expressed in terms of the liquid phase activities to account for the non-ideal mixing behavior of the reaction components in the liquid phase:

$$\mathfrak{R} = a_{AcAc} a_{PrOH} - \frac{a_{PrAc} a_{H_2O}}{K} \quad (4.6)$$

where K is the equilibrium constant, and its temperature dependency is given by Eq.(5.2). The lowest boiling component propanol is chosen as the reference point for $n_{T,ref}$.

Taking into account the dimerization reaction of acetic acid in the vapor phase, the vapor mole fraction y_i can be calculated by:

$$y_i \cdot p \cdot z_i = x_i \cdot \gamma_i(x_j, T) \cdot p_i^{sat}(T) \quad (4.7)$$

where the saturated pressures (p_i^{sat}) are calculated by the Antoine equation, and the liquid phase activity coefficients (γ_i) are calculated by the NRTL equation [50]. z_i are the dimerization correction factors described e.g. by Marek and Standart [25, 53]. For the detailed information of the thermodynamic model, please refer to the Appendix A.4.

For separation, a porous polyester membrane (Whatman, UK) is considered here; this membrane is a commercially available product which is manufactured by track-etched processes. Thus, the membrane pores are nearly cylindrical ($\tau = 1$). The membrane thickness is reported to be 6 μm and the membrane porosity is 4.7% being calculated from the reported pore density, 6×10^8 pores/ cm^2 . The smallest available membrane pore diameter, 100 nm, is

used for the following analysis. The permeation of molecules through the specified membrane is described here by the dusty gas model. In practice, it will be important to avoid capillary condensation of the permeating vapor within the membrane pores. This can be achieved by an extra heat supply to the membrane.

4.2.1 Residue curve maps and retentate phase diagrams

Figure 4.7a shows the residue curve map for non-reactive distillation at isothermal conditions, i.e. $T = 105\text{ }^{\circ}\text{C}$. There are three non-reactive binary azeotropes in the RCM. The azeotrope between propyl acetate and water (Az. 1) is the unstable node, while the other two (Az. 2 and Az. 3) are the saddle points. Pure propanol, propyl acetate and water are also saddle points, and acetic acid is the only stable node for the simple distillation. Residue curves originate from the unstable node, first approach the saddle points, and finally converge to the stable node. The information of all singular points is listed in Table 4.1.

Table 4.1 List of singular points in Fig. 4.7 (Legend: \circ Unstable Node, \square Saddle Point, \bullet Stable Node).

Name	Composition	Type	Pressure [bar]	Da			x_1	x_2	X_3
				0	1	∞			
Azeotrope 1	PrAc/H ₂ O	Unstable	2.38	\circ			0	0	0.3774
Azeotrope 2	PrOH/ H ₂ O	Saddle	1.91	\square	\square	\square	0	0.4347	0
Azeotrope 3	PrOH/PrAc	Saddle	1.44	\square	\square	\square	0	0.7311	0.2689
Azeotrope 4	AcAc/PrOH /PrAc/H ₂ O	Unstable	2.29		\circ		0.0210	0.1193	0.2929
Azeotrope 5	AcAc/PrOH /PrAc/H ₂ O	Unstable	2.06			\circ	0.0599	0.3331	0.1260
Propanol	PrOH	Saddle/ Stable	1.35	\square	\bullet	\bullet	0	1	0
Water	H ₂ O	Saddle	1.20	\square	\square	\square	0	0	0
Propyl acetate	PrAc	Saddle	1.13	\square	\square	\square	0	0	1
Acetic acid	AcAc	Stable	0.67	\bullet	\bullet	\bullet	1	0	0

When $Da = 1$ (as Figure 4.7b), Az. 2 and Az. 3 still remain their positions and stability, while the unstable node (Az. 1) no longer exists since propyl acetate and water start reacting. Instead, the unstable node moves into the composition tetrahedron and becomes the quaternary kinetic azeotrope. Moreover, the propanol apex becomes a stable node instead of a saddle point.

At $Da \rightarrow \infty$ (as Figure 4.7c), the reaction approaches its chemical equilibrium and the residue curves are first dominated by the reaction stoichiometry and then move along the equilibrium surface (as Figure 4.8) to the stable node. The unstable node meets a saddle point

branch, which emerges from the propanol-water edge (when $Da > 3.54$), on the equilibrium surface and results in the quaternary reactive azeotrope.

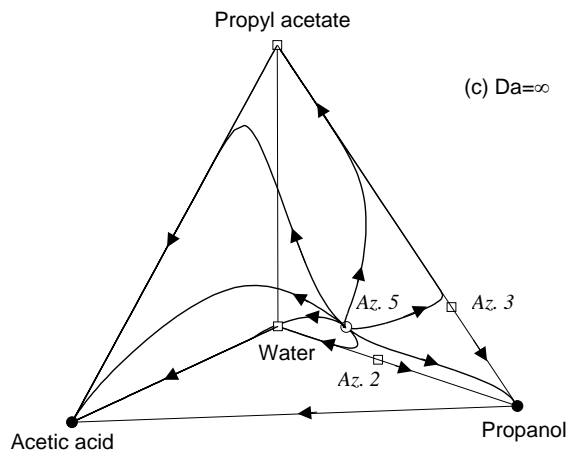
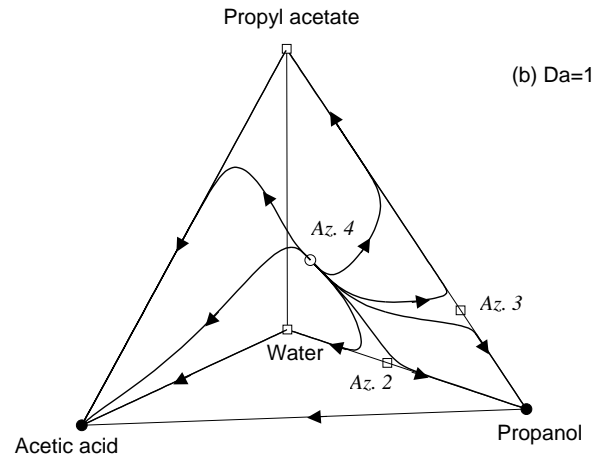
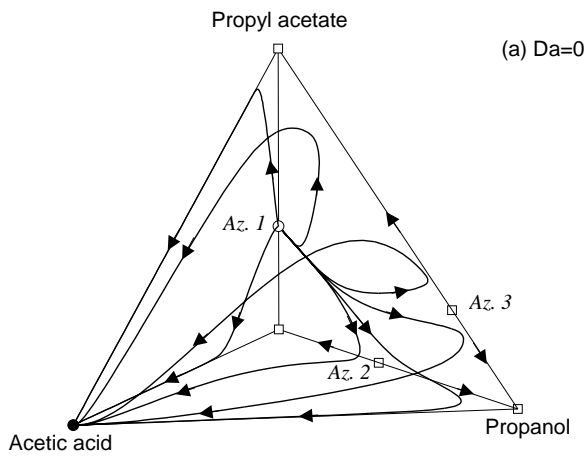


Figure 4.7 Residue curve maps for reactive distillation of propyl acetate synthesis reaction system at $T = 105\text{ }^\circ\text{C}$; (a) no chemical reaction, (b) kinetically controlled chemical reaction, (c) equilibrium controlled chemical reaction.

Abbreviation: Az = (Reactive, or kinetic) Azeotrope.

Legend: o Unstable Node, □ Saddle Point, ● Stable Node.

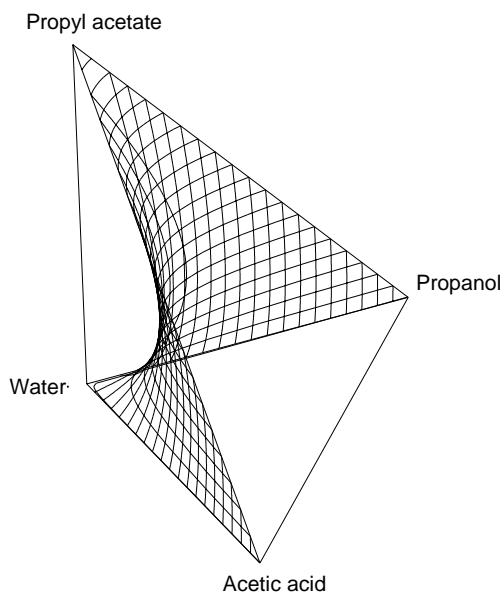


Figure 4.8 Surface of chemical equilibrium compositions for propyl acetate synthesis reaction system at $T = 105\text{ }^\circ\text{C}$.

With the help of the proposed theory, a similar analysis can be carried out for membrane reactors. Figure 4.9a shows the retentate phase diagram for the non-reactive membrane process at 105 °C. There are three non-reactive binary arrheotropes in the retentate diagram. The arrheotrope between propyl acetate and water (Ar. 1) is an unstable node, while the other two (Ar. 2, Ar. 3) are saddle points. Pure propanol, propyl acetate and water are also saddle points, while acetic acid is the only stable node at given conditions. Composition trajectory lines originate from the unstable node, first approaching the saddle points, and eventually converging to the stable node. All singular points are also listed in Table 4.2.

Table 4.2 List of singular points in Fig. 4.9 (Legend: o Unstable Node, □ Saddle Point, ● Stable Node).

Name	Composition	Type	Pressure [bar]	Da			x_1	x_2	x_3
				0	1	∞			
Arrheotrope 1	PrAc/H ₂ O	Unstable	2.40	o			0	0	0.3365
Arrheotrope 2	PrOH/ H ₂ O	Saddle	1.92	□	□	□	0	0.3707	0
Arrheotrope 3	PrOH/PrAc	Saddle	1.44	□	□	□	0	0.7742	0.2258
Arrheotrope 4	AcAc/PrOH /PrAc/H ₂ O	Unstable	2.31		o		0.0172	0.0890	0.2716
Arrheotrope 5	AcAc/PrOH /PrAc/H ₂ O	Unstable	2.06			o	0.0567	0.3027	0.0908
Propanol	PrOH	Saddle/ Stable	1.35	□	●	●	0	1	0
Water	H ₂ O	Saddle	1.20	□	□	□	0	0	0
Propyl acetate	PrAc	Saddle	1.13	□	□	□	0	0	1
Acetic acid	AcAc	Stable	0.67	●	●	●	1	0	0

If $Da = 1$ (Figure 4.9b), Ar. 2 and Ar. 3 still keep their locations and stabilities, but the unstable node (Ar. 1) no longer exists since propyl acetate and water start to react. Instead, the unstable node moves into the composition tetrahedron and becomes a quaternary unstable node Ar. 4 (*kinetic arrheotrope*). Moreover, the propanol apex turns to be a stable node instead of a saddle point.

At $Da \rightarrow \infty$ (Figure 4.9c), chemical equilibrium is established and the composition trajectories first approach the equilibrium surface following the reaction stoichiometry, and then move along this surface to the stable nodes A or B. The unstable node meets a saddle point branch, which emerges from the propanol-water edge (for $Da > 5.71$), on the equilibrium surface and results in the quaternary *reactive arrheotrope*, Ar. 5.

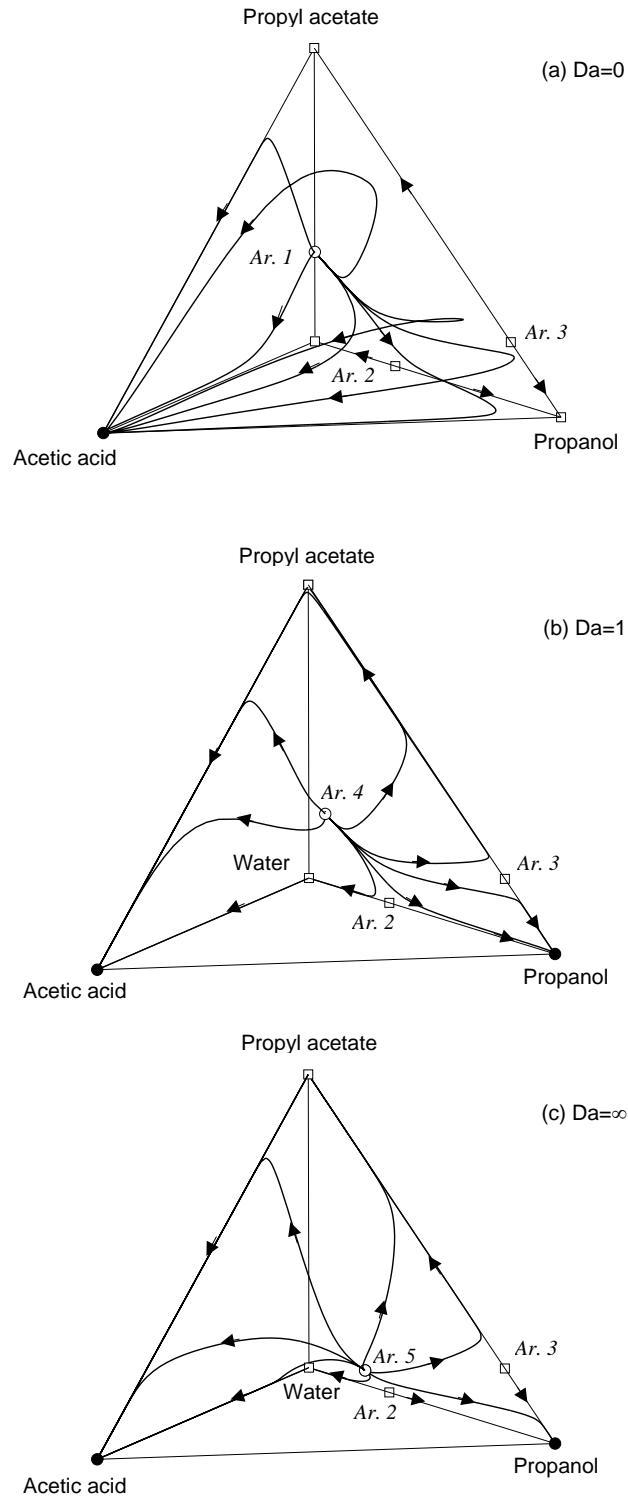


Figure 4.9 Retentate phase diagrams for propyl acetate synthesis reaction coupled with permeation through polyester membrane of 100 nm pore diameter at $T = 105\text{ }^{\circ}\text{C}$; (a) no chemical reaction, (b) kinetically controlled chemical reaction, (c) equilibrium controlled chemical reaction. Abbreviation: Ar = (Reactive, or kinetic) Arrheotrope. Legend: o Unstable Node, \square Saddle Point, \bullet Stable Node.

4.2.2 Singular point analysis

As can be seen from Section 4.2.1, the singular points influence and structure the topology of the retentate phase diagrams. Thus, bifurcation analysis of these points yields fast information on the feasibility of a certain process variant.

Figure 4.10a shows the bifurcation behavior of a simple reactive distillation process. The binary azeotrope between propyl acetate and water, Az. 1, moves into the composition tetrahedron when chemical reaction takes place ($Da > 0$). On the other hand, the binary azeotropes of propanol-water (Az. 2) and propanol-propyl acetate (Az. 3), still remain in reactive cases since these binary pairs do not react with each other. However, a saddle point branch emerges from Az. 2 when Da is larger than a critical value about 3.54, and then meets the unstable node branch at the reactive azeotrope when $Da \rightarrow \infty$. The other singular points remain their positions and stability at any Da , only except that propanol changes from a saddle point to a stable node when Da exceeds the critical value, 0.89.

Figure 4.10b also shows the bifurcation behavior but in the form of pressure versus the normalized Damköhler number, $Da / (Da + 1)$. It shows that in the non-reactive case, Az. 1 is the lightest component and therefore the unstable node, while acetic acid has the lowest pressure and behaves as a stable node. With the increasing Da , Az. 1 does not remain but moves towards the reactive azeotrope (Az. 5) instead. When $Da > 0.89$, propanol becomes another stable node in addition to acetic acid. When $Da > 3.54$, there appears another quaternary azeotrope as a saddle point, which joins the reactive azeotrope when $Da \rightarrow \infty$.

Analogously, Figure 4.11 shows the singular point analysis of the membrane reactor. Figure 4.10 and Figure 4.11 are qualitatively similar due to the reason that the selectivity induced by the 100 nm-pore-diameter membrane at 105 °C is quite limited. Quantitatively speaking, the loci of potential singular point curves (Figure 4.10a and Figure 4.11a) are different, and the critical values at which the additional saddle point branch emerges are 3.54 (Figure 4.10b) and 5.23 (Figure 4.11b), respectively.

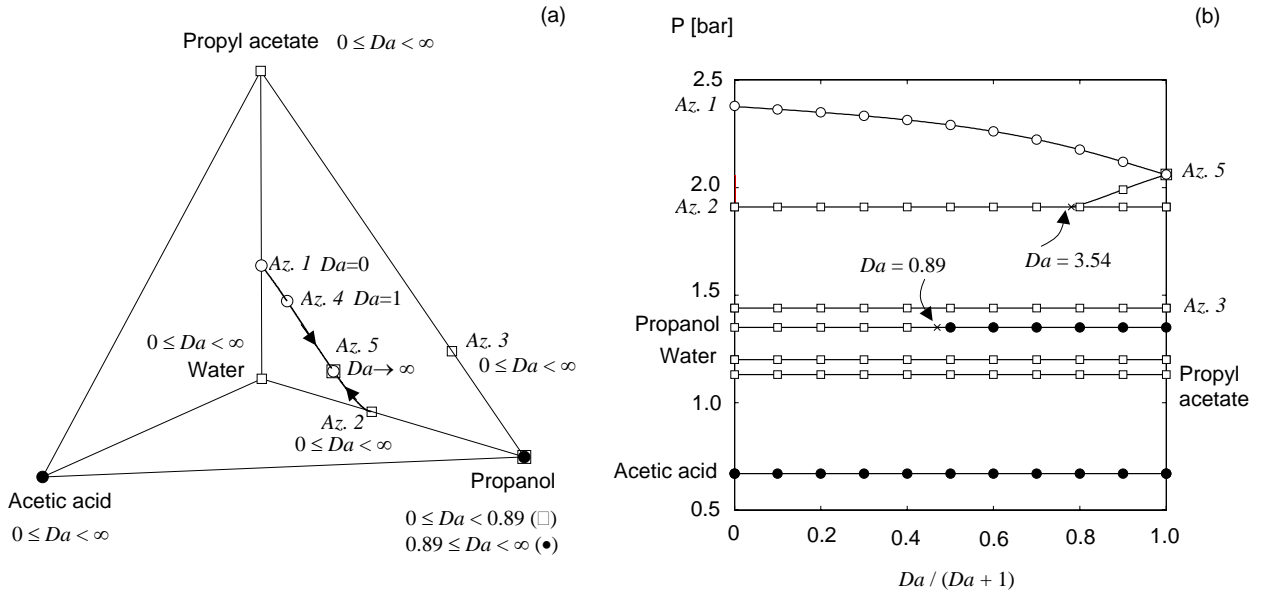


Figure 4.10 (a) Singular point loci and bifurcation behavior for reactive distillation at 105 °C. (b) Bifurcation behavior of reactive distillation at 105 °C, in the form of pressure versus normalized Damköhler number. Legend: o Unstable Node, □ Saddle Point, ● Stable Node.

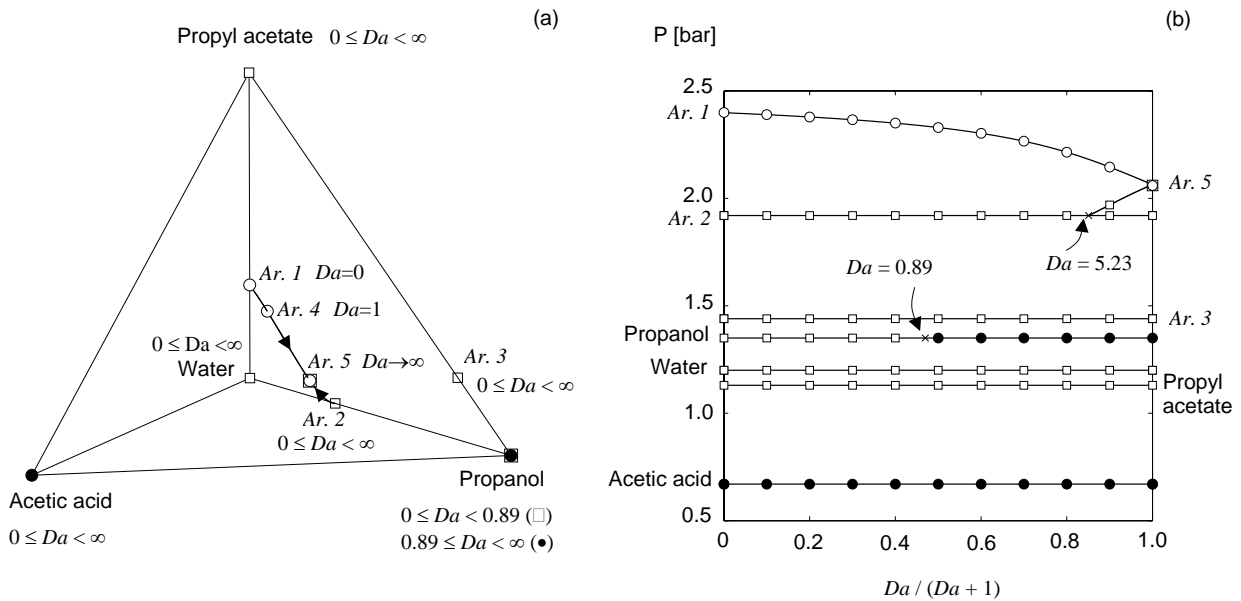


Figure 4.11 Potential singular point curve and bifurcation behavior for propyl acetate synthesis reaction coupled with permeation through polyester membrane of 100 nm pore size at 105 °C; (a) within the composition tetrahedron, (b) in the form of pressure versus normalized Damköhler number. Abbreviation: Ar = (Reactive or kinetic) Arrheotrope. Legend: o Unstable Node, □ Saddle Point, ● Stable Node

For the considered porous membranes, the pore diameter d_p is the most important property which can be changed to influence the selectivity. Thus, singular point analysis is performed with respect to the pore diameter (see Figure 4.12). At chemical equilibrium controlled operation ($Da \rightarrow \infty$), there are two binary azeotrope branches between propanol / propyl acetate and propanol / water, and a quaternary branch. These singular point branches approach the (reactive) azeotropes if the pore diameter is larger than a few microns. In this situation, the membrane does not induce any additional selectivity to the separation process. If the pore diameter is less than a few nanometers, the membrane induces the maximum additional selectivity which is exerted by Knudsen diffusion as accounted for in the dusty gas model.

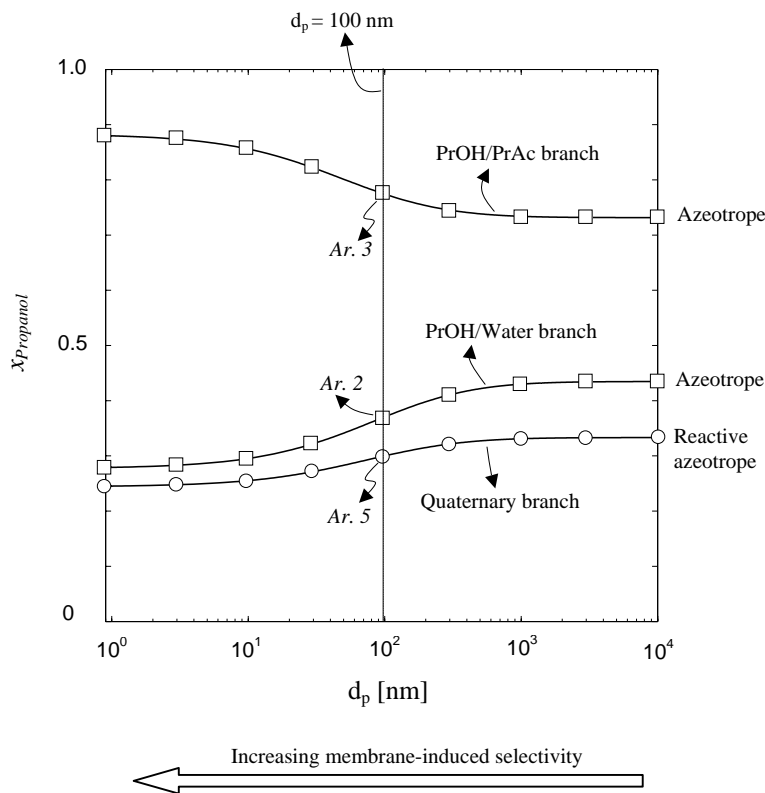


Figure 4.12 Bifurcation behavior with respect to pore diameter (at $Da \rightarrow \infty$) for propyl acetate synthesis reaction coupled with permeation through polyester membrane at 105 °C. Abbreviation: Ar = (Reactive) Arrhenius. Legend: o Unstable Node, □ Saddle Point, • Stable Node.

4.3 Chapter conclusions

In this chapter, the proposed analysis methodology is applied to two examples of quaternary systems. In the first hypothetical system, it has been shown that the membrane with low selectivity can change the locations of singular points; with the even higher selectivity, the membrane can even change the stability of those singular points. This implies certain desired products which are not attainable by simple open distillation can be attained with the help of suitable membranes.

Geometrically speaking, the reactive azeotropic conditions for a quaternary system give two surfaces in the composition space, and the intersection of these two surfaces determines the curve on which all potential singular points are located. Singular points analysis can be carried out not only with respect to the Damköhler number but also with respect to the properties of membranes. This can give valuable information on the selection of a suitable membrane material.

In the practical example, the esterification of acetic acid with propanol, the dusty gas model is applied to describe the diffusion through porous polyester membranes. The locations of singular points can be shifted due to the different transport rates through the membrane. Bifurcation analysis has been carried out with respect to the Damköhler number and the membrane pore size. In particular when $Da \rightarrow \infty$, the occurrence of a quaternary reactive azeotrope is predicted. Experiments are presented to validate the prediction in Chapter 6.

5. Kinetics of propyl acetate synthesis reaction

Information on reaction kinetics is needed for the feasibility study within the transition from non-reactive conditions to equilibrium controlled reactive conditions (i.e. for $0 < Da < \infty$). For the propyl acetate synthesis reaction catalyzed by the commercial cation-exchange resin Amberlyst 15, the reaction kinetics is not available in the literature. Moreover, the chemical equilibrium constant extracted from the literature [54-55] does not result in a good prediction for the subsequent residue curve map measurement (see Chapter 6). Therefore the kinetics of this reaction is investigated experimentally [52].

The reaction scheme reads as Eq.(4.5); the chemical equilibrium constant was first determined separately by long time experiments. Totally fourteen sets of kinetic data were then measured with different conditions. Three typical kinetic models, viz. the pseudo-homogeneous (PH), Rideal-Eley (RE), and Langmuir-Hinshelwood-Hougen-Watson (LHHW) models were applied to interpret the experimental data. The parameters of the kinetic models and their confidence intervals were estimated by the in-house software DIVA. The influences of the operating parameters such as temperature, initial molar ratio of reactants and catalyst amount were also checked.

In the literature, the parameter identification of LHHW models has been reported several times to suffer from convergence problems especially for esterification reactions (e.g. [56-58]). To overcome this convergence problem, a useful solution was proposed in this chapter such that the parameter identification of LHHW model for the esterification reaction can be accomplished directly from the kinetic data, without carrying out any extra non-reactive adsorption experiments (e.g. [56, 59]), and without any presumptions concerning negligible parameters (e.g. [54, 60]).

5.1 Experiments

5.1.1 Materials

Acetic acid (99-100%, Merck), propanol (>99%, Merck) and propyl acetate (>98%,

Merck) were used as reactants; the commercial cation-exchange resin, Amberlyst[®] 15, was used to catalyze the reaction. The specifications of the Amberlyst 15 catalyst are listed in Table 5.1; the particle size and pore diameter are confirmed by SEM (Figure 5.1).

Table 5.1 Specifications of Amberlyst 15 catalyst

Appearance	Beige, grey-brown spherules
Particle size (mm)	0.355 ~ 1.18 (> 90 %)
Average pore diameter (nm)	30 ~ 80
Density (g/cm ³)	0.6
Surface area (m ² /g)	50
Proton concentration (meq H ⁺ /g)	4.7 (dry)
Degree of cross-linking (wt.%)	20
Porosity	0.36
Temperature tolerance	< 120 °C

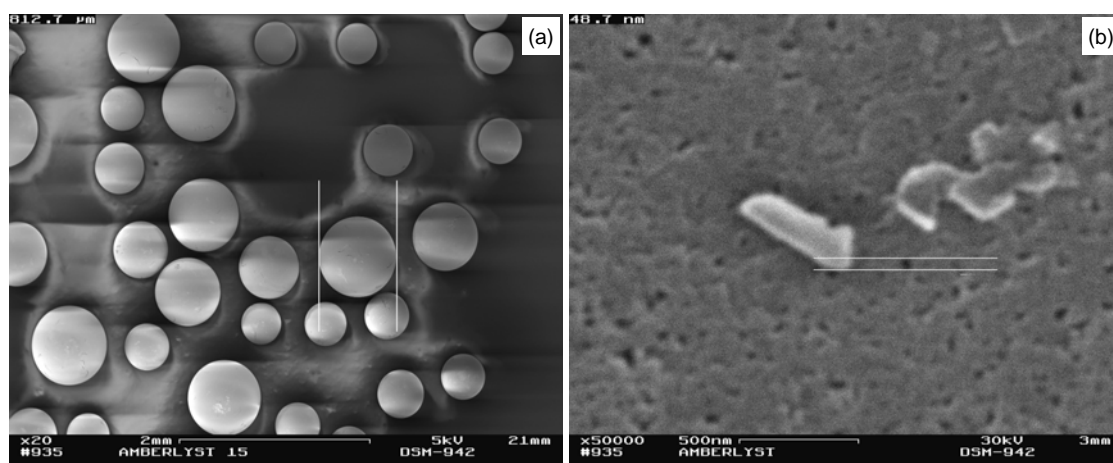


Figure 5.1 SEM image of Amberlyst 15: (a) Particle size (b) Pore diameter.

5.1.2 Experimental setup

To minimize the liquid composition change due to evaporation, the experiments were carried out in a sealed, steel-jacketed reactor of 1.57 liters volume (10 cm inner diameter × 20 cm height). It was operated isothermally in the batch mode and magnetically stirred. The reactor was equipped with temperature and pressure sensors, and a blow-off safety valve. The

set temperature was regulated by the thermostat (Julabo, F30-C). Samples were taken via the sampling hole, which was sealed with the silicone pad; the syringe capped with the 30 cm-long needle (Rettberg, Germany) pierced through the pad to take samples from the reacting liquid phase.

5.1.3 Analysis of liquid phase composition

The samples were analyzed by a gas chromatography (Hewlett-Packard, HP6890 series) where the mixtures were separated in a cross-linked polyethylene glycol column (HP-INNOWAX, Part No: 19091N-133). The column temperature was programmed with a 2 minutes initial hold at 50 °C, followed by a 50 °C/min ramp up to 130 °C and held for 2.5 minutes. Both the thermal conductivity detector (TCD) and the flame ionization detector (FID) were used for peak detection. Due to the fact that propanol and water have an inseparable peak time in the column, the water amount was calculated by subtraction of the TCD and FID signals. To guarantee a controlled error of such a subtraction method, the GC was recalibrated when the compositions calculated by TCD and FID differed from each other for more than 1.5%.

Table 5.2 Experimental conditions of the reaction kinetic study.

Run No.	Temperature (K)	Catalyst (g)	$x_{AcAc,0}$	$x_{PrOHc,0}$	$x_{PrAc,0}$
1	353	5.0	0.5	0.5	0
2	338	5.0	0.2	0.8	0
3	368	3.5	0.2	0.8	0
4	368	2.0	0.2	0.8	0
5	368	5.0	0.2	0.8	0
6	353	3.5	0.8	0.2	0
7	368	5.0	0.5	0.5	0
8	338	3.5	0.8	0.2	0
9	338	5.0	0.5	0.5	0
10	368	2.0	0.8	0.2	0
11	353	2.0	0.8	0.2	0
12	338	3.5	0.5	0.5	0
13	368	2.0	0.5	0.5	0
14	353	5.0	0.35	0.35	0.3

5.1.4 Procedure

Mixtures of totally three moles were prepared with different initial molar ratios, and then poured into the reactor. The reactor was then closed and heated. When the liquid mixture was heated up to the set temperature, the catalyst was added into the reactor through a peephole on the lid, which was then sealed, and this moment was considered as the starting time. Samples of approximately 1 ml were taken every 5 ~ 10 minutes for the first hour, and 20 ~ 40 minutes for the next 3 ~ 4 hours. Totally 14 runs, as listed in Table 5.2, were performed and used to discriminate the kinetic models.

5.2 Results

5.2.1 Exclusion of external mass transfer influence

The reactor of 10 cm inner diameter was stirred by an 8 cm-long triangular magnetic bar. To confirm the exclusion of solid-liquid interphase mass transfer effects on the kinetics, three stirring speeds (150, 250 and 300 rpm) were tested preliminarily. There was no appreciable difference among these agitation conditions. The magnetic stirrer was operated at a speed of 300 rpm in the subsequent experiments.

5.2.2 Chemical equilibrium constant

In principle, the chemical equilibrium constant can be determined either by the thermodynamic data (the enthalpies and free energies of formation of all components, $\Delta_f H$ and $\Delta_f G$), or by long time experiments. However, the estimation based on the thermodynamic data is usually much less reliable due to the fact that a small deviation in $\Delta_f H$ and $\Delta_f G$ can lead to a relatively large error in the reaction enthalpy $\Delta_r H$ and the reaction free energy $\Delta_r G$, and thus the equilibrium constant K . Moreover, for the considered reaction system, the necessary thermodynamic data of propyl acetate are not available; therefore, the equilibrium constant is determined experimentally.

Long time experiments were performed independently to determine the equilibrium constant K . The procedure was similar as described previously, but fewer samples were taken. Each run lasted for longer time (≥ 10 hours), and the equilibrium was judged to be reached when no measurable concentration changes were observed. The results are listed in Table 5.3.

Table 5.3 Equilibrium constants at different conditions.

Temperature (K)	$x_{AcAc,0} : x_{PrOH,0}$	K
338	1 : 1	18.706
353	1 : 1	19.643
353	1 : 4	21.409
353	4 : 1	17.474
368	1 : 1	20.971
368	1 : 4	22.382
368	4 : 1	19.202

The equilibrium constants are formulated in terms of the liquid phase activity (Eq. 5.1); while the activity coefficients (γ_i) are calculated by the NRTL equation [50].

$$K = \frac{a_{PrAc} \cdot a_{H_2O}}{a_{AcAc} \cdot a_{PrOH}} = \frac{x_{PrAc} \cdot x_{H_2O}}{x_{AcAc} \cdot x_{PrOH}} \cdot \frac{\gamma_{PrAc} \cdot \gamma_{H_2O}}{\gamma_{AcAc} \cdot \gamma_{PrOH}} \quad (5.1)$$

It can be seen from Table 5.3 that the equilibrium constant is slightly temperature dependent within the range 338 K ~ 368 K. The temperature dependence of K can be found by the linear regression of all data points in the plot of $\ln K$ versus the reciprocal temperature ($1/T$) as shown in Figure 5.2:

$$\ln K = \frac{-475.42}{T} + 4.3223 \quad (5.2)$$

5.2.3 Reaction enthalpy, entropy and free energy

If a constant reaction enthalpy is assumed within the operating temperature range, the reaction enthalpy ($\Delta_r H$) and entropy ($\Delta_r S$) can be estimated by setting the experimental values of Eq.(5.2) into Eq.(5.3):

$$\ln K = \frac{-\Delta_r H}{RT} + \frac{\Delta_r S}{R} \quad (5.3)$$

Consequently the reaction enthalpy $\Delta_r H$ and reaction entropy $\Delta_r S$ are found to be 3952.6 J/mol and 35.9356 J/mol·K respectively. Furthermore, the liquid phase reaction free energy change can be calculated to be:

$$\Delta_r G = \Delta_r H - T \cdot \Delta_r S = 3952.6 - 298 \times 35.9356 = -6756.2 \quad (\text{J/mol}) \quad (5.4)$$

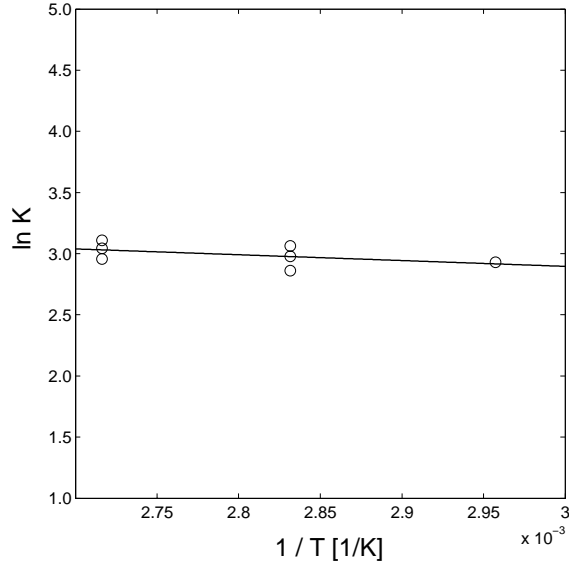


Figure 5.2 Regression of $\ln K$ v.s $1/T$

5.2.4 Effect of catalyst amount

The concentration profile is plotted for different catalyst amounts in Figure 5.3a. For the same conditions of temperature and initial molar fraction, the reaction rate increases in proportion to the catalyst amount added. This can be seen from Figure 5.3b that the increase in catalyst amount results in equal acceleration of the initial reaction rate $R_i (t \rightarrow 0)$. Thus it is reasonable to presume the proportionality of reaction rate R_i and M_{cat} .

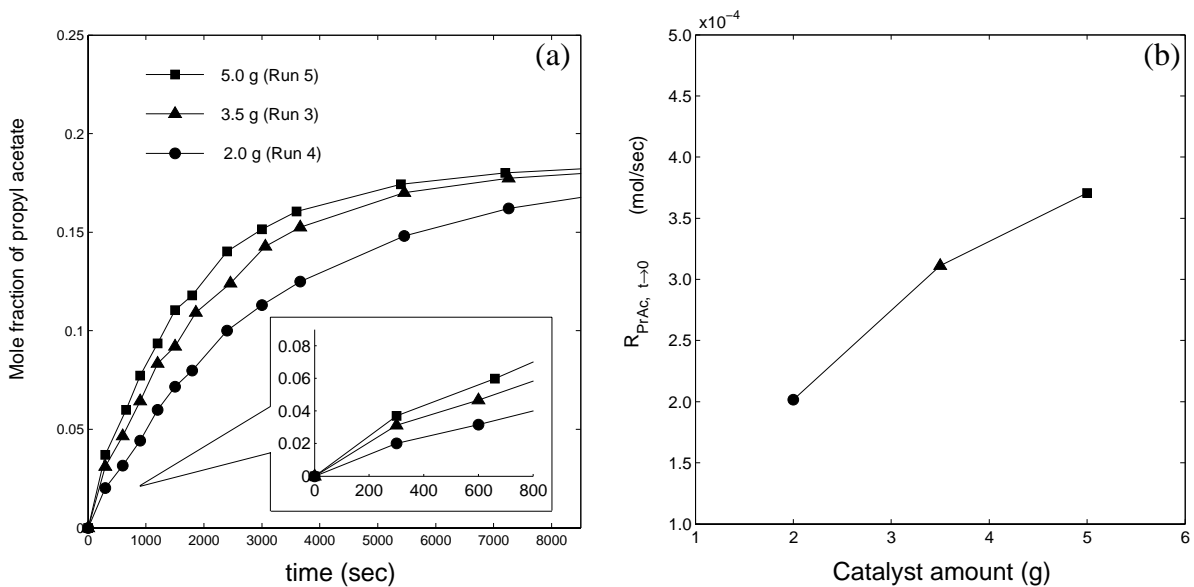


Figure 5.3 Effect of catalyst loading ($T = 368 \text{ K}$, $N_{tot} = 3.0 \text{ mol}$, $x_{AcAc,0} / x_{PrOH,0} = 1 : 4$). (a) Mole fraction profiles of different M_{cat} ; (b) Initial reaction rates v.s. M_{cat} .

5.2.5 Effect of temperature

The influence of the temperature on the reaction rate is illustrated in Figure 5.4. As expected, the reaction rate increases with temperature. The temperature dependency of the forward rate constant k_f is assumed to obey the Arrhenius equation and the activation energy will be estimated from the kinetic data as shown later.

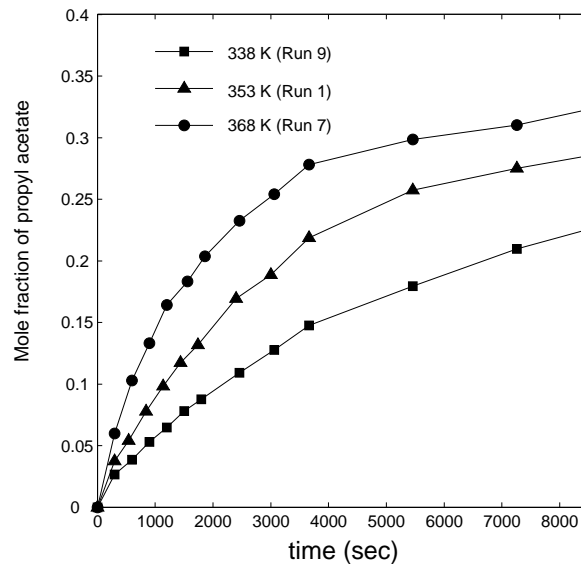


Figure 5.4 Effect of temperature. ($N_{tot} = 3.0$ mol, $x_{AcAc,0} / x_{PrOH,0} = 1 : 1$, $M_{cat} = 5.0$ g).

5.2.6 Effect of initial mole fraction

The concentration profile of propyl acetate is plotted for different initial molar ratios between acetic acid and propanol in Figure 5.5. Qualitatively speaking, equal initial molar ratios lead to the highest equilibrium composition of propyl acetate; while for asymmetric initial molar ratios, the run with higher acetic acid content ($x_{AcAc,0} : x_{PrOH,0} = 4 : 1$) shows a higher reaction rate than with an excess of propanol (1 : 4).

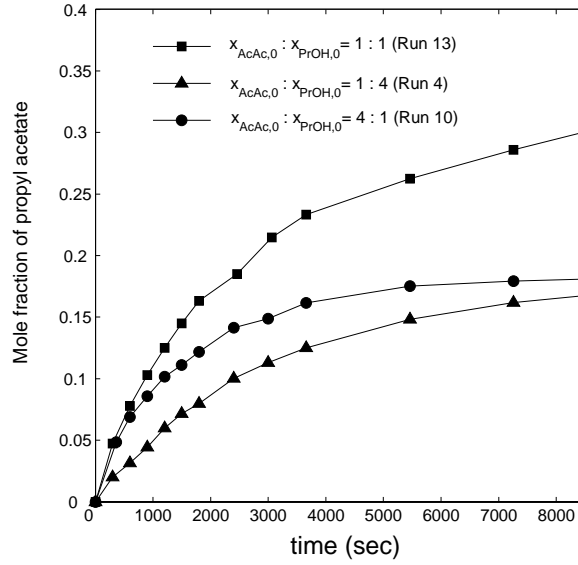


Figure 5.5 Effect of initial molar ratio of acetic acid and propanol ($T = 368\text{ K}$, $N_{tot} = 3.0\text{ mol}$, $M_{cat} = 2.0\text{ g}$).

5.2.7 Mathematical formulation of kinetic models

In this work three typical kinetic models were selected to interpret the obtained kinetic data, that is, the pseudo-homogeneous (PH), Rideal-Eley (RE) and Langmuir-Hinshelwood-Hougen-Watson (LHHW) models. The PH rate equation for the esterification reads as:

$$R_i \equiv N_{tot} \cdot \frac{dx_i}{dt} = M_{cat} \cdot r_i = M_{cat} \cdot \nu_i \cdot k_f \cdot \left(a_{AcAc} a_{PrOH} - \frac{1}{K} a_{PrAc} a_{H_2O} \right) \quad (5.5)$$

where R_i is the apparent reaction rate, defined as the increasing (or decreasing) amount of component i per unit time. r_i is the intensive reaction rate, defined as R_i divided by the catalyst amount. N_{tot} is total number of moles, ν_i the stoichiometric coefficient of component i , M_{cat} the catalyst amount, k_f the forward rate constant, $a_i = x_i \gamma_i$ the activity of component i , and K the equilibrium constant.

The heterogeneous LHHW model represents a mechanism wherein all components can be adsorbed on the catalyst surface, and the chemical reaction occurs between the adsorbed molecules. Assuming that the surface reaction in the adsorbed phase is the rate-determining step, the LHHW rate equation can be derived (see Appendix A.5) as:

$$\begin{aligned}
R_i &\equiv N_{tot} \cdot \frac{dx_i}{dt} = M_{cat} \cdot r_i \\
&= M_{cat} \cdot v_i \cdot k_f \cdot \frac{\left(a_{AcAc} a_{PrOH} - \frac{1}{K} a_{PrAc} a_{H_2O} \right)}{\left(1 + K_{S,AcAc} a_{AcAc} + K_{S,PrOH} a_{PrOH} + K_{S,PrAc} a_{PrAc} + K_{S,H_2O} a_{H_2O} \right)^2}
\end{aligned} \tag{5.6}$$

Comparing with the PH model, the extra parameters in Eq.(5.6) are the adsorption constants ($K_{S,i}$), which are considered temperature independent within the experimental range.

In contrast to the LHHW model, the RE model assumes that one (or some) of the components is not adsorbed by the catalyst. If propyl acetate is considered non-adsorbable on the catalyst, the RE rate equation can be written as (see Appendix A.5):

$$\begin{aligned}
R_i &\equiv N_{tot} \cdot \frac{dx_i}{dt} = M_{cat} \cdot r_i \\
&= M_{cat} \cdot v_i \cdot k_f \cdot \frac{\left(a_{AcAc} a_{PrOH} - \frac{1}{K} a_{PrAc} a_{H_2O} \right)}{\left(1 + K_{S,AcAc} a_{AcAc} + K_{S,PrOH} a_{PrOH} + K_{S,H_2O} a_{H_2O} \right)^2}
\end{aligned} \tag{5.7}$$

The temperature dependency of forward rate constant k_f in Eqs. (5.5) ~ (5.7) is assumed to obey the Arrhenius equation:

$$k_f = k_{f0} \cdot \exp(-E_f / RT) \tag{5.8}$$

where the pre-exponential term k_{f0} represents the frequency factor, and E_f the activation energy.

5.2.8 Parameter identification

The kinetic data were obtained to identify the parameters of the above kinetic models. Since the equilibrium constant is determined by Eq. (5.2), the adjustable parameters in Eqs. (5.5) ~ (5.7) include the frequency factor k_{f0} , the activation energy E_f , and the adsorption constants $K_{S,i}$. Thus, the numbers of parameters to be identified in the PH, LHHW and RE models are 2, 6, and 5 respectively.

The objective of the data-fitting procedure is to minimize the quadratic sum (QS) of the deviation between the experimental data and the model prediction.

$$QS = \sum_{all\ samples} (x_{PrAc, exp} - x_{PrAc, model})^2 \tag{5.9}$$

The parameter identification was realized by the in-house software DIVA (Dynamic Simulator für Verfahrenstechnische Anlagen) [61]. For parameter identification problems, the confidence interval is also of primary importance because it provides a measure to judge the accuracy of parameter estimates. For the non-linear rate equations, Eqs.(5.5)-(5.7), the confidence interval of each parameter can be obtained by the linearization approximation (e.g. [62]). The fitting results and the confidence intervals are given in Table 5.4.

Table 5.4 Results of parameter identification and confidence interval estimation for kinetic models

Model	k_{f0} (mol/g.sec)	E_f (J/mol)	$K_{S,AcAc}$	$K_{S,PrOH}$	$K_{S,PrAc}$	$K_{S,H2O}$	QS
PH	1.2556×10^4 $\pm 0.044\%$	5.0791×10^4 $\pm 0.002\%$	-	-	-	-	0.418
LHHW	2.7163×10^6 $\pm 1.498\%$	5.4572×10^4 $\pm 0.002\%$	4.5383 $\pm 0.910\%$	7.9183 $\pm 0.834\%$	1.4662 $\pm 1.134\%$	8.7032 $\pm 0.774\%$	0.100
RE	2.7414×10^6 $\pm 0.248\%$	5.5084×10^4 $\pm 0.002\%$	4.1074 $\pm 0.150\%$	7.1982 $\pm 0.136\%$	-	8.9547 $\pm 0.132\%$	0.104

According to the quadratic sum of deviation, QS , the heterogeneous (LHHW, RE) models fit the experimental data significantly better than the PH model. The obtained adsorption constants show that water is the most adsorbable on the catalyst, followed by propanol, acetic acid, and then propyl acetate. The comparison of predicted curves and the experimental data is illustrated in Figure 5.6. Moreover, upon the results of LHHW and RE models, the activation energy E_f is estimated to be 54.828 ± 0.256 kJ/mol.

Generally speaking, the confidence intervals of estimated parameters are satisfactorily small in Table 5.4. Nevertheless, two evident characteristics can be seen from the result. First, in all three models the confidence interval of activation energy E_f is much smaller than the other parameters, because it is the unique parameter that reflects the temperature dependency and thus can be easily discriminated. Second, the confidence intervals of parameters in the PH model are most satisfactory, followed by the RE model, while the confidence intervals are relatively large in the LHHW model. This is due to the reason that the frequency factor k_{f0} is correlated with the adsorption constants $K_{S,i}$ in the heterogeneous kinetic models.

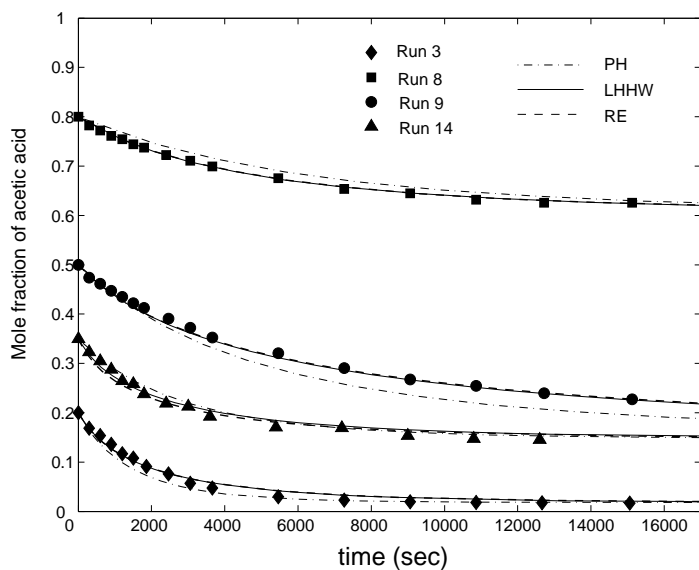


Figure 5.6 Comparison of experimental data and model prediction for three different kinetic models.

5.3 LHHW model parameter identification issue

In a previous work of the same reaction system [55], the authors reported that an RE model wherein the adsorption of acetic acid is the rate determining step, gave the best fitting results among the thirteen mechanisms of consideration. However, from the mathematical point of view, the RE models can be regarded as a subset of the LHHW models when one or some of the components are not adsorbable on the catalyst (e.g. $K_{S,PrAc} = 0$); therefore it is unreasonable that RE models could give better fitting results than the LHHW models, unless the fitting procedures are not treated equally well for both models. It is believed that, similar as reported elsewhere (e.g. [56-58]), the authors of [55] either had a convergence problem or got the negative adsorption constant values for LHHW model, which they did not point out.

This convergence problem of identifying the LHHW model parameters has been reported several times in the literature especially for the esterification reactions. Previously, to apply LHHW models to the esterification reactions, researchers either predetermined the adsorption constants by separate non-reactive adsorption experiments, or presumed some of them negligible. In fact, such a convergence difficulty was also encountered in this work at first, but this could be easily solved by the incorporation of an additional experiment 14 (*cf.* Table 5.2), wherein the molar concentrations of ester and water were kept different.

Mathematically speaking, this convergence problem is due to the fact that the adsorption effects of the ester and water are “coupled” to each other. As a convention of

kinetics study of esterification reactions, the experiments are often conducted with the initial compositions of the acid and the alcohol; consequently, the mole fractions of ester and water are always the same through the whole experiment because of the reaction stoichiometry. The adsorption constants of ester and water can be “decoupled” by applying the initial molar ratio that bears significant difference between the concentrations of ester and water, for example, Run 14 in this work.

5.4 Chapter conclusions

The reaction kinetics of esterification of acetic acid with propanol has been studied. The reaction was catalyzed by the cation-exchange resin Amberlyst 15. The kinetic data were obtained in a batch reactor within the temperature range 338 K - 368 K. The equilibrium constant was determined experimentally and found to be slightly temperature-dependent. The standard reaction enthalpy and free energy were estimated to be $\Delta_r H = 3952.6 \text{ J/mol}$ and $\Delta_r G = -6756.2 \text{ J/mol}$, respectively. Three kinetic models (PH, RE, LHHW) were then developed to interpret the kinetic data. Parameters of the kinetic models and the confidence interval of each parameter were estimated from the obtained kinetic data. The LHHW model gives the best fitting result, followed by the RE model, and then the PH model, while the confidence interval of estimated parameters ranks in the reverse order. The activation energy was estimated from the heterogeneous kinetic models as $54.828 \pm 0.256 \text{ kJ/mol}$. An additional run of kinetic measurements wherein the initial concentration of propyl acetate and water were different was incorporated to solve the convergence problem of parameter identification in the LHHW model.

6. Experimental validation of proposed theory

In this chapter, experiments were carried out to validate the existence of a reactive azeotrope and a reactive arrheotrope in the propyl acetate synthesis reaction system. The residue curve map and retentate phase diagram of chemical equilibrium controlled case (i.e. $Da \rightarrow \infty$) were measured. The experiments were first performed for reactive distillation to indicate the location of the reactive azeotrope, and provide a basis for the subsequent comparison with the membrane process. Then, similar measurements were implemented with the incorporation of a porous polymeric membrane of 100 nm pore diameter to demonstrate the effect of mass transfer kinetics, in particular on the displacement of the unstable node from the reactive azeotrope to the reactive arrheotrope.

In both cases the isothermal heating policy was applied. For reactive distillation, the system was operated at 105 °C to provide a positive gauge pressure in the vessel, in order to drive out the vapor through the outlet valve. On the other hand, for the membrane case vacuum was applied on the permeation side which adequately provides the driving force for membrane permeation. According to the dusty gas model, the selectivity of porous membranes decreases sharply with the increasing system pressure; therefore, the experiments were preferably operated at a lower temperature⁴ 80 °C mainly for two reasons: (i) to sustain a significant membrane selectivity, and (ii) to reduce the capillary condensation phenomenon within the membrane pores by keeping a sufficient temperature difference between the permeating vapors and the membrane, which has a reported maximum temperature tolerance of 140 °C.

⁴ The lowered temperature was found helpful to relieve the capillary condensation problem. However, the displacement between the reactive azeotrope and reactive arrheotrope is not caused by the different operating temperatures, but by the membrane (see Appendix A.6).

6.1 Experimental setup for reactive distillation process

The materials and the composition analysis method are the same as described in the previous chapter. The experiments were carried out in the same steel-jacketed vessel as described in Section 5.1.2, except that a regulating valve was installed to allow the vapor outlet as shown in Figure 6.1. It was operated in a batch mode, and magnetically stirred at 300 rpm. The set temperature, 105 °C, was regulated by the thermostat.

According to the simulation result shown in Figure 4.7c, there exists a quaternary reactive azeotrope in this reaction system when $Da \rightarrow \infty$. Residue curves were measured to validate this prediction.

Mixtures of initial compositions close to the reactive azeotrope, which is an unstable node, were prepared to start a residue curve. The mixture and the catalyst were added into the reactor, closed and heated up to the set temperature of 105 °C. The liquid composition was measured by taking samples (~0.5 ml/sample) every 10 minutes, which were analyzed by gas chromatography. When the liquid residue amount was too small to take any more samples, this run was ended. The subsequent run was started with the initial composition close to the final point of the previous run. Several runs were repeated until they constituted a sufficient portion of one residue curve. To guarantee a sufficiently high Da , the relationship of catalyst concentration and escaping flow rate was checked. The escaping flow rate was controlled ~40 ml/hr by the regulating valve; under this condition, 25 g dry catalyst in 300 ml initial liquid volume could approach the prediction well. To give the safety factor of 20%, 30 g catalyst was used in the initial liquid volume of 300 ml in this work.

Due to the partial solubility between propyl acetate and water, special attention was paid to check the possible liquid phase splitting when taking every sample [63]. Nevertheless the phase splitting was not observed through the whole experiments. The heterogeneous reactive azeotrope predicted in the literature [63] is based on a higher equilibrium constant ($K = 48.8$) extrapolated from [55], which is different from the result of kinetics study in the previous chapter. The residue curve map prediction based on this higher equilibrium constant also doesn't fit well with the following experimental results.

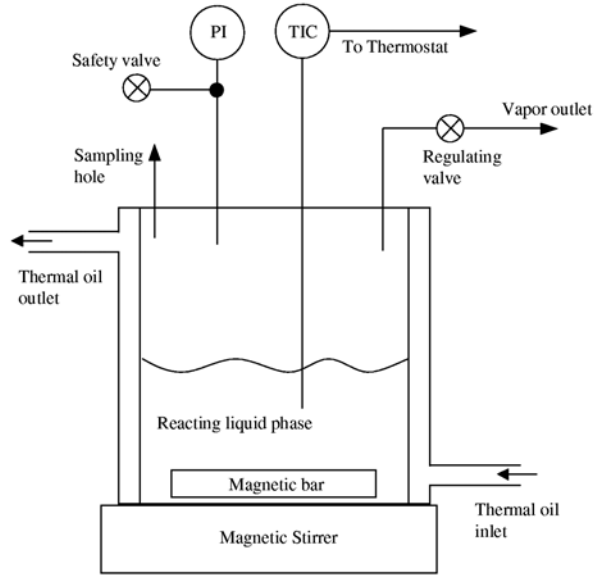


Figure 6.1 Experimental setup for reactive distillation residue curves measurement.

6.2 Validation of reactive azeotrope

The measurement results in the reactive distillation process are plotted as in Figure 6.2. For better visualization, the transformed coordinates are used [26, 45] where propyl acetate is selected as the reference component as in Eq.(6.1). One should note that Figure 6.2 and Figure 4.7c are equivalent, but plotted in different coordinates.

$$\begin{aligned}
 X_A &= x_{AcAc} + x_{PrAc} \\
 X_B &= x_{PrOH} + x_{PrAc} \\
 X_C &= x_{H_2O} - x_{PrAc} = 1 - X_A - X_B
 \end{aligned}
 \tag{6.1}$$

Different residue curves are designated by different symbols, and different colors in one curve represent different runs of experiments. Total 36 runs were performed to constitute eight curves originating around the reactive azeotrope whose molar fraction is 5.99% acetic acid, 33.31% propanol, 12.60% propyl acetate and 48.10% water. The liquid composition changes slowly near the unstable node so that data points cluster closely. The experimental results are in good agreement with the prediction and thus validate the existence of a reactive azeotrope under the isothermal operation (*c.f.* [22]).

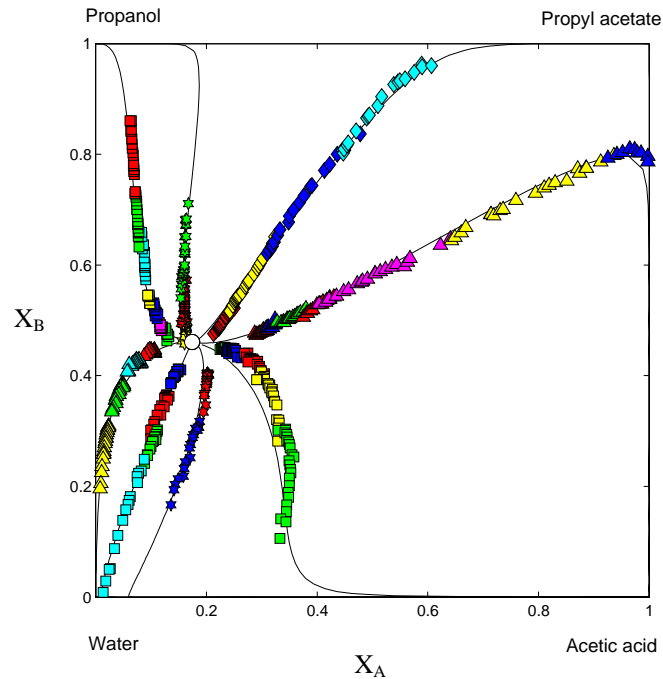


Figure 6.2 Residue curve map for reactive distillation of propyl acetate synthesis reaction ($Da \rightarrow \infty$) at $T = 105$ °C. Legend: o reactive azeotrope; solid lines (—): simulated residue curves; colorful symbols ($\Delta \diamond \square \dots$): experimental data.

6.3 Experimental setup for membrane reactor process

As predicted in Section 4.2, the permeation through porous media can shift the location of the reactive azeotrope (validated in Figure 6.2) towards the reactive arrheotrope. To verify this prediction, a porous polyester membrane with 100 nm pore diameter is applied. This commercially available membrane (Whatman, UK) is made of a transparent polyester film; the pores are opened by the track-etch process and thus have a rather narrow size distribution. The membrane was installed onto the lid, and mechanically supported by the porous steel plate with 1 mm diameter pores on top. Vacuum was applied on the permeation side to provide the driving force of permeation, and the reacting liquid phase was kept at 80 °C by the thermostat.

The goal of this experiment is to validate the prediction of a reactive arrheotrope under the influence of a membrane that is quantified by the dusty gas model (DGM). Mass transfer mechanisms other than the DGM must be suppressed. These include the boundary layer mass transfer resistance on the retentate side of the membrane and the capillary condensation in the membrane pores.

The preliminary measurements were not successful. Improvements were then made to accomplish the measurements, and the experiment with an initial composition between the reactive azeotrope and reactive arrheotrope (*c.f.* Figure 6.3) was used as the indication for troubleshooting. If the membrane-induced selectivity functions well, the composition trajectory goes upwards; if the membrane selectivity is eliminated by other mechanisms, it goes downwards (as in the reactive distillation case). The resulting experimental setup is depicted as Figure 6.4, and the improvement actions are summarized in the following sections.

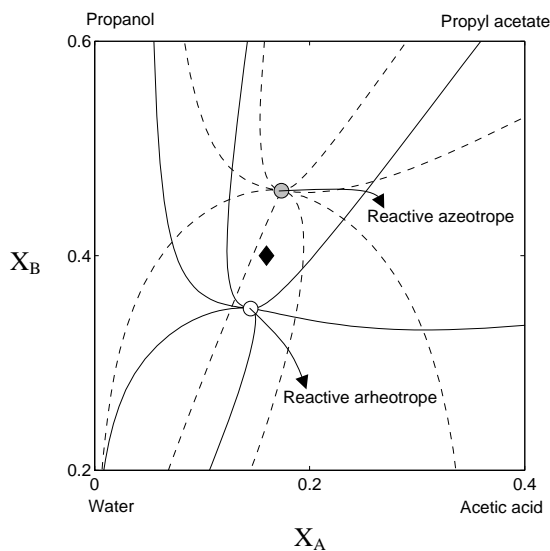


Figure 6.3 Sketch map of a suitable initial composition (◆) for troubleshooting. If the membrane-induced selectivity exists, the measured curve goes upwards; otherwise the curve goes downwards as in the reactive distillation case.

Legend: solid lines (—): simulated curves with membrane; dashed line (---): simulated curves without membrane.

6.3.1 Mass transfer resistance through the boundary layer

For selective membrane diffusion processes, concentration polarization may occur. The less permeable substances will accumulate more than the preferentially permeable components near the membrane because of the different transport rates through the membrane. This concentration polarization phenomenon always leads to the higher driving force for less permeable components, and reduces the driving force for preferentially permeable components. As a result, it has a counteraction effect in the selective diffusion process, and cancels out the selectivity.

This concentration polarization phenomenon is more often described as the boundary layer effect. For liquid mixtures on the retentate side, the boundary layer mass transfer resistance is usually non-negligible, and the mass transfer coefficients are estimated by the analogy between heat and mass transfer (e.g. [64]). In the considered system, there is a bulk vapor phase on the retentate side of the membrane; thus the boundary layer resistance is much smaller than in the liquid phase. Two stirring propellers were placed beneath the

membrane and driven magnetically to further minimize the mass transfer resistance in the boundary layer (as in Figure 6.4). The maximum stirring speed was found to be 500 rpm for long time stability. Measurements without the mixing propellers were effective for the first few samples but failed quickly afterwards. The subsequent measurements were performed with the stirring propellers.

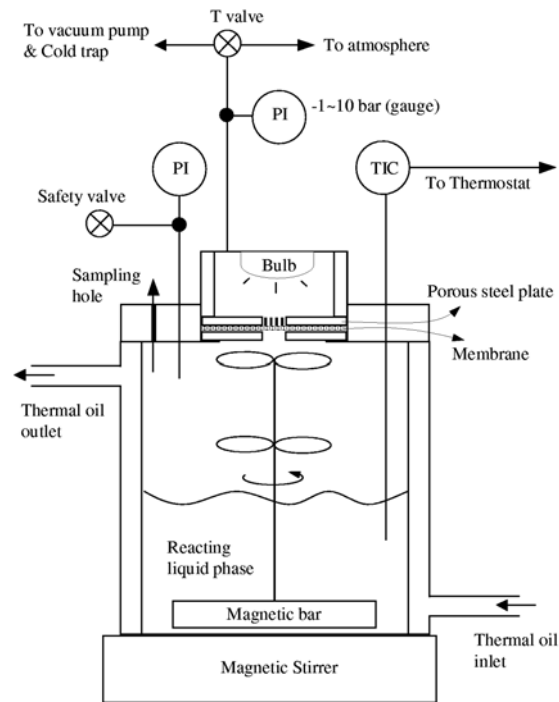


Figure 6.4 Experimental setup for the retentate phase diagram measurement of MR.

6.3.2 Capillary condensation in the membrane pores

When condensable vapors permeate through porous media, the capillary condensation could take place due to the curvature of the surface in contact. The relation between the capillary condensation pressure and the saturated vapor pressure can be formulated by the Kelvin equation (e.g. [64-67]):

$$\frac{p^{cond}}{p^{sat}} = \exp\left(\frac{-2 \cdot \sigma \cdot \cos\theta}{r_c \cdot c \cdot R \cdot T}\right) \quad (6.2)$$

where p^{cond} represents the condensation pressure in the pore, p^{sat} the saturated vapor pressure, σ the interfacial tension, θ the contact angle, r_c the radius of curvature, and c the molar density of the vapor.

To avoid capillary condensation within the membrane pores, a temperature difference between the permeating vapors and the membrane is needed so that the vapors entering the membrane pores are no longer saturated at the elevated membrane temperature. This extra heat supply through vacuum to the membrane was achieved by a heating bulb (as in Figure 6.4). The membrane temperature, which has a maximum tolerance 140 °C as reported by the provider, was controlled to be 120 °C by regulating the power input of the heating bulb.

6.3.3 Selection of polymer membrane material

From Eq.(6.2) it can be seen that another way to suppress the capillary condensation phenomenon is to increase the contact angle θ . This can be achieved by selecting an appropriate membrane material for the chemical species in use to lower the affinity between the vapors and the polymer surface. There are two types of polymer materials available for the track-etch porous membranes, i.e. the polycarbonate (PC) and polyester (PET) membranes. The polycarbonate membrane was first chosen because it has a smaller pore diameter (50 nm) available as the commercial products. However, the measurements with the polycarbonate membrane were only partially successful on the left hand side of the predicted reactive arrheotrope (where the concentration of propyl acetate was low). The experiments on the right half of the map always failed. However, the results implied that the flux of propyl acetate was always higher than expected.

If a certain component condensates on the wall of pores, it leads to an additional condensed phase flux of this substance. Therefore, it was suspected that propyl acetate had a strong affinity with the polycarbonate polymer (whose molecular structure is shown as Figure 6.5a.), and the capillary condensation could not be avoided when the propyl acetate concentration was high. This speculation was then confirmed by Hansen's solubility parameter (HSP) [68-69], which quantified the affinities between chemical solvents and solid materials by considering the dispersion interactions, the dipole-dipole interactions and the hydrogen-bonding interactions.

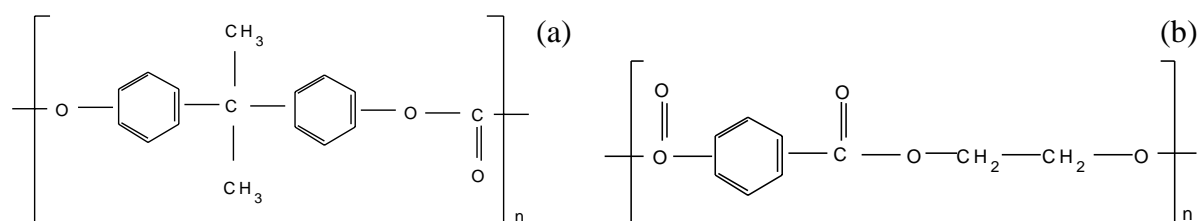


Figure 6.5 Molecular structures of (a) Polycarbonate (b) Polyester.

A concise index derived from Hansen’s solubility parameter (HSP) is the relative energy difference (RED) number between the chemicals and the solid materials. If a solvent and a solid material have a large RED number, it indicates that they have a low affinity and thus a large contact angle. The RED numbers of the polycarbonate polymer with the considered chemicals and some other solvents are listed in Table 6.1. In this work to prevent the capillary condensation, large RED numbers are favored. Nevertheless, It can be seen from Table 6.1 that the RED number between propyl acetate and the polycarbonate polymer is exceptionally low, which explains our experimental observation.

Table 6.1 Relative energy difference (RED) numbers of polycarbonate and polyester polymers with the considered chemicals and some other solvents (derived from HSP for polymers [68] and for chemicals [69]).

	Acetic acid	<i>n</i> -Propanol	Propyl acetate	Water
Polycarbonate	10.625	15.080	5.381	139.169
Polyester	14.291	10.335	11.952	83.943
	Acetone	Chloroform	<i>i</i> -Propanol	Cyclohexanol
Polycarbonate	2.796	3.506	13.593	8.170
Polyester	14.206	6.800	10.098	4.492

On the other hand, the polyester polymer (whose molecular structure is shown as Figure 6.5b) has sufficiently high RED numbers with all the four components, and thus provides the possibility to measure the whole diagram without the hindrance of capillary condensation effect. Briefly speaking, the polyester (PET) membrane is less hydrophobic than the polycarbonate (PC) membrane; therefore, the capillary condensation problem of propyl acetate can be relieved. Further trial experiments confirmed that the polyester membrane functioned well in all directions around the predicted reactive arthrope. Thus, the PET membrane with the smallest available pore diameter, 100 nm, was selected in the subsequent experiments.

6.3.4 Control of permeation flux

If the permeation flux is high, the boundary layer and capillary condensation problems will be deteriorated, because the accumulation of less permeable substances becomes faster and the heat input rate of the heating bulb is not sufficient to compensate the heat uptake by

the permeating vapors. Therefore, the tolerable permeation flux was found to be ~ 6 ml/hr and controlled by the open area of the porous steel support.

Due to the low permeation flux, the sufficiently high Damköhler number Da was easily ensured, but the rate of the composition trajectory progress was much slower than the reactive distillation measurement. Therefore, the initial liquid volume was reduced to 150 ml, and 20 g dry Amberlyst 15 was added to catalyze the reaction. Samples were taken every 20 minutes and analyzed by gas chromatography. Mixtures with initial compositions close to the predicted reactive azeotrope were prepared to start a new curve, and successive runs were repeated until a significant portion of a curve was depicted.

6.4 Validation of reactive azeotrope

The experiment results are plotted versus the predicted curves in Figure 6.6 wherein the transformed coordinates (Eq. 6.1) are again adopted for better visualization (*cf.* Figure 4.9c). The RCM of reactive distillation is also drawn with the dashed line for comparison. Because water has the lightest molecular weight and thus permeates through the porous membrane faster than other molecules, it can be seen that the quaternary unstable node is shifted towards the water corner. Total 45 runs were performed to constitute six curves originating around the reactive azeotrope whose molar composition is 6.29% acetic acid, 26.86% propanol, 8.22% propyl acetate and 58.63% water. The measurements fit the predicted curves very well, and therefore validate the existence of the reactive azeotrope.

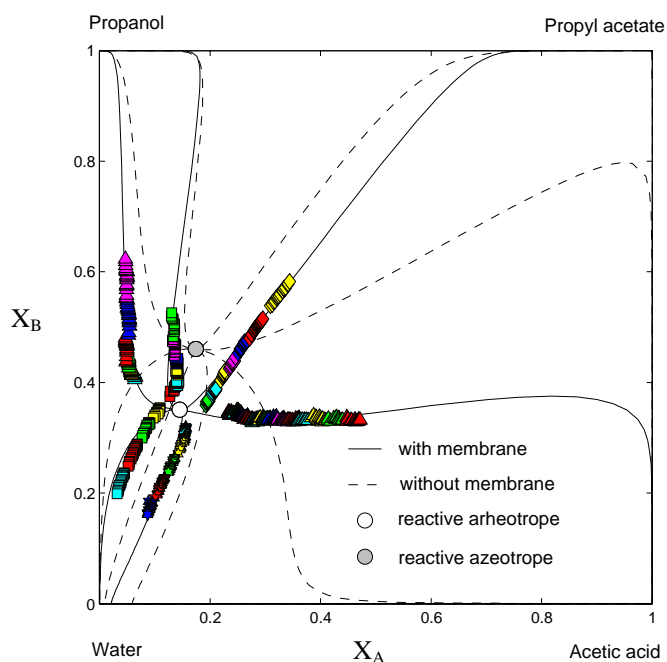


Figure 6.6 Validation of reactive azeotrope ($Da \rightarrow \infty$) under the influence of porous polyester membrane of pore diameter 100 nm. ($T = 80$ °C).

Legend: o reactive azeotrope or reactive azeotrope (shadowed); solid lines (—): simulated curves with membrane; dashed line (---): simulated curves without membrane; colorful symbols (Δ \diamond \square ...): experimental data.

6.5 Chapter conclusions

In this chapter, the predicted reactive azeotrope and reactive arrheotrope in the propyl acetate synthesis reaction have been verified experimentally. First, the residue curve map of reactive distillation (at $Da \rightarrow \infty$) was presented. Eight residue curves were measured with starting compositions around the reactive azeotrope; experimental results and the model prediction fitted well and thus indicated the existence of the reactive azeotrope. A similar work on the reactive azeotrope validation was reported in the literature [22].

For the validation of the reactive arrheotrope, a porous polyester membrane with 100 nm pore diameter was applied to exert the mass transfer selectivity. Improvements were made to suppress the boundary layer effect and the capillary condensation phenomenon, including the installation of stirring propellers and a heating bulb, the selection of a proper membrane polymer material, and the control of the permeation flux. The maximum tolerable permeation flow rate was found to be ~6 ml/hr, and the low permeation flow made the measurements much more time-consuming than the reactive distillation case. Six curves were measured around the reactive arrheotrope, and the results agreed well with the model prediction. Therefore, the existence of a reactive arrheotrope has been validated experimentally, which has never been reported before.

7. Conclusions and outlook

The main contribution of this work is to set up a new methodology to investigate the mass transfer effects on the attainable products of membrane reactors. The proposed method is generalized from the feasibility analysis of reactive distillation that has been well established in the literature, and the kernel of this generalization consists in the flux-based formulation of the material balance. As a result this modification constructs a methodical frame wherein the mass transfer kinetics can be considered independently. Additionally, the heat input strategy has been released from the autonomous heating policy so that the theoretical study of membrane reactors can be realized experimentally.

It is also shown that the theory proposed in this work could be retrieved back to that of reactive distillation if there is no selectivity induced by mass transfer kinetics. The governing equation of liquid phase composition proves to have analogous structures in a dynamic batch process and a continuous process at steady state. Therefore, the phase diagrams acquired from a batch process can be used in the design of a continuous membrane reactor.

Two types of membrane diffusion formulations are considered in this work to exemplify the proposed theory. The first one is the partial pressure driven membrane diffusion wherein the membrane properties are characterized by the mass transfer coefficient $[k]$ -matrix. The second one is the dusty gas model; the main purpose of this case is to show how a conventional transport model can be implemented in the frame of the proposed methodology.

Singular points represent the stationary compositions, and stable nodes in particular stand for the feasible products of the process. The singular points of non-reactive membrane separation process are termed as “arrheotrope”, which means in translation “the liquid composition is not changing with flux”, while the singular points of a membrane reactor are called “reactive arrheotropes” accordingly. By introducing a new set of transformed composition variables proposed in this work, the reactive arheotropic condition of a membrane reactor can be transformed into an analogous form to that of simple distillation,

and the resulting equation defines a curve on which all singular points for different Damköhler numbers will be located.

Two ternary as well as two quaternary examples are then applied to illustrate the proposed methodology. It is shown in all examples that membrane mass transfer effects can significantly change the loci of the potential singular point curves (PSPC) and thus the topology of retentate phase diagrams. In the ideal ternary system, the shape (ellipse / hyperbola) and orientation of PSPC can be directly identified by a simple rule derived from the reactive azeotropic condition. In the second ternary system, the synthesis reaction of tetrahydrofuran (THF) from 1,4-butanediol (1,4-BD), it is found that a Knudsen membrane can rotate the orientation of the PSPC so that the feasible product of the Knudsen membrane reactor at high Damköhler numbers is changed from water to THF. The result of this strongly non-ideal system agrees well with the prediction of the ideal one.

For quaternary systems, it is further demonstrated that the singular point analysis can be performed not only with respect to the Damköhler number (Da), but also to the properties of membranes (e.g. membrane pore size). In the ideal system, the PSPC can be interpreted as the intersection of two surfaces defined by the reactive azeotropic conditions, and the trajectory of the PSPC determines whether a system exhibits reactive azeotropes or not. In the last example, the esterification reaction of acetic acid with *n*-propanol, a porous polyester membrane is employed to study the mass transfer effects, which were quantified by the conventional dusty gas model. It is shown that there exists a quaternary unstable node (reactive azeotrope) in the system, and this unstable node can be shifted towards the reactive azeotrope by the applied membrane.

Afterwards experiments were performed to validate the prediction in the esterification example. First the heterogeneous kinetics of the propyl acetate synthesis reaction catalyzed by Amberlyst 15 was determined experimentally in this work. To describe the kinetics, pseudo-homogeneous (PH), Rideal-Eley (RE) and Langmuir-Hinshelwood-Hougen-Watson (LHHW) rate expressions were developed. The parameter identification was done with help of the in-house software DIVA, and the confidence interval of each parameter was also estimated. The LHHW model gives the best fitting result, followed by the RE model and the PH model, while the confidence of parameter accuracy ranks in the reverse order.

The residue curve map and retentate phase diagram at equilibrium reaction conditions were then measured. In the case of reactive distillation, the residue curves were measured

with the initial compositions around the reactive azeotrope so that its existence has been validated under isothermal conditions. A porous polyester membrane was incorporated to exert the mass transfer selectivity. The occurrence of the reactive azeotrope was predicted under the influence of such a membrane. Several actions were taken to suppress mass transfer mechanisms other than the dusty gas model. The existence of the reactive azeotrope was then validated by the experiments successfully, which in turn verified the proposed theory.

Based on the results of this work and following the track of reactive distillation development, one can portray an outlook for the future work. First, the proposed transformed composition variables facilitate the dynamic simulation of membrane reactor columns with the help of wave propagation theory [70], and thus the development of process control of membrane reactors can be approached in a more systematical way. Second, the transformed coordinates can be easily extended to multiple reaction systems, which is necessary when the considered system undergoes more than one chemical reaction. Furthermore, the proposed flux-based formulation is a rather flexible concept such that it should be applicable to many kinds of reactive separation processes with some modification, for instance, reactive stripping and reactive crystallization (*c.f.* [71-72]) in which phase equilibrium can not be assumed and mass transfer effects have to be considered.

Appendix

A.1 Derivation of transformed composition variables

Potential singular point curves (PSPC) [48] allow more insight into the intrinsic process types and the effect of incorporating a membrane. We start with the component and total material balances, Eqs.(2.3) and (2.4). To eliminate the reaction term ($H_r \cdot k_f \cdot \mathcal{R}$) in both equations, so that the potential singular point curve covers all extents of reaction, it is convenient to utilize the material balance for a reference component k :

$$\frac{d(H \cdot x_k)}{dt} = -n_k + v_k \cdot H_r \cdot k_f \cdot \mathcal{R} \quad (\text{A1.1})$$

and substituting this result into Eq.(2.3) yields

$$H \frac{d}{dt} \left(\frac{x_i - x_k}{v_i - v_k} \right) + \left(\frac{x_i - x_k}{v_i - v_k} \right) \frac{dH}{dt} = - \begin{cases} \left(\frac{n_i}{v_i} - \frac{n_k}{v_k} \right) & i = 1 \dots NC - 1 \\ & i \neq k \end{cases} \quad (\text{A1.2})$$

Applying Eq.(A1.1) to the overall material balance Eq.(2.4) gives:

$$\frac{dH}{dt} = - \left(\frac{v_k n_T - v_T n_k}{v_k - v_T x_k} \right) + H \frac{v_T}{(v_k - v_T x_k)} \frac{dx_k}{dt} \quad (\text{A1.3})$$

Eq.(A1.2) and Eq.(A1.3) can be combined to

$$H \left[\frac{d}{dt} \left(\frac{x_i - x_k}{v_i - v_k} \right) + \left(\frac{x_i - x_k}{v_i - v_k} \right) \left(\frac{v_T}{v_k - v_T x_k} \right) \frac{dx_k}{dt} \right] = - \left[\left(\frac{n_i}{v_i} - \frac{n_k}{v_k} \right) - \left(\frac{x_i - x_k}{v_i - v_k} \right) \left(\frac{v_k n_T - v_T n_k}{v_k - v_T x_k} \right) \right] \quad (\text{A1.4})$$

$$\begin{matrix} i = 1 \dots NC - 1 \\ i \neq k \end{matrix}$$

This set of equations can be written in a compact form if one defines transformed composition variables as follows:

$$X_i = \frac{(v_k x_i - v_i x_k)}{(v_k - v_T x_k)} \quad Y_i = \frac{(v_k n_i - v_i n_k)}{(v_k n_T - v_T n_k)} \quad (\text{A1.5})$$

With the transformed variables, Eqs.(A1.4) become

$$\frac{dX_i}{dt} = - \frac{(v_k n_T - v_T n_k)}{H(v_k - v_T x_k)} (Y_i - X_i) \quad \begin{matrix} i = 1 \dots NC - 1 \\ i \neq k \end{matrix} \quad (\text{A1.6})$$

and by defining the time variable, Eq.(A1.7),

$$d\tau = \frac{(v_k n_T - v_T n_k)}{H(v_k - v_T x_k)} dt \quad (\text{A1.7})$$

one gets the final ($NC-2$) linearly independent reduced equations, in analogous manner to distillation and reactive distillation [25-26]:

$$\frac{dX_i}{d\tau} = X_i - Y_i \quad \begin{array}{l} i = 1 \cdots NC - 1 \\ i \neq k \end{array} \quad (\text{A1.8})$$

It is worth noticing that, if all fluxes n_i are positive (i.e. directed from reacting phase to permeate phase) as the usual condition of membrane reactors, the dimensionless time τ can be guaranteed to increase monotonically with t , by selecting the reference component k as:

- (i) a reactant, if $v_T > 0$,
- (ii) a product, if $v_T < 0$,
- (iii) arbitrarily, if $v_T = 0$.

Additionally, X_i and Y_i obey the following summation equations:

$$\sum_{\substack{i=1 \\ i \neq k}}^{NC} X_i = 1 \quad \sum_{\substack{i=1 \\ i \neq k}}^{NC} Y_i = 1 \quad (\text{A1.9})$$

As a consequence of Eq.(A1.8), at the singular points of membrane reactors, the transformed vapor and liquid phase mole fractions are equal:

$$X_i = Y_i \quad \begin{array}{l} i = 1 \cdots NC - 1 \\ i \neq k \end{array} \quad (\text{A1.10})$$

The analogous transformation can be easily derived for the continuous process (*cf.* Figure 2.2), starting with Eqs.(2.19) and (2.20). The repeated derivation can well be omitted.

A.2 Matrix formulation of dusty gas model

In Section 2.2.2, the conventional dusty gas model formulation Eq.(2.27) can be cast into the matrix form Eq.(2.31) as following:

$$-\frac{1}{RT} \nabla p_i - \frac{1}{RT} \frac{B_0 p_i}{\mu D_{K,i}^e} \nabla p = \sum_{j=1}^{NC} \frac{y_j n_i - y_i n_j}{D_{ij}^e} + \frac{n_i}{D_{K,i}^e} \quad (2.27)$$

$$\Rightarrow -\frac{1}{RT} \nabla p_i - \frac{1}{RT} \frac{B_0 p_i}{\mu D_{K,i}^e} \nabla p = \sum_{j=1}^{NC} \frac{y_j n_i}{D_{ij}^e} - \sum_{j=1}^{NC} \frac{y_i n_j}{D_{ij}^e} + \frac{n_i}{D_{K,i}^e} \quad (A2.1)$$

$$\Rightarrow -\frac{1}{RT} \nabla p_i - \frac{1}{RT} \frac{B_0 p_i}{\mu D_{K,i}^e} \nabla p = \left(\sum_{j=1}^{NC} \frac{y_j}{D_{ij}^e} + \frac{1}{D_{K,i}^e} \right) \cdot n_i + \sum_{j=1}^{NC} \left(\frac{-y_i}{D_{ij}^e} \cdot n_j \right) \quad (A2.2)$$

$$\Rightarrow -\frac{1}{RT} \nabla p_i - \frac{1}{RT} \frac{B_0 p_i}{\mu D_{K,i}^e} \nabla p = B_{ii}^e \cdot n_i + \sum_{j=1}^{NC} (B_{ij}^e \cdot n_j) \quad (A2.3)$$

Eq.(A2.3) represents the i^{th} element of the following vector form

$$\left(-\frac{1}{RT} \nabla p_i - \frac{1}{RT} \frac{B_0 p_i}{\mu D_{K,i}^e} \nabla p \right) = [B^e] \cdot (n_i) \quad (A2.4)$$

$$\Rightarrow (n_i) = [B^e]^{-1} \cdot \left(-\frac{1}{RT} \nabla p_i - \frac{1}{RT} \frac{B_0 p_i}{\mu D_{K,i}^e} \nabla p \right) \quad (A2.5)$$

$$\Rightarrow (n_i) = -\frac{1}{RT} [k] \left(\Delta p_i + \frac{y_i \cdot p \cdot B_0}{\mu \cdot D_{K,i}^e} \Delta p \right) \quad (2.31)$$

with $[k]$ and the B_{ii}^e , B_{ij}^e defined by Eq.(2.32).

$$[k] = [B^e]^{-1} / \delta \quad (2.32a)$$

$$B_{ii}^e = \frac{1}{D_{K,i}^e} + \sum_{\substack{j=1 \\ j \neq i}}^{NC} \frac{y_j}{D_{ij}^e} \quad (2.32b)$$

$$B_{ij}^e = -\frac{y_i}{D_{ij}^e} \quad (2.32c)$$

A.3 Thermodynamic data of THF reaction system

The saturated vapor pressure of each component is calculated by the Antoine equation:

$$\log_{10} p_i^{sat} = A + \frac{B}{T + C}, \quad p_i^{sat} \text{ in pa, } T \text{ in K} \quad (\text{A3.1})$$

The liquid phase activity coefficients were calculated from the Wilson equation using the interaction parameters and molar volumes listed as Table A3.1.

Table A3.1 Thermodynamic data for the THF synthesis reaction system.

Component	1,4-Butanediol	Tetrahydrofuran	Water
Normal boiling point (K)	503.15	339.15	373.15
Antoine coefficients			
<i>A</i>	13.0236	9.2727	10.3274
<i>B</i>	-3905.1	-1442.3	-1985.0
<i>C</i>	-15.96	0	0
Wilson coeff. (<i>A_{ij}</i> [cal/mol])	<i>j</i> = 1,4-BD	<i>j</i> = THF	<i>j</i> = Water
<i>i</i> = 1,4-BD	—	1030.1867	410.4832
<i>i</i> = THF	105.6295	—	1140.7179
<i>i</i> = Water	675.7784	1819.4033	—
Molar volume (<i>V^L</i> [m ³ /mol])	1,4-BD	THF	Water
	8.835 x 10 ⁻⁵	8.155 x 10 ⁻⁵	1.807 x 10 ⁻⁵

A.4 Thermodynamic data of propyl acetate reaction system

In Eq.(4.7), the saturated vapor pressure of each component is calculated by the Antoine equation:

$$\ln p_i^{sat} = A + \frac{B}{T + C}, \quad p_i^{sat} \text{ in pa, } T \text{ in K} \quad (\text{A4.1})$$

The dimerization correction factor (z_i) is calculated using the following equations

$$z_A = \frac{1 + (1 + 4k_A p_1^{sat})^{0.5}}{1 + (1 + 4k_A P y_A (2 - y_A))^{0.5}} \quad (\text{A4.2})$$

for the associating molecule (acetic acid), and

$$z_N = \frac{2(1 - y_A + (1 + 4k_A P y_A (2 - y_A))^{0.5})}{(2 - y_A)(1 + (1 + 4k_A P y_A (2 - y_A))^{0.5})} \quad (\text{A4.3})$$

for the other three components; where k_A , the dimerization equilibrium constant, is calculated by

$$\log_{10} k_A = D_1 + \frac{D_2}{T}, \quad k_A \text{ in pa}^{-1}, T \text{ in K} \quad (\text{A4.4})$$

The thermodynamic data are listed in Table A4.1

Table A4.1 Thermodynamic data for the propyl acetate system.

Component	Acetic acid	Propanol	Propyl acetate	Water
Normal boiling point (K)	391.15	370.35	374.65	373.15
Antoine coefficients				
<i>A</i>	22.1001	22.72435	21.6266	23.2256
<i>B</i>	-3654.62	-3310.394	-3249.98	-3835.18
<i>C</i>	-45.392	-74.687	-52.84	-45.343
Dimerization constants				
<i>D</i> ₁	-12.5459	—	—	—
<i>D</i> ₂	3166.0	—	—	—
NRTL coeff. (<i>N</i> _{<i>ij</i>})	<i>j</i> = Acetic acid	<i>j</i> = Propanol	<i>j</i> = Propyl acetate	<i>j</i> = Water
<i>i</i> = Acetic acid	—	-147.4298	-410.3887	-342.1961
<i>i</i> = Propanol	104.1007	—	1055.3593	152.5084
<i>i</i> = Propyl acetate	1050.5581	-433.1348	—	720.1784
<i>i</i> = Water	1175.7145	1866.3369	3497.7669	—
NRTL coeff. (α_{ij})	<i>j</i> = Acetic acid	<i>j</i> = Propanol	<i>j</i> = Propyl acetate	<i>j</i> = Water
<i>i</i> = Acetic acid	—	0.3007	0.2970	0.2952
<i>i</i> = Propanol	0.3007	—	0.3011	0.3747
<i>i</i> = Propyl acetate	0.2970	0.3011	—	0.2942
<i>i</i> = Water	0.2952	0.3747	0.2942	—

A.5 Derivation of heterogeneous kinetic models for propyl acetate reaction system

Langmuir-Hinshelwood-Hougen-Watson (LHHW) model

In the LHHW model, all the components are considered adsorbable on the catalyst surface, and the chemical reaction only takes place in the adsorbed phase. Furthermore, the following assumptions are made for the subsequent derivation: (1) the adsorption sites are uniformly energetic; (2) a monolayer coverage on the catalyst surface is assumed; (3) a molecule on site 1 does not influence what attaches onto a nearby site 2.

Providing θ_{AcAc} , θ_{PrOH} , θ_{PrAc} and θ_{H_2O} denote the surface occupation fractions of acetic acid, propanol, propyl acetate and water respectively, the fraction of vacant sites, θ_0 , is given as:

$$\theta_0 = (1 - \theta_{AcAc} - \theta_{PrOH} - \theta_{PrAc} - \theta_{H_2O}) \quad (A5.1)$$

The reaction mechanism includes five steps, i.e. the adsorption of acetic acid and propanol, the chemical reaction taking place in the adsorbed phase, and the desorption of propyl acetate and water. The rate equation of each step can be expressed as following:

Step 1 (adsorption of acetic acid)



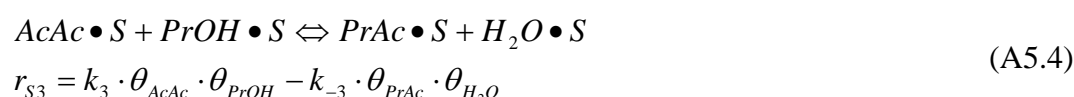
where S represents the vacant adsorption site and $AcAc \bullet S$ denotes the adsorbed molecule of acetic acid. r_{S1} is the rate of Step 1, while k_1 and k_{-1} are the forward and backward rate constants of Step 1. Similarly, the adsorption of propanol reads as:

Step 2 (adsorption of propanol)



The chemical reaction then takes place in the adsorbed phase on the catalyst surface:

Step 3 (chemical reaction in the adsorbed phase)



The products propyl acetate and water are then desorbed from the adsorption sites:

Step 4 (desorption of propyl acetate)



Step 5 (desorption of water)



In this work, the chemical reaction in the adsorbed phase (Step 3) is considered as the rate-controlling step so that the other four steps are in equilibrium. Therefore, r_{S1} , r_{S2} , r_{S4} and r_{S5} are set zero, which gives:

$$\theta_{AcAc} = \frac{k_1}{k_{-1}} \cdot a_{AcAc} \cdot \theta_0 \equiv K_{S,AcAc} \cdot a_{AcAc} \cdot \theta_0 \quad (A5.7)$$

$$\theta_{PrOH} = \frac{k_2}{k_{-2}} \cdot a_{PrOH} \cdot \theta_0 \equiv K_{S,PrOH} \cdot a_{PrOH} \cdot \theta_0 \quad (A5.8)$$

$$\theta_{PrAc} = \frac{k_{-4}}{k_4} \cdot a_{PrAc} \cdot \theta_0 \equiv K_{S,PrAc} \cdot a_{PrAc} \cdot \theta_0 \quad (A5.9)$$

$$\theta_{H_2O} = \frac{k_{-5}}{k_5} \cdot a_{H_2O} \cdot \theta_0 \equiv K_{S,H_2O} \cdot a_{H_2O} \cdot \theta_0 \quad (A5.10)$$

Summing up Eqs.(A5.7)~(A5.10) and comparing with Eq.(A5.1) gives:

$$\sum_{j=AcAc}^{H_2O} \theta_j = \theta_0 \cdot \sum_{j=AcAc}^{H_2O} (K_{S,j} \cdot a_j) = 1 - \theta_0 \quad (A5.11)$$

θ_0 can be deduced from Eq.(A5.11) as:

$$\theta_0 = \left(\frac{1}{1 + \sum_{j=AcAc}^{H_2O} (K_{S,j} \cdot a_j)} \right) \quad (A5.12)$$

and thus

$$\theta_i = \left(\frac{K_{S,i} \cdot a_i}{1 + \sum_{j=AcAc}^{H_2O} (K_{S,j} \cdot a_j)} \right) \quad \text{for } i = AcAc \dots H_2O \quad (A5.13)$$

The overall reaction rate is equal to the rate of the controlling step (Step 3). Substituting Eq.(A5.12) and Eq.(A5.13) into Eq.(A5.4) gives:

$$\begin{aligned} |r_i| = r_{S3} &= \frac{k_3 \cdot K_{S,AcAc} \cdot K_{S,PrOH} \cdot a_{AcAc} \cdot a_{PrOH} - k_{-3} \cdot K_{S,PrAc} \cdot K_{S,H_2O} \cdot a_{PrAc} \cdot a_{H_2O}}{\left(1 + \sum_{j=AcAc}^{H_2O} K_{S,j} \cdot a_j \right)^2} \\ &\equiv \frac{k_f \cdot \left(a_{AcAc} \cdot a_{PrOH} - \frac{1}{K} \cdot a_{PrAc} \cdot a_{H_2O} \right)}{\left(1 + \sum_{j=AcAc}^{H_2O} K_{S,j} \cdot a_j \right)^2} \end{aligned} \quad (A5.14)$$

with

$$k_f = k_3 \cdot K_{S,AcAc} \cdot K_{S,PrOH} \quad (A5.15)$$

$$K = \frac{k_3 \cdot K_{S,AcAc} \cdot K_{S,PrOH}}{k_{-3} \cdot K_{S,PrAc} \cdot K_{S,H_2O}} \quad (A5.16)$$

Considering the effect of catalyst amount and the reaction stoichiometry, the resulting rate equation is given as:

$$R_i = M_{cat} \cdot r_i = \frac{M_{cat} \cdot v_i \cdot k_f \cdot \left(a_{AcAc} \cdot a_{PrOH} - \frac{1}{K} \cdot a_{PrAc} \cdot a_{H_2O} \right)}{\left(1 + \sum_{j=AcAc}^{H_2O} K_{S,j} \cdot a_j \right)^2} \quad (5.6)$$

Rideal-Eley (RE) model

For the RE model wherein propyl acetate is assumed non-adsorbable (i.e. $K_{S,PrAc} = 0$), the fraction of vacant sites, θ_0 , is calculated as

$$\theta_0 = \left(1 - \theta_{AcAc} - \theta_{PrOH} - \theta_{H_2O} \right) \quad (A5.17)$$

The reaction mechanism includes four steps, i.e. the adsorption of acetic acid and propanol, the surface reaction, and the desorption of water. The rate equation of each step can be expressed as following:

Step 1 (adsorption of acetic acid)

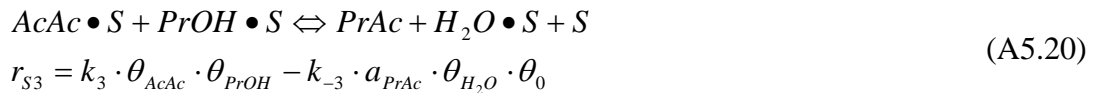


Step 2 (adsorption of propanol)



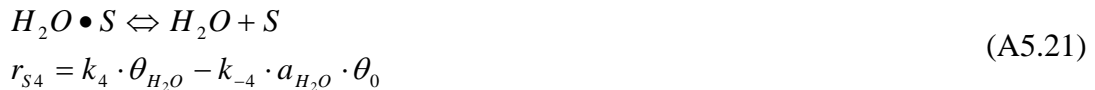
The meanings of symbols are similar as in the previous derivation of the LHHW model. The chemical reaction then takes place between the adsorbed acetic acid and adsorbed propanol, and gives the adsorbed water and the un-adsorbed propyl acetate as the products:

Step 3 (chemical reaction in the adsorbed phase)



The byproduct water is then desorbed from the adsorption site:

Step 4 (desorption of water)



Again the chemical reaction in the adsorbed phase (Step 3) is considered as the rate-controlling step so that Steps 1, 2 and 4 are in equilibrium. Therefore, r_{S1} , r_{S2} and r_{S4} equal zero, which gives:

$$\theta_{AcAc} = \frac{k_1}{k_{-1}} \cdot a_{AcAc} \cdot \theta_0 \equiv K_{S,AcAc} \cdot a_{AcAc} \cdot \theta_0 \quad (A5.22)$$

$$\theta_{PrOH} = \frac{k_2}{k_{-2}} \cdot a_{PrOH} \cdot \theta_0 \equiv K_{S,PrOH} \cdot a_{PrOH} \cdot \theta_0 \quad (A5.23)$$

$$\theta_{H_2O} = \frac{k_{-4}}{k_4} \cdot a_{H_2O} \cdot \theta_0 \equiv K_{S,H_2O} \cdot a_{H_2O} \cdot \theta_0 \quad (A5.24)$$

Summing up Eqs.(A5.22)~(A5.24) and comparing with Eq.(A5.17) gives:

$$\sum_{i \neq PrAc} \theta_i = \theta_0 \cdot \sum_{i \neq PrAc} (K_{S,i} \cdot a_i) = 1 - \theta_0 \quad (A5.25)$$

θ_0 can be solved from Eq.(A5.25) as:

$$\theta_0 = \left(\frac{1}{1 + \sum_{j \neq PrAc} (K_{S,j} \cdot a_j)} \right) \quad (A5.26)$$

and thus

$$\theta_i = \left(\frac{K_{S,i} \cdot a_i}{1 + \sum_{j \neq PrAc} (K_{S,j} \cdot a_j)} \right) \quad \text{for } i = AcAc, PrOH, \text{ and } H_2O \quad (A5.27)$$

The overall reaction rate is equal to the rate of controlling step (Step 3). Substituting Eq.(A5.26) and Eq.(A5.27) into Eq.(A5.20) gives:

$$\begin{aligned} |r_i| = r_{S3} &= \frac{k_3 \cdot K_{S,AcAc} \cdot K_{S,PrOH} \cdot a_{AcAc} \cdot a_{PrOH} - k_{-3} \cdot K_{S,H_2O} \cdot a_{PrAc} \cdot a_{H_2O}}{\left(1 + \sum_{j \neq PrAc} K_{S,j} \cdot a_j \right)^2} \\ &\equiv \frac{k_f \cdot \left(a_{AcAc} \cdot a_{PrOH} - \frac{1}{K} \cdot a_{PrAc} \cdot a_{H_2O} \right)}{\left(1 + \sum_{j \neq PrAc} K_{S,j} \cdot a_j \right)^2} \end{aligned} \quad (A5.28)$$

with

$$k_f = k_3 \cdot K_{S,AcAc} \cdot K_{S,PrOH} \quad (A5.29)$$

$$K = \frac{k_3 \cdot K_{S,AcAc} \cdot K_{S,PrOH}}{k_{-3} \cdot K_{S,H_2O}} \quad (A5.30)$$

Considering the effect of catalyst amount and the reaction stoichiometry, the resulting rate equation is given as:

$$R_i = M_{cat} \cdot r_i = \frac{M_{cat} \cdot v_i \cdot k_f \cdot \left(a_{AcAc} \cdot a_{PrOH} - \frac{1}{K} \cdot a_{PrAc} \cdot a_{H_2O} \right)}{\left(1 + \sum_{j \neq PrAc} K_{S,j} \cdot a_j \right)^2} \quad (5.7)$$

A.6 Influence of temperature on the quaternary unstable node in propyl acetate reaction system

In the experimental validation of the reactive arrheotrope, the operating temperature was lowered from 105 °C to 80 °C, to reduce the capillary condensation phenomenon. However, the displacement between the reactive azeotrope (Figure 6.2) and reactive arrheotrope (Figure 6.6) is not caused by different operating temperatures, but by the membrane. As can be seen from Figure A6.1, the locations of reactive azeotropes at 80 °C and 105 °C are pretty close. Moreover, for the 100 nm pore diameter membrane, the membrane selectivity is lower if the system temperature is 105 °C so that the displacement of the unstable node is smaller. Compositions of these unstable nodes are listed in Table A6.1.

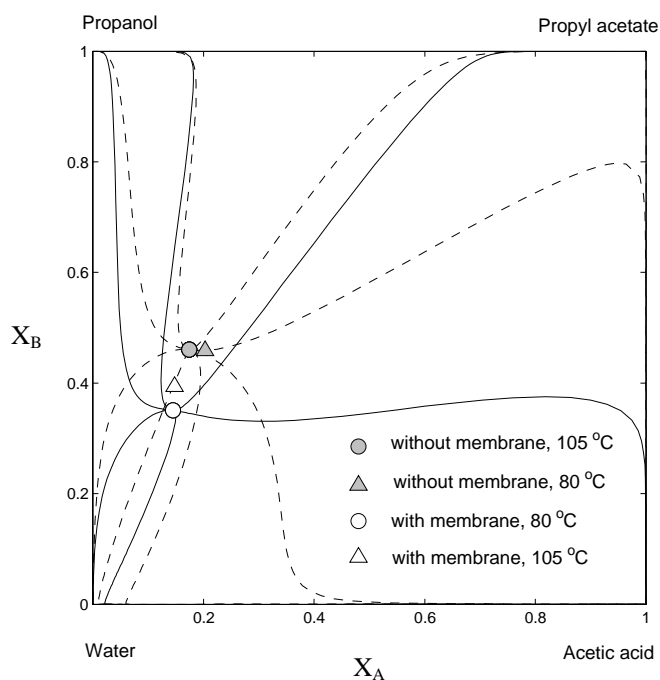


Figure A6.1 Locations of the reactive azeotrope and reactive arrheotrope ($d_p = 100$ nm) at different temperatures ($T = 80$ °C and 105 °C).

Table A6.1 Compositions of the quaternary unstable node at different conditions.

Membrane pore size	Temperature	Pressure [bar]	x_1	x_2	x_3	Note
Without	80 °C	0.824	0.0722	0.3167	0.1414	
Without	105 °C	2.062	0.0599	0.3331	0.1260	Validated in Sec. 6.2
100 nm	80 °C	0.821	0.0629	0.2686	0.0822	Validated in Sec. 6.4
100 nm	105 °C	2.059	0.0567	0.3027	0.0908	

References

- [1] Doherty, M.F., & Buzad, G. (1992). Reactive distillation by design, *Chemical Engineering Research and Design, Transaction of the Institution of Chemical Engineers, Part A*, 70, 448-458.
- [2] Taylor, R., & Krishna, R. (2000). Modelling reactive distillation, *Chemical Engineering Science*, 55, 5183-5229.
- [3] Sundmacher, K., & Kienle, A., Eds. (2003). *Reactive Distillation – Current Status and Future Directions*, Wiley-VCH, Weinheim, Germany.
- [4] Zhu, Y., & Chen, H. (1998). Pervaporation separation and pervaporation-esterification coupling using crosslinked PVA composite catalytic membranes on porous ceramic plate, *Journal of Membrane Science*, 138, 123-134.
- [5] Tuchlenski, A., Uchytíl, P., & Seidel-Morgenstern, A. (1998). An experimental study of combined gas phase and surface diffusion in porous glass, *Journal of Membrane Science*, 140, 165-184.
- [6] van de Graaf, J.M., Zwiep, M., Kapteijn, F., & Moulijn, J.A. (1999). Application of a silicalite-1 membrane reactor in metathesis reactions, *Applied Catalysis A: General*, 178, 225-241.
- [7] Domingues, L., Recasens, F., & Larrayoz, M.A. (1999). Studies of a pervaporation reactor: Kinetics and equilibrium shift in benzyl alcohol acetylation, *Chemical Engineering Science*, 54, 1461-1465.
- [8] Beers, A.E.W., Spruijt, R.A., Nijhuis, T.A., Kapteijn F., & Moulijn, J.A. (2001). Esterification in a structured catalytic reactor with counter-current water removal, *Catalysis Today*, 66, 175-181.
- [9] Piera, E., Tellez, C., Coronas, J., Menendez, M., & Santamaria, J. (2001). Use of zeolite membrane reactors for selectivity enhancement: application to the liquid-phase oligomerization of i-butene, *Catalysis Today*, 67, 127-138.
- [10] Tanaka, K., Yoshikawa, R., Ying, C., Kita, H., & Okamoto, K.-I. (2001). Application of zeolite membranes to esterification reactions, *Catalysis Today*, 67, 121-125.

- [11] Bernal, M.P., Coronas, J., Menendez, M., & Santamaria, J. (2002). Coupling of reaction and separation at the microscopic level: esterification processes in a H-ZSM-5 membrane reactor, *Chemical Engineering Science*, 57, 1557-1562.
- [12] Jafar, J.J., Budd, P.M., & Hughes, R. (2002). Enhancement of esterification reaction yield using zeolite A vapour permeation membrane, *Journal of Membrane Science*, 199, 117-123.
- [13] Feng, X., & Huang, R.Y.M. (1996). Studies of a membrane reactor: Esterification facilitated by pervaporation, *Chemical Engineering Science*, 51, 4673-4679.
- [14] Moon, W.S., & Park, S.B. (2000). Design guide of a membrane for a membrane reactor in terms of permeability and selectivity, *Journal of Membrane Science*, 170, 43-51.
- [15] Lim, S.Y., Park, B., Hung, F., Sahimi, M., & Tsotsis, T.T. (2002). Design issues of pervaporation membrane reactors for esterification, *Chemical Engineering Science*, 57, 4933-4946.
- [16] Assabumrungrat, S., Kiatkittipong, W., Prasertdam, P., & Goto, S. (2003). Simulation of pervaporation membrane reactors for liquid phase synthesis of ethyl tert-butyl ether from tert-butyl alcohol and ethanol, *Catalysis Today*, 79-80, 249-257.
- [17] Venimadhavan, G., Buzad, G., Doherty M. F., & Malone, M. F. (1994). Effect of kinetics on residue curve maps for reactive distillation, *A.I.Ch.E. Journal*, 40, 1814-1824.
- [18] Ung, S., & Doherty, M.F. (1995). Calculation of residue curve maps for mixtures with multiple equilibrium chemical reactions, *Industrial and Engineering Chemical Research*, 34, 3195.
- [19] Thiel, C., Sundmacher, K., & Hoffmann, U. (1997). Residue curve maps for heterogeneously catalysed reactive distillation of fuel ethers MTBE and TAME, *Chemical Engineering Science*, 52, 993-1005.
- [20] Qi, Z., Kolah, A., & Sundmacher, K. (2002). Residue curve maps for reactive distillation systems with liquid phase splitting. *Chemical Engineering Science*, 57, 163-178.
- [21] Steyer, F., Qi, Z., & Sundmacher, K. (2002). Synthesis of cyclohexanol by three-phase reactive distillation: influence of kinetics on phase equilibria, *Chemical Engineering Science*, 57, 1511-1520.

- [22] Song, W., Huss, R.S., Doherty, M.F., & Malone, M.F. (1997) Discovery of a reactive azeotrope, *Nature*, 388, 561-563.
- [23] Huang, Y.-S., Sundmacher, K., Tulashie S., & Schlünder, E.-U. (2005). Theoretical and experimental study on residue curve maps of propyl acetate synthesis reaction, *Chemical Engineering Science*, 60, 3363-3371.
- [24] Chiplunkar, M., Hong, M., Malone, M.F., & Doherty, M.F. (2005). Experimental study of feasibility in kinetically-controlled reactive distillation, *A.I.Ch.E. Journal*, 51, 464-479.
- [25] Barbosa, D., & Doherty, M.F. (1988). The influence of equilibrium chemical reactions on vapor-liquid phase diagrams, *Chemical Engineering Science*, 43, 529-540.
- [26] Barbosa, D., & Doherty, M.F. (1988). The simple distillation of homogeneous reactive mixtures, *Chemical Engineering Science*, 43, 541-550.
- [27] Ung, S., & Doherty, M.F. (1995). Vapor-liquid phase equilibrium in systems with multiple chemical reactions, *Chemical Engineering Science*, 50, 23-48.
- [28] Rev, E. (1994). Reactive distillation and kinetic azeotropy, *Industrial and Engineering Chemical Research*, 33, 2174-2179.
- [29] Venimadhavan, G., Malone M.F., & Doherty, M.F. (1999). Bifurcation study of kinetic effects in reactive distillation, *A.I.Ch.E. Journal*, 45, 546-556.
- [30] Okasinski, M.J., & Doherty, M.F. (1997). Thermodynamic behavior of reactive azeotropes, *A.I.Ch.E. Journal*, 43, 2227-2238.
- [31] Qi, Z., & Sundmacher, K. (2002). Bifurcation analysis of reactive distillation systems with liquid-phase splitting, *Computers in Chemical Engineering*, 26, 1459-1471.
- [32] Kooijman, H.A., & Taylor, R. (1995). Modelling mass transfer in multicomponent distillation, *Chemical Engineering Journal*, 57, 177-188.
- [33] Castillo, F.J.L., & Towler, G.P. (1998). Influence of multicomponent mass transfer on homogeneous azeotropic distillation, *Chemical Engineering Science*, 53, 963-976.
- [34] Springer, P.A.M., Baur, R., & Krishna, R. (2002). Influence of interface mass transfer on the composition trajectories and crossing of boundaries in ternary azeotropic distillation, *Separation and Purification Technology*, 29, 1-13.

- [35] Schlünder, E.-U. (1977). Über den Einfluß der Stoffübertragung auf die Selektivität der Thermischen Trennverfahren - dargestellt am Beispiel der Schlepptitteldestillation, *Verfahrenstechnik*, 11, 682-686.
- [36] Schlünder, E.-U. (1979). The effect of diffusion on the selectivity of entraining distillation, *International Chemical Engineering*, 19, 373-379.
- [37] Fullarton, D., & Schlünder, E.-U. (1986). Diffusion distillation – a new separation process for azeotropic mixtures, *Chemical Engineering and Processing*, 20, 255-263.
- [38] Nguyen, Q.T., & Clement, R. (1991). Analysis of some cases of pseudo-azeotropes in pervaporation, *Journal of Membrane Science*, 55, 1-19.
- [39] Nisoli, A., Doherty, M.F., & Malone, M.F. (2004). Effects of vapor-liquid mass transfer on feasibility of reactive distillation, *A.I.Ch.E. Journal*, 50, 1795-1813.
- [40] Aiouache, F., & Goto, S. (2003). Reactive distillation – pervaporation hybrid column for tert.-amyl alcohol etherification with ethanol, *Chemical Engineering Science*, 58, 2465-2477.
- [41] Taylor, R., & Krishna, R. (1993). *Multicomponent mass transfer*, Wiley, New York.
- [42] Mason, E.A., & Malinauskas, A.P. (1983). *Gas transport in porous media: the dusty gas-model*, Elsevier, Amsterdam.
- [43] Krishna, R., & Wesselingh, J.A. (1997). The Maxwell-Stefan approach to mass transfer, *Chemical Engineering Science*, 52, 861-911.
- [44] Reid, R.C., Prausnitz, J.M., & Poling, B.E. (1987). *The properties of gases and liquids*. McGraw-Hill, New York.
- [45] Huang, Y.-S., Sundmacher, K., Qi, Z., & Schlünder, E.-U. (2004). Residue curve maps of reactive membrane separation, *Chemical Engineering Science*, 59, 2863-2879.
- [46] Wade, J., & Merriman, R. W. (1911). Influence of water on the boiling point of ethyl alcohol at pressures above and below the atmospheric pressure, *Journal of the Chemical Society, Transaction*, 99, 997-1011.
- [47] Atkins, P.W. (1990). *Physikalische Chemie*, VCH, Weinheim, Germany.
- [48] Qi, Z., Flockerzi, D., & Sundmacher, K. (2004). Singular points of reactive distillation systems, *A.I.Ch.E. Journal*, 50, 2866-2876.

- [49] Limbeck, U., Altwicker, C., Kunz, U. & Hoffmann, U. (2001). Rate expression for THF synthesis on acidic ion exchange resin, *Chemical Engineering Science*, 56, 2171-2178.
- [50] Gmehling, J., & Onken, U. (1977). *Vapour-liquid equilibrium data collection, chemistry data series*, Frankfurt am Main, DECHEMA.
- [51] Huang, Y.-S., Schlünder, E.-U., & Sundmacher, K. (2005). Feasibility analysis of membrane reactors – discovery of reactive arrheotropes, *Catalysis Today*, 104, 360-371.
- [52] Huang, Y.-S., & Sundmacher, K. (2005). Kinetics study of propyl acetate synthesis reaction catalyzed by Amberlyst 15, *International Journal of Chemical Kinetics*, submitted.
- [53] Marek, J., & Standart, G. (1954). Vapor-liquid equilibria in mixtures containing an associating substance. I. Equilibrium relationships for systems with an associating component, *Collection of Czechoslovak Chemical Communication, English Edition*, 19, 1074-1084.
- [54] Krishnaiah, D. & Bhagvanth Rao, M. (1984). Kinetics of esterification of n-propyl alcohol with acetic acid catalysed by Dowex-50w. *Indian Journal of Technology*, 22, 268-271.
- [55] Bart, H. J., Kaltenbrunner, W., & Landschützer, H. (1996). Kinetics of esterification of acetic acid with propyl alcohol by heterogeneous catalysis, *International Journal of Chemical Kinetics*, 28, 649-656.
- [56] Song, W., Venimadhavan, G., Manning, J.M., Malone, M.F., & Doherty, M.F. (1998). Measurement of residue curve maps and heterogeneous kinetics in methyl acetate synthesis, *Industrial and Engineering Chemical Research*, 37, 1917-1928.
- [57] Gangadwala, J., Mankar, S., Mahajani, S., Kienle, A., & Stein, E. (2003). Esterification of Acetic Acid with Butanol in the Presence of Ion-Exchange Resins as Catalysts, *Industrial and Engineering Chemical Research*, 42, 2146-2155.
- [58] Parra, D., Tejero, J., Cunill, F., Iborra, M., & Izquierdo, J.F. (1994). Kinetic study of MTBE liquid-phase synthesis using C4 olefinic cut, *Chemical Engineering Science*, 49, 4563-4578.
- [59] Pöpken, T., Götze, L., & Gmehling, J. (2000). Reaction Kinetics and Chemical Equilibrium of Homogeneously and Heterogeneously Catalyzed Acetic Acid

- Esterification with Methanol and Methyl Acetate Hydrolysis, *Industrial and Engineering Chemical Research*, 39, 2601-2611.
- [60] Silva, V.M.T.M., & Rodrigues, A.E. (2001). Synthesis of diethylacetal: thermodynamic and kinetic studies, *Chemical Engineering Science*, 56, 1255-1263.
- [61] Majer, C. (1998). *Parameterschätzung, Versuchsplanung und Trajektorienoptimierung für verfahrenstechnische Prozesse*, Ph.D. Thesis. University of Stuttgart, Germany.
- [62] Marsili-Libelli, S., Guerrizio, S., & Checchi, N. (2003). Confidence regions of estimated parameters for ecological systems. *Ecological Modelling*, 165, 127-146.
- [63] Okasinski, M. J., & Doherty, M. F. (2000). Prediction of heterogeneous reactive azeotropes in esterification systems, *Chemical Engineering Science*, 55, 5263-5271.
- [64] Lawson, K.W., & Lloyd, D.R. (1997). Membrane distillation, *Journal of Membrane Science*, 124, 1-25.
- [65] Lee, K.H., & Hwang, S.T. (1986). The transport of condensible vapors through a microporous Vycor glass membrane, *Journal of Colloid and Interface Science*, 110, 544-555.
- [66] Yeh, G.C., Yeh, B.V., Schmidt, S.T., Yeh, M.S., McCarthy, A.M., & Celenza, W.J. (1991). Vapor-liquid equilibrium in capillary distillation, *Desalination*, 81, 161-187.
- [67] Uchytíl, P., Petrickovic, R., Thomas, S., & Seidel-Morgenstern, A. (2003). Influence of capillary condensation effects on mass transport through porous membranes, *Separation and Purification Technology*, 33, 273-281.
- [68] Hansen, C.M. (2000). *Hansen Solubility Parameters*, CRC Press LLC, Washington.
- [69] Hansen, C.M., & Just, L. (2001). Prediction of environmental stress cracking in plastics with Hansen solubility parameters, *Industrial and Engineering Chemical Research*, 40, 21-25.
- [70] Grüner, S., Mangold, M., & Kienle, A. (2004). Dynamics of reaction separation processes in the limit of chemical equilibrium, *A.I.Ch.E. Journal*, submitted.
- [71] Sundmacher, K., Seidel-Morgenstern, A., & Kienle, A., Eds. (2004). *Integrated Chemical Processes*, Wiley-VCH, Weinheim.

[72] Ivanova, M., Qi, Z., Schlünder, E.-U., & Sundmacher, K. (2005). Analysis of potential singular point surface of reactive stripping processes, *Chemical Engineering Science*, accepted.

Publication list

Journal & Book contribution

- [1] Huang, Y.-S., Sundmacher, K., Qi, Z., & Schlünder, E.-U. (2004). Residue curve maps of reactive membrane separation, *Chemical Engineering Science*, 59, 2863-2879.
- [2] Huang, Y.-S., Sundmacher, K., Tulashie S., & Schlünder, E.-U. (2005). Theoretical and experimental study on residue curve maps of propyl acetate synthesis reaction, *Chemical Engineering Science*, 60, 3363-3371.
- [3] Huang, Y.-S., Schlünder, E.-U., & Sundmacher, K. (2005). Feasibility analysis of membrane reactors – discovery of reactive azeotropes, *Catalysis Today*, 104, 360-371.
- [4] Sundmacher, K., Qi, Z., Huang, Y.-S., & Schlünder, E.-U. (2005). Thermodynamic and kinetic effects on the feasible products of reactive distillation: Azeotropes and Arrheotropes, page 87-148, in Sundmacher, K., Seidel-Morgenstern, A., Kienle, A. (Eds.) *Integrated Chemical Processes*, Wiley-VCH, Weinheim.
- [5] Huang, Y.-S., & Sundmacher, K. (2005). Kinetics study of propyl acetate synthesis reaction catalyzed by Amberlyst 15, *International Journal of Chemical Kinetics*, submitted.
- [6] Huang, Y.-S., & Sundmacher, K. (2005). Experimental validation of reactive azeotropes, in preparation.

Conference contribution

- [1] Huang, Y.-S., Schlünder, E.-U., & Sundmacher, K. (Poster). Mass transfer effects on residue curve maps for membrane reactors. *The 3rd International Symposium on Multifunctional Reactors – ISMR3*, 27-30 August 2003, Bath, UK.
- [2] Sundmacher, K., Qi, Z., Huang, Y.-S., & Schlünder, E.-U. (Oral). Thermodynamic and kinetic effects on the feasible products of reactive distillation: Azeotropes and Arrheotropes. *International Max-Planck Symposium on Integrated Chemical Processes*, 22-24 March 2004, Magdeburg, Germany.
- [3] Huang, Y.-S., Schlünder, E.-U., & Sundmacher, K. (Oral). Feasibility analysis of membrane reactors - Discovery of reactive azeotropes. *The 6th International*

Conference on Catalysis in Membrane Reactors – ICCMR6, 6-9 July 2004, Lahnstein, Germany.

- [4] Huang, Y.-S., & Sundmacher, K. (Oral). From reactive distillation to reactive membrane separation: a generalized approach for feasibility analysis. *AIChE Annual Meeting*, 7-12 November 2004, Austin, USA.

Curriculum Vitae

Surname Huang
First name Yuan-Sheng
Date of birth 18.06.1973
Place of birth Hualien
Nationality Taiwan
Gender Male
Marital status Single
Current address Breiter Weg 258, 39104 Magdeburg
Telephone 0391 - 5446910 (Private); 0391 - 6110276 (Office)
E-mail huang@mpi-magdeburg.mpg.de

Education profile:

11/2001 ~ Present *PhD (Process Systems Engineering)*
Faculty of Process and Systems Engineering,
Otto-Von-Guericke University
Supervisor: Prof. Dr. Kai Sundmacher
Research Subject: Mass Transfer Effects on Reactive Separation
Processes – Discovery of Reactive Arrheotropes

07/1995 ~ 06/1997 *M.Sc. (Chemical Engineering)*
Dept. of Chemical Engineering, National Taiwan University.
Supervisor: Prof. Cheng-Liang Chen
Master thesis: The Self-Tuning Fuzzy Logic Controller

07/1991 ~ 06/1995 *B.Sc. (Chemical Engineering)*
Dept. of Chemical Engineering, National Taiwan University.

Work Experience:

11/2001 ~ Present *Research Fellow*
Max-Planck-Institute for Dynamics of Complex Technical Systems

12/1999 ~ 05/2001 *Process Engineer*
Taiwan Semiconductor Manufacturing Company.

Magdeburg, 30.10.2005